

# NOTE TO USERS

This reproduction is the best copy available.

**UMI**<sup>®</sup>



B1566791

# QUANTIFYING PROPICONAZOLE IN WOOD BY RAMAN MICROSCOPY

by

Erlet Kurti

(Bachelor of Science, University of Tirana, Albania, 1996)

A Thesis

presented to Ryerson University

in partial fulfillment of the

requirements for the degree

of Master of Applied Science

in the Program of

Chemical Engineering

PROPERTY OF  
RYERSON UNIVERSITY LIBRARY

Toronto, Ontario, Canada, 2004

© Erlet Kurti 2004

UMI Number: EC52968

### INFORMATION TO USERS

The quality of this reproduction is dependent upon the quality of the copy submitted. Broken or indistinct print, colored or poor quality illustrations and photographs, print bleed-through, substandard margins, and improper alignment can adversely affect reproduction.

In the unlikely event that the author did not send a complete manuscript and there are missing pages, these will be noted. Also, if unauthorized copyright material had to be removed, a note will indicate the deletion.

**UMI**<sup>®</sup>

---

UMI Microform EC52968

Copyright 2008 by ProQuest LLC.

All rights reserved. This microform edition is protected against unauthorized copying under Title 17, United States Code.

ProQuest LLC  
789 E. Eisenhower Parkway  
PO Box 1346  
Ann Arbor, MI 48106-1346

## **Borrower's Page**

Ryerson University requires the signatures of all persons using or photocopying this thesis. Please sign below, and give address and date.

## Abstract

### QUANTIFYING PROPICONAZOLE IN WOOD BY RAMAN MICROSCOPY

Erlet Kurti, 2004,

Master of Applied Science,

Chemical Engineering Department, Ryerson University.

Raman spectra of wood blocks treated with different propiconazole solutions (4 %, 2 % and 1%) in mineral spirits were recorded using a Raman microscope, equipped with a NIR (785 nm) laser. The strong propiconazole Raman band, in the uncongested region 647-693  $\text{cm}^{-1}$  was chosen as the analytical band. The normalized intensity of analytical band was used to determine the propiconazole distribution in white spruce. Mapping measurements on radial face of the treated samples revealed that on average the propiconazole concentration in summerwood was much higher than concentration in springwood. GC-MS analyses were carried out on methanol extractions of soaked samples milled at ~1.5 mm intervals. The depth profiles in longitudinal directions, obtained by Raman and GC-MS measurements, suggested that propiconazole tended to bloom to the surface during drying. A linear calibration plot was produced from averaged Raman normalized intensity and GC-MS-measured concentrations. By using the regression line, concentration in the longitudinal direction was predicted for another wood block soaked in 3 % propiconazole solution.

## ACKNOWLEDGEMENTS

Throughout the completion of this thesis I was grateful to have the encouragement of professors, friends and family. While this work is dedicated to all of them, I owe a major debt of gratitude to my supervisors, Dr. Darrick. V. Heyd and Dr. Stephen. R. Wylie. Thank you for giving me the opportunity to work on this project. Thank you, for the time, guidance and support that you provided me during the realization of this project. Not only your academic directions played a critical role in my professional development, but also your encouragement and kindness made my life enjoyable while completing this study. Thank you!

For their input and technical assistance, I would also express my appreciation to the technologists of Ryerson University, especially Dennis Walsmley, Ali Hemmati and Peter Scharping.

I would like to thank the Materials and Manufacturing Ontario (MMO), and the Natural Sciences and Engineering Research Council (NSERC), and Janssen Pharmaceuticals for funding this project.

## TABLE OF CONTENTS

|  | Page     |
|--|----------|
| Abstract                               | iv       |
| Acknowledgements                       | v        |
| List of Figures                        | x        |
| List of Tables                         | xiii     |
| List of Equations                      | xiv      |
| <b>Chapter 1 INTRODUCTION</b>          | <b>1</b> |
| 1.1 Objectives                         | 2        |
| <b>Chapter 2 LITERATURE REVIEW</b>     | <b>4</b> |
| 2.1 Overview                           | 4        |
| 2.2 Propiconazole                      | 4        |
| 2.2.1 Structure                        | 5        |
| 2.2.2 Toxicity                         | 6        |
| 2.2.3 Fate in the Environment          | 7        |
| 2.3 Wood Structure                     | 8        |
| 2.3.1 Macroscopic Structure of Wood    | 8        |
| 2.3.1.1 Annual Rings                   | 8        |
| 2.3.1.2 Sapwood and Heartwood          | 9        |
| 2.3.2 Physical Characteristics of Wood | 10       |
| 2.3.2.1 Colour                         | 10       |
| 2.3.2.2 Weight and Specific Gravity    | 10       |
| 2.3.3 Microscopic Structure of Wood    | 10       |

|         |   |    |
|---------|---|----|
| 2.3.3.1 | Pits  | 11 |
| 2.3.3.2 | Softwood  | 11 |
| 2.3.3.3 | Hardwood  | 12 |
| 2.3.4   | Chemical Composition and Ultrastructure of Wood             | 12 |
| 2.3.4.1 | Organic Components of Wood; Cellulose                       | 12 |
| 2.3.4.2 | Lignin  | 13 |
| 2.3.4.3 | Extractives   | 14 |
| 2.3.4.4 | Cell Wall Structure   | 15 |
| 2.4     | Wood Preservation   | 16 |
| 2.4.1   | Fungal Attack   | 17 |
| 2.4.2   | Preservatives   | 18 |
| 2.4.3   | Wood Treating Methods                                       | 18 |
| 2.4.3.1 | Pressure Processes  | 19 |
| 2.4.3.2 | Non-Pressure Processes                                      | 20 |
| 2.4.4   | Factors Influencing the Effectiveness of Wood Preservatives | 22 |
| 2.4.4.1 | Flow of Fluids Through a Porous Medium                      | 23 |
| 2.4.4.2 | Impregnation Model  | 25 |
| 2.5     | Raman Phenomena   | 28 |
| 2.5.1   | Polarizability and Selection Rules                          | 30 |
| 2.5.2   | Rotational Raman Effect                                     | 32 |
| 2.5.3   | Quantitative Analysis                                       | 32 |
| 2.5.3.1 | Area Normalization  | 34 |
| 2.5.4   | Raman Microscopy  | 34 |

|                  |  |    |
|------------------|--|----|
| 2.6              | Application of Raman Spectroscopy in Wood Analysis                     | 36 |
| 2.6.1            | Spruce Spectra   | 36 |
| 2.6.2            | Pine Spectra and Distinguishing Features of Hardwoods                  | 39 |
| 2.6.3            | Lignin   | 41 |
| 2.6.4            | Mapping of Wood Compounds and Chemical Treatments                      | 44 |
| <b>Chapter 3</b> | <b>METHODOLOGY</b>   | 48 |
| 3.1              | Species  | 48 |
| 3.2              | Sample Preparation and Extraction                                      | 48 |
| 3.3              | Internal Standard  | 50 |
| 3.4              | GC-MS Determination of Propiconazole                                   | 50 |
| 3.5              | Raman Spectra  | 52 |
| 3.6              | Raman Instrument   | 53 |
| 3.6.1            | Overview of System Operation   | 53 |
| 3.6.2            | Experiment Set-up  | 56 |
| 3.6.3            | Laser Source   | 57 |
| 3.6.3.1          | Quenching Fluorescence   | 57 |
| <b>Chapter 4</b> | <b>RESULTS AND DISCUSSION</b>  | 59 |
| 4.1              | Normalization Procedure  | 59 |
| 4.2              | Fluorescence   | 60 |
| 4.3              | Distribution of Propiconazole  | 65 |
| 4.3.1            | Deposition on Wood Surface   | 65 |
| 4.3.2            | Mapping Measurements of Propiconazole Distribution in Seasonal<br>Wood | 68 |

|                  |  |    |
|------------------|--|----|
| 4.4              | GC-MS Determination of Propiconazole Depth Profile | 72 |
| 4.5              | Raman Depth Profiles                               | 80 |
| 4.6              | Calibration Curve                                  | 84 |
| 4.6.1            | Raman Predicted Concentration                      | 86 |
| 4.6.2            | Weighted Regression Line                           | 88 |
| <b>Chapter 5</b> | <b>GENERAL CONCLUSIONS</b>                         | 91 |
| 5.1              | Recommendations                                    | 92 |
|                  | Appendix A   | 93 |
|                  | Appendix B   | 94 |
|                  | References   | 96 |

## LIST OF FIGURES

| <u>Figure</u> | <u>Description</u>   | <u>Page</u> |
|---------------|--|-------------|
| 1             | Structure of Propiconazole   | 6           |
| 2             | Principal Features of a Tree Stem  | 9           |
| 3             | Structure of a Cellulose Unit  | 13          |
| 4             | Catechin Structure   | 15          |
| 5             | Diagram of Tracheid Cell Wall Structure  | 16          |
| 6             | Wood and Biodegraded Wood  | 17          |
| 7             | Schematic Presentation of Liquid Penetration into a Submerged Porous Body  | 25          |
| 8             | Concentration Profiles Following Softwood Impregnation with NaOH   | 28          |
| 9             | Schematic of a Raman Microscope and Polarization Induced in a Molecule's Electron Cloud by an Incident Electric Field ( $h\nu_0$ ) | 35          |
| 10            | FT-Raman Spectra of Untreated Pine Wood  | 39          |
| 11            | Raman Spectra Collected from a Single Location in the Latewood, Secondary Wall of Black Spruce                                     | 42          |
| 12            | Changes in Intensity of $\nu_1$ Band Intensity Obtained by Raman Measurements of Transverse Faces                                  | 46          |
| 13            | Line Maps of Various Raman Spectra in the Longitudinal Direction   | 46          |
| 14            | Azaconazole Structure  | 50          |
| 15            | SIM Chromatogram   | 51          |
| 16            | Raman Measurements Points on the Radial Face of Wood Blocks  | 52          |
| 17            | Schematic Diagram of Renishaw Raman System 2000  | 54          |

|    |   |    |
|----|---|----|
| 18 | Renishaw Raman System 2000 at Ryerson University  | 54 |
| 19 | Raman Spectra of Spruce, Spruce Treated with Propiconazole, and Standard Propiconazole  | 60 |
| 20 | Different Species Intensity at $300\text{ cm}^{-1}$   | 62 |
| 21 | Red pine Heartwood and Sapwood Intensities at $300\text{ cm}^{-1}$  | 62 |
| 22 | Quenching Fluorescence  | 64 |
| 23 | Raman Surface Calibration Curve   | 65 |
| 24 | Mapping Measurement on Transversal Surface of a Propiconazole Treated Sample  | 67 |
| 25 | White Light Image from 2-D Mapping Measurements and Average integrated intensity of analytical region ( $647\text{-}693\text{ cm}^{-1}$ ) | 69 |
| 26 | White Light Image and Normalized Raman Intensity from 1-D Mapping   | 70 |
| 27 | Depth Profile of Propiconazole in Block A by GC-MS  | 72 |
| 28 | Surface-Excluded Depth Profile of Propiconazole in Block A by GC-MS   | 73 |
| 29 | Depth Profile of Propiconazole in Block B by GC-MS  | 74 |
| 30 | Surface Excluded Depth Profile of Propiconazole in Block B by GC-MS   | 75 |
| 31 | Depth Profile of Propiconazole in Block C by GC-MS  | 76 |
| 32 | Surface Excluded Depth Profile of Propiconazole in Block C by GC-MS   | 77 |
| 33 | Raman Depth Profiles for Block-A  | 80 |

|    |  |    |
|----|--|----|
| 34 | Raman Depth Profiles for Block-B   | 81 |
| 35 | Raman Depth Profiles for Block-C   | 82 |
| 36 | Calibration Curve  | 84 |
| 37 | 95 % Confidence Limits for the Unweighted Regression                                 | 85 |
| 38 | Raman Depth Profiles for the Block Soaked in 3% Propiconazole Solution               | 86 |
| 39 | Predicted Concentration From the Regression Line Equation                            | 87 |
| 40 | GC-MS Measured Concentration and Raman Predicted Values                              | 88 |
| 41 | 95 % Confidence Limits for Predicted Concentration by Using Weighted Regression Line | 89 |
| A1 | Raman Spectra of Different Species   | 93 |
| B1 | Calibration Curve with Error Bars from SDs   | 94 |

## LIST OF TABLES

| <u>Table</u> | <u>Description</u>  | <u>Page</u> |
|--------------|---|-------------|
| 1            | Raman Bands in the Spectrum of Black Spruce                                   | 37          |
| 2            | Band Assignment for Cellulose and Lignin in Black Spruce Spectrum             | 38          |
| 3            | Experiment Set-up   | 56          |
| B2           | Predicted Concentration Values by Unweighted and Weighted<br>Regression lines | 95          |
| B3           | Relative Error in the Predicted Concentration                                 | 95          |

## LIST OF EQUATIONS

| <u>Equation</u> | <u>Description</u>  | <u>Page</u> |
|-----------------|---|-------------|
| 1               | Darcy's Law for Liquids                                       | 22          |
| 2               | Flow of an Incompressible Liquid                              | 24          |
| 3               | Pressure Differential   | 24          |
| 4               | Jurin's Law   | 24          |
| 5               | Second Fick's Law (Cylindrical Coordinates, Radial Direction) | 26          |
| 6               | Analytical Solution for Second Fick's Law in Radial Direction | 26          |
| 7               | Second Fick's Law (Cylindrical Coordinates, Axial Direction)  | 27          |
| 8               | Analytical Solution for Second Fick's Law in Axial Direction  | 27          |
| 9               | Polarization  | 30          |
| 10              | Classical Derivation from Polarization Equation               | 30          |
| 11              | Transition Moment Integral                                    | 31          |
| 12              | Intensity of Raman Scattered Light                            | 32          |
| 13              | Intensity for Modern Instruments                              | 33          |
| 14              | Frequency Independent Cross-Section                           | 33          |
| 15              | Calculated Raman Shift  | 55          |
| 16              | Normalized Intensity  | 60          |

## Chapter 1

### INTRODUCTION

While it does not have the historical longevity of stone, the unique characteristics and comparative abundance of wood have made it a natural material for homes, frames, furniture, decorative objects, *etc.* Wood has many uses because of its excellent strength-to-weight ratio, thermal conductivity, durability and workability. Unfortunately, wood is susceptible to chemical, physical and biological degradation. In many cases, the attack by fungi, insects, bacteria, *etc.*, may degrade wood completely. Several antifungal strategies may be used to eliminate or reduce biodeterioration of wood. Fungi attack the wood when four essential requirements are met: food, moisture, temperature and air. The wood itself throughout its organic composition provides the necessary food for fungus survival. Keeping wood dry can prevent deterioration but not much can be done about oxygen.

One of the most effective methods for preserving wood is by treating it with preservatives. Preservatives can extend wood life by 30 to 50 years. Some preservatives are more effective than others and some are more adaptable to specific purposes. In North America, for a number of decades, CCA (Chromated Copper Arsenate) has been an effective treatment of wood used in residential equipment. As of December 31, 2003, negative publicity mainly focused on the presence of arsenic led to a voluntary withdrawal of CCA from the marketplace. New alternatives are emerging for treating wood in applications such as window frames, patio walkways, picnic tables, play structures, porches and fences. For example, propiconazole-containing solutions are being successfully used in applications where wood is in close contact with humans.

Propiconazole is a systemic foliar antifungal agent that has protective and curative action. Nowadays propiconazole is considered a safer alternative than a number of traditionally used preservatives like azaconazole, pentachlorophenols and inorganic arsenical preservatives [EXTOXNET, 2001].

The effectiveness of wood preservation depends on several treatment factors including depth of penetration, selection of wood, *etc.* The current analytical methods [AWPA, A24-94] for determining propiconazole depth of penetration are time consuming and require lengthy multistep sample preparation. Moreover, these methods involve milling that may lead to irreversible chemical changes in the lignin structures or may partially evaporate some of the volatile extractives due to the heat induced in the samples [Dence, 1992]. Evidently, there is a need for a practical and non-destructive technique that would not require extensive sample preparation and analysis time.

### **1.1 Objectives**

This study was aimed at developing a quantitative, rapid, analytical technique for analysis of propiconazole distribution in treated wood. The feasibility of using Raman microscopy as a rapid means of determining the propiconazole depth of penetration, was studied. Both Raman microscopy and GC-MS (gas chromatography-mass spectroscopy) were utilized for quantification of propiconazole concentration in the longitudinal direction.

Raman is very well suited as an *in situ* technique for analysis of heterogeneous materials like wood. This technique is advantageous since samples can be measured directly, as is, without complex procedures for sample preparation. In addition, Raman

measurements are not expected to cause any sample damage because the induced energy of the excitation laser (NIR) is low. Further considering that presence of water in a sample is not a problem (unlike IR) gives Raman microscopy capabilities that are not provided by any other method [Wariishi *et al.* 1997; Agarwal, 1999].

The distribution of propiconazole related to particular wood structures such as summerwood and springwood was also investigated. Raman microscopy has the capability to analyze microscopic regions with high spatial resolution. The information obtained is unique given that the resolving power of the microscope is smaller than the sizes of microstructures of wood. Finally, Raman predicted results were validated with traditional GC-MS method.

## Chapter 2

### LITERATURE REVIEW

#### 2.1 Overview

First, this chapter discusses general information about propiconazole and wood. Wood treating methods, flow in porous medium and an impregnation model are also reviewed. Second, a brief description of Raman phenomena and Raman microscopy is given. In addition, application of Raman techniques to analyses of wood, wood components and treated wood is described in section 6 of this chapter.

#### 2.2 Propiconazole

Within the last decades, triazole fungicides have become important in controlling a wide range of plant diseases. Although initially developed as fungicides for seeds and plants, the value of triazoles as wood preservatives was quickly recognized thanks to their excellent protective, curative and systemic power.

Propiconazole is a triazole fungistatic agent with a broad spectrum of activity. It was first developed in 1979 by Janssen Pharmaceuticals of Belgium [EXTOXNET, 2001] and marketed in early 1980's by Ciba-Geigy. Initially intended for pharmaceutical use, propiconazole was later applied against powdery mildew, rust, scab and leaf spot diseases on different crops. The current uses include treatments for wheat, oat, canola, grasses and the prevention of sapstain, mould and decay of wood.

Stipes *et al.* [1986] first noticed that the minimal inhibitory concentration of propiconazole against *Ophistoma ulmi*, a fungus that causes Dutch Elm disease, was as

low as 1ppb. This concentration was much lower than for any other fungicide tested in their research. Immediately propiconazole became the new focus of arborist attention, while the use of fungicides like thiabendazole was almost abandoned.

Propiconazole exhibits strong activity against a number of different fungi, including *Ophistoma ulmi*, [Stipes *et al.* 1986], *Sclerotinia homoeocarpa* [Hsiang *et al.* 1997], *Coniophora puteana*, *Gleophyllum trabeum*, *Poria placenta*, and *Coriolus versicolour* [Hughes, 2004]. Propiconazole is an ergosterol biosynthesis inhibitor. In general, all azoles including imidiazoles and triazoles interfere with the activity of fungal lanosterol 14 $\alpha$ -demethylase, a member of the cytochrome P450 family. Lanosterol 14 $\alpha$ -demethylase is responsible for transforming lanosterol to ergosterol. Blocking biosynthesis of ergosterol, which is crucial to the fungal cytoplasmic membrane, would result in fungal cell disorganization, and finally stop fungal growth [Herbert, 2001].

### 2.2.1 Structure

Typically, triazole derivatives have a common structural moiety, the 1,2,4-triazole ring that is connected to a hydrophobic backbone through position 1. Propiconazole has two chiral centers located at the 2- and 4- positions of the central dioxolane ring, therefore it exists as four stereoisomers, two enantiomer pairs, one *cis* and one *trans*. Both isomers are biologically important, but *cis*-stereomers usually show higher antifungal activity than the racemates [Zirngibl, 1998].

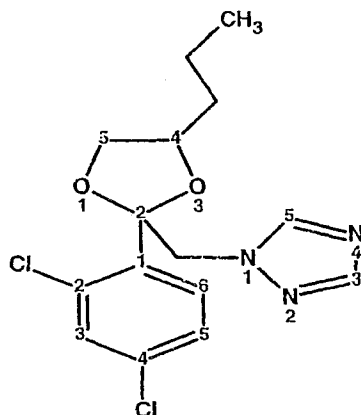


Figure 1. Structure of Propiconazole. (1-[[2-(2,4-dichlorophenyl)-4-propyl-1,3-dioxolane-2-yl]methyl]-1*H*-1,2,4-triazole)

The presence of nitrogen atoms gives propiconazole the characteristics of a base. Due to the basic nature of the propiconazole molecule, Tadeo and Laflente [1987] reported increased recoveries of propiconazole from citrus fruits when the extracting solvent was pH adjusted to 8.0.

Propiconazole is light to dark yellow in appearance and is a highly viscous liquid. It is miscible with methanol, mineral spirit, acetone and toluene [PMRA, 2000].

### 2.2.2 Toxicity

Propiconazole exhibits minimal toxicity to nontarget species. The oral acute dose (LD<sub>50</sub>) found in rats is 1517 mg/kg, while in rabbits is 1344 mg/kg. Propiconazole is neither mutagenic nor teratogenic [PMRA, 2000]. In a two-year feeding study in rats, the no-effect-level (NOEL) was established at 100 ppm. Propiconazole has low solubility in water (110 mg/L at 20°C) and is not bioaccumulative (log K<sub>ow</sub>=3.65). The U.S.

Environmental Protection Agency has classified propiconazole as Group "C" for carcinogenicity (possible human carcinogen) [EXTOXNET, 2001].

### 2.2.3 Fate in the Environment

Propiconazole is resistant to hydrolysis and phototransformation. It shows a maximum absorption ( $\lambda_{max}$ ) at 269 nm and at wavelengths longer than 290 nm the absorption is very weak. When exposed to solar light, the photodegradation of propiconazole is slow with the half-life estimated at  $85 \pm 10$  hours. The phototransformation occurs about 30 % faster in natural water than in pure water due to the humic acids that are able to enhance the rate of propiconazole disappearance [Vialaton *et al.* 2001]. Propiconazole will partition readily into sediments, where it can be moderately persistent under aerobic conditions and persistent in anaerobic environments. Its vapour pressure ( $1.3 \times 10^{-4}$  Pa) and Henry's Law constant ( $3.99 \times 10^{-9}$  atm m<sup>3</sup>/mol) indicate little potential for volatilization [PMRA, 2000].

In plants, propiconazole is metabolized by hydroxylation of the n-propyl group to give four beta-hydroxy isomers that form sugar conjugates. Cleavage of the dioxolane ring and deketalization yields the alkanol metabolite. Moreover, hydroxylation and dechlorination of the phenyl ring occur to some degree.

A degradation study in an aqueous environment (pH 6.0) similar to that of elm tree (*Ulmus americana*) has revealed that the half-life of propiconazole is 67-101 days [Amstrong, 1999]. From activation energy ( $E_a$ ) calculations, Amstrong [1999] indicated that degradation of propiconazole is temperature dependent. When the tree sap was at elevated temperatures (50°C) a rapid degradation occurred, whereas in the wintertime

degradation was slower. The only degradation products positively identified in Armstrong's study were 1-(2,4-dichlorophenyl)-2-ethanone and 1,2-pentanediol.

## **2.3 Wood Structure**

Trees belong to seed-bearing plants (*Spermatophytae*) that are subdivided in two distinct classes, referred to as softwoods and hardwoods. The softwoods are derived from the *Coniferales* order of the *Gymnospermae*, while the hardwoods derive from the *Angiospermae* order. Approximately 520 softwood tree species are known; the more commercially important softwoods include genus like Pine, Spruce, Fir, Cedar, *etc.* The *Angiosperms*, comprising around 30000 species, include trees like Oak, Beech, Maple, *etc* [Sjöstoröm, 1993].

### **2.3.1 Macroscopic Structure of Wood**

In a cross-section of the main stem in a tree three parts can be distinguished: *pith*, *wood and bark*. Between wood and bark there is a microscopic tissue, called *cambium* (fig.2). When cambium is growing, it produces wood toward the inside and bark toward the outside of the tree.

#### **2.3.1.1 Annual Rings**

Wood is characterized by the presence of more or less obvious concentric layers, known as annual (growth) rings. In most species, growth rings can be easily distinguished from one another because of differences between earlywood (springwood) and latewood

(summerwood). At the beginning of the growth season, light-coloured and porous earlywood is formed. Later the rate of growth decreases and latewood is produced. The portion of ring formed in spring is primarily designed for sap conduction while summerwood is more suited to give mechanical strength and is darker and denser than springwood [Sjöstoröm, 1993].

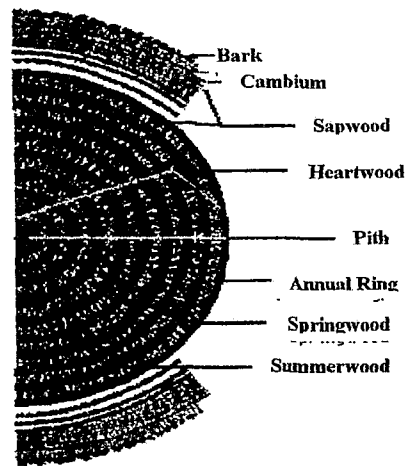


Figure 2. Principal Features of a Tree Stem; cross sectional view. Adapted from Milton [2002]

### 2.3.1.2 Sapwood and Heartwood

In many species at a certain age the inner wood begins to change to dead heartwood that is associated with a darkening of the tissue. The dying cells produce organic deposits such as resins, phenolic substances, tannins, gums etc. The peripheral portion of the stem is called sapwood. Sapwood is less durable and more permeable than heartwood

## **2.3.2 Physical Characteristics of Wood**

### **2.3.2.1 Colour**

Generally colour is imparted to wood by extractives that are mainly deposited in heartwood. Wood colour can vary from almost white, as in the sapwood of many species, to the jet black of the heartwood of black ebony (*Diospyros ebenum*). Dark natural colour is an indication for high durability. The presence of extractives, which are toxic to wood decaying fungi, is the cause of high durability of woods like cedar, oak, and black luster [Tsounis, 1968].

### **2.3.2.2 Weight and Specific Gravity**

The weight of wood is influenced by different factors, such as sapwood and heartwood, proportion of earlywood and latewood, and especially by moisture content. For comparative purposes, the specific gravity is a better-suited concept. Specific gravity is the ratio of the weight to the volume of wood and is based on standard hygrometric conditions.

### **2.3.3 Microscopic Structure of Wood**

The microscopic structure of wood is highly heterogeneous. Microscopic observation shows not only differences between various species as well as between softwood and hardwood, but also differences within the same sample, such as sapwood and heartwood, earlywood and latewood.

### 2.3.3.1 Pits

*Pits* are recesses in the secondary wall between adjacent cells. *Bordered pits* are holes in cell walls that are enlarged towards the pit membrane forming a cavity. Typically they occur in softwood tracheids (see 2.3.3.2) and hardwood fibers or vessels. In some species the central area of the pit membrane is thickened with an amorphous material. This central part is called the *torus* and is surrounded by a membrane called the *margo*, which consists of strands of microfibrils and allows fluids and small particles to penetrate through the pit membrane. Aspiration occurs when the torus is pressed against the aperture and the pit is closed irreversibly. Caused by pressure differences within adjacent cells, aspiration affects the permeability of wood.

### 2.3.3.2 Softwood

Softwoods have a relatively simple structure as they consist of 90-95 % tracheids. Most of the tracheids are oriented longitudinally but in some softwoods like spruce, pine and douglas fir there are tracheids oriented radially (ray tracheids). Tracheids give softwood the mechanical strength and provide liquid transport through the bordered pits. These long and slender cells with flattened or tapered closed edges differ in diameter evolving from earlywood to latewood. Tracheid diameters are on the average 0.02-0.04 mm, but in some species may range from 0.007 mm for last latewood tracheids to 0.032 mm for the first earlywood tracheids. In most softwoods, average lengths of tracheids vary from 2 to 4 mm [Sjöstoröm, 1993; Fengel and Stoll. 1973]. The *parenchyma cells* (storage cells) include *ray parenchyma* and *epithelial cells*. In spruce wood, most of the

ray cells are parenchyma cells. Epithelial cells secrete oleoresins in the resin canal, which are vertical and radial cavities within the tissue of most softwoods.

### **2.3.3.3 Hardwood**

In hardwoods the supporting tissue consists mainly of libriform cells (fibers), which are elongated, thick-walled cells with small cavities. The dimensions of fibers in hardwood are smaller than dimensions of softwood tracheids [Fengel and Wegener, 1984]. Hardwood conducting vessels are composed of thin-walled and rather short and wide elements, which are placed on top of each other to form long tubes. In some hardwoods, like aspen and birch these vessels constitute about 25 % of wood volume.

Hardwood rays are comprised of parenchyma cells that are short, compact, radially arranged cells with stubby ends. Axial parenchymas are long tapered longitudinal cells with thin cell walls that function as nutrient storage sites [Thomas, 1979].

## **2.3.4 Chemical Composition and Ultrastructure of Wood**

### **2.3.4.1 Organic Components of Wood; Cellulose**

All wood is composed of cellulose, hemicelluloses, and lignin. The approximate proportions in softwood and hardwood are: cellulose 40-45 %; lignin 25-35 % in softwoods and 15-25 % in hardwoods; hemicelluloses, 25-30 % in softwoods and 25-35 % in hardwoods [Douglas, 1987].

Cellulose is composed of molecules of glucose ( $C_6H_{12}O_6$ ) that are linked together to form long cellulose chain molecules. Linkage of any two glucose units is a cellobiose unit with a length of 10.3Å.

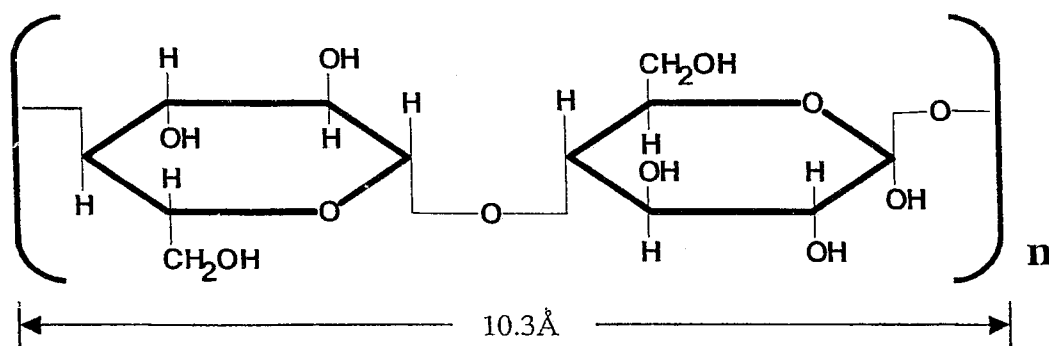


Figure 3. Structure of a Cellobiose Unit

The hydroxyl groups of cellulose molecules are able to form hydrogen bonds with other glucose units or with water molecules [Fengel and Wegener. 1984]. Cellulose molecules aggregate together to form *microfibrils*, which build up fibrils and finally cellulose fibers. Cellulose is the major determinant of mechanical and hygroscopic properties of the cell wall. In contrast to cellulose, which is exclusively composed of glucose, *Hemicelluloses* include a variety of monosaccharides like mannose, xylose *etc.*

#### 2.3.4.2 Lignin

Lignin, a phenolic component of the cell wall, differentiates wood from other cellulosic materials. A lignin formula presented by Adler [1987] consisted of 16 phenyl propane units that represent only a segment of the macromolecule. Softwoods typically consist of guaiacyl lignin (4-hydroxy-3-methoxyphenyl), while hardwoods mainly consist of syringyl (3,5-dimethoxy-4-hydroxyphenyl) with guaiacyl lignin as a minor component.

### 2.3.4.3 Extractives

The variety of chemical components that are extractable from wood with various solvents are called extractives. Extractives are compounds that contribute to properties of wood such as colour, odour, resistance, specific gravity and permeability. The proportion of extractives varies from less than 1 % to 10 % of the wood volume. The amount of extractives differs markedly even within the same tree. In pines, for example, the heartwood contains much more extractives than sapwood [Sjöstoröm, 1993].

Resin is a collective name for a variety of oily non-phenolic lipophilic extractives soluble in non-polar organic solvents but insoluble in water. Terpenes are one of the most important constituents of resins. Terpenes that are present in softwood extractives include classes from mono- to tetra-terpenes. In hardwood extractives typically higher terpene classes are found. Apart from resins, other compounds like fats, waxes, steroids, fatty acids and phenolic substances are also present in wood extractives [Fengel and Wegener, 1984].

Fats are glycerol esters of fatty acids, whereas waxes are esters of fatty acids with higher ( $C_{18}$ - $C_{24}$ ) alcohols, terpene alcohols or sterols. Most common fatty acids include palmitic ( $C_{16}$ ), stearic ( $C_{18}$ ), linolenic ( $C_{18}$ ) and eicosatreinoic ( $C_{20}$ ) acids. The isomer of linolenic acid, pinolenic acid, is the major fatty acid in spruces and pines [Sjöstoröm, 1993].

Wood extractives also contain low molecular phenols that are mainly concentrated in heartwood with only traces present in sapwood. *Stilbenes*, which have a conjugated double bond system (*e.g.* pinosylvin), are a phenolic group particularly present in heartwood pines. Vanillin, conifer aldehyde, guaiacylglycerol and syringin are some of

the *simple phenols* isolated in spruce extractives [Ekman, 1976]. Other phenolic compounds found in wood extractives include *lignans*, *flavonoids*, *condensed and hydrolysable tannins*. Lignans are always associated with the softwood extractives, whereas flavonoids and related compounds are the major components on the extractives of the so-called coloured woods, *e.g.* red woods, blue and yellow wood [Fengel and Wegener, 1984]. Condensed tannins, which are polymers of flavonoids, occur in species like chestnut, oak, quebracho, spruce, pine, larch etc [Hillis, 1962]. Catechin (flavan-3-ols) is a well-known structural unit of condensed tannins. Hydrolysable tannins are esters of gallic acid and its dimers, with glucose. Tannins of this type are unusual in wood.

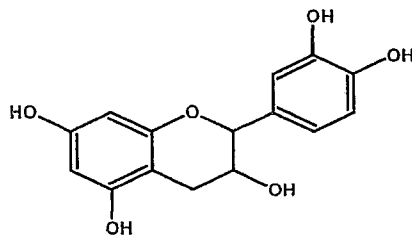


Figure 4. Catechin Structure

Certain inorganic (*ash*) materials, such as calcium, potassium and magnesium are also considered as extractives since they are not cell-wall components. Their percentage is low (<1%) and may differ significantly with species.

#### 2.3.4.4 Cell Wall Structure

Electron photomicrographs have revealed that several layers build up the tracheid cell wall. These layers are (fig. 5): middle lamella (M), primary wall (P), outer layer of secondary wall ( $S_1$ ), middle layer of secondary wall ( $S_2$ ), inner layer of secondary wall

(S<sub>3</sub>), and warty layer (W). The above layers differ from one another with respect to structure and chemical compositions. In the outer (S<sub>1</sub>) layer microfibrils are oriented nearly normal to fiber axis, whereas in the secondary wall (S<sub>2</sub>) they are angled by almost 20° from the fiber axis. The angle of microfibrils in the S<sub>3</sub> layer varies from 50 to 90° [Tsounis, 1968]. The S<sub>2</sub> layer, which is the thickest one, contains the highest percentage of cellulose (~54 %). The middle lamella is a highly lignified layer (~75 %) and is located between the cells serving as a cell binder [Panshin and De Zeeuw, 1980]. The warty layer (W), typically found in conifer species, is a thin amorphous membrane in the inner surface of the cell wall.

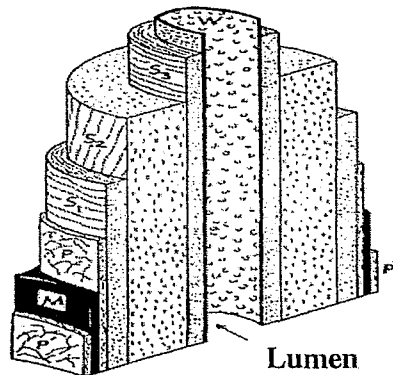


Figure 5. Diagram of Tracheid Cell Wall Structure. Adapted from Siau [1984].

## 2.4 Wood Preservation

Wood is subject to degradation because of its organic chemical composition and its physical structure. The degradation may take place while wood is part of a living tree, during storage, or preparation for use and service. In fact, cellulose and lignin are the two most abundant organic compounds on the earth and without fungi and insects that biodegrade them, the landscape would be littered with downed and dead trees. The

problem is that these recyclers do not distinguish between wood in a living tree or in use and wood lying dead on the forest floor [Stephen, 1996].

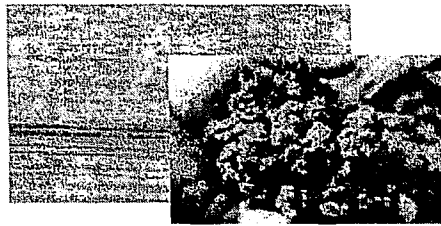


Figure 6. Wood and Biodegraded Wood.

#### 2.4.1 Fungal Attack

Fungi may cause both *stains* and *decay*. *Sap stain (blue stain)*, one of the most common fungal stains, can develop when fungi attack the sapwood in logs, lumber and (rarely) on dying trees. Blue stain is caused by a number of fungi, such as *Ceratocystis*, *Graphium*, and others. These fungi spread throughout the wood passing from cell to cell mostly through pits. Wood attains a bluish colour and since the stain is not superficial sanding or planing cannot remove it [Tsounis, 1968].

*Decay (rot)* can affect wood in living trees, logs lumber and other wood products. Fungi that cause decay belong to two main classes: *brown rot* and *white rot*. Wood that is decayed by brown rot becomes brown, checked and it can be easily pulverized. White rot makes wood spongy or fibrous. White rot fungi are able to decompose both carbohydrates and lignin, whereas brown rot fungi primarily metabolize (breakdown) cellulose and hemicelluloses [Tsounis, 1968].

### **2.4.2 Preservatives**

Generally, preservatives fall into the following major groups: oil-borne, water-borne, and creosote. The oil-born preservatives include members such as pentachlorophenol (Penta), copper and zinc naphthenate, tributyl tin oxide (TBTO) *etc.* In use since the 1930s, these preservatives are carried in organic solvents and applied to utility and building poles, fence posts, and highway timbers. Nowadays, formulators are concentrating their efforts to make these preservatives emulsifiable in water and more environmental friendly. Propiconazole is an organic triazole biocide that is currently being used commercially for aboveground and sapstain control applications [Wayne, 1994; Forest Products Society, 1999].

Wood treated with water-borne preservatives is used in residential, commercial and industrial buildings. Typical members are: chromated copper arsenate (CCA), ammoniacal copper arsenate (ACA), alkaline copper quat (ACQ), copper azole (CBA-A & CA-B) and sodium borates (SBX).

Creosote is a toxic distillate of coal tar with an offensive odour. It is highly effective against fungi, insects, and marine borers, and is primarily used for treating railroad ties, guardrail posts, and timbers used in marine structures.

### **2.4.3 Wood Treating Methods**

Historically, there have been almost as many methods for applying preservatives into service wood, as there are different preservatives. Most of the industrial scale methods can be classified as either pressure or nonpressure processes.

### 2.4.3.1 Pressure Processes

Pressure treatment is a common industrial application that involves placement of wood material in an airtight steel cylinder or retort and filling it with preservative under pressure to force the preservative into wood. Most units vary from 2-3 m in diameter and up to 45 m in length and are built to resist working pressures up to 1720 kPa. The basic variations of the pressure treatment methods are: full-cell (Bethell) process, and empty-cell (Rueping/Lowry) process. The "empty" and "full" terms refer to the level of preservative retained in the wood cells.

The main steps involved in the full-cell process are listed below [Stephen, 1996]:

- The charge of wood is placed inside a pressure vessel and vacuum is applied in order to remove as much air as possible from the wood and from the cylinder.
- The preservative (either heated or at ambient temperature) enters the cylinder.
- After being flooded with preservative, in order to drive the solution into wood, the cylinder is pressurized until no more preservative will enter the wood, or until the desired preservative retention is achieved
- At the end of the pressure period, pressure is released, preservative is removed from the cylinder and a final vacuum may be applied to remove the preservative dripping from the wood.

Generally, high retention and penetration of the treating solution is expected after the full-cell process. Retention is a measure of the amount of preservative or other liquid in wood and is usually expressed in pounds of preservative per cubic foot of wood (lbs/ft<sup>3</sup>). Retention may also be expressed as the fraction of voids filled by liquid (fractional

volumetric retention) and calculated by dividing the volume of the retained liquid by the volume of the voids in the wood [Siau, 1984].

In the empty-cell processes, no initial vacuum is drawn, therefore only the cell walls are treated with these processes. These processes require less preservative and are usually applied when the treated wood will not be exposed to extreme conditions. Rueping process involves filling of the wood cells with pressurized air prior to preservative injection. Pressurization time varies with wood species, where more resistant species may require up to 1 hour pressure period. Typically, the air pressure varies from 172 to 690 kPa depending on the desired retention. After the initial pressurization period, preservative is pumped into the treating cylinder under hydraulic pressure and forced into the wood. Pressure is raised above that of the initial air and maintained until the desired retention level is achieved. After the pressure-release, the expanding air, aided by a small-applied vacuum, pushes preservative out the cell cavities leaving them empty. The Lowry process, which is also an empty-cell process, is operated with no initial pressure. Preservative is pumped into the treating cylinder and pressure is applied after the cylinder is filled. The rest of the steps are the same as in the Rueping process [Stephen, 1996].

#### **2.4.3.2 Non-Pressure Processes**

Dipping, Soaking, Spraying, and Vacuum are some of the methods included in non-pressurized processes. Treatment by dipping involves immersing wood in tanks filled with preservative solution for several minutes. Dipping tanks vary in dimensions (typically 2x2.5x0.5 m) and most of them have draining racks. After dipping the treated wood is left to drip-dry so that chemical losses are minimised. Given the nature of this

method, some splashing and evaporation of preservative solution is inevitable. Dipping applications provide limited protection to wood, however they do have value for exterior woodwork and millwork that is painted and not in contact with the ground [Forest Products Society, 1999].

Soaking is the same method as dipping, except that immersion of wood into the treating solution lasts from days to weeks. Soaking wood for several days in preservative solutions provides considerable better penetration and retention levels than the dipping method. Cold soaking well-seasoned wood for several hours or days in oil preservatives has been successfully applied on window frames, fence post, exterior trim, lumber and timbers. For example, pine posts treated by cold soaking for 24 to 48 h or longer in a solution containing 5% of pentachlorophenol have shown an average life of 16 to 20 years or longer. The sapwood in these posts is well penetrated, and preservative solution retention levels ranged from 32 to 96 kg/m<sup>3</sup> (2 to 6 lb/ft<sup>3</sup>), which is within specified requirements for this application [Forest Products Society, 1999].

Spraying is a treatment most widely used for protecting areas of previously treated wood that have been cut or machined. With this method penetration and retention are unpredictable, so only limited protection is expected.

Vacuum methods involve enclosing wood in an airtight container from which air will be removed with a vacuum pump. In some applications, the container is filled with preservatives with or without additional pressure and without air re-entering. The preservatives are driven into wood by the slight pressure created from removal of air from cell cavities, followed by addition of the preservatives [Forest Products Society, 1999].

Combinations of vacuum with pressure methods, such as double vacuum and pressure, are also being successfully applied in the wood treatment industry. In double vacuum methods, air is pumped out and the treatment vessel is filled with preservative under pressure, so deep penetration is achieved. Next, a second vacuum is applied in order to evacuate the excess amount of preservative. At the end of the process the treated wood is almost dry and the amount of wasted chemicals is minimal [EverDry Forest Products, 2003].

#### **2.4.4 Factors Influencing the Effectiveness of Wood Preservatives**

Even with a high quality preservative, inadequate preservative penetration may allow fungi to spread through the shell of treated wood to the inner part of unprotected wood. The depth of penetration depends not only on the treatment process used, but also on the wood species and the portion of sapwood to heartwood.

Permeability plays an important role on the liquid penetration in the wood structures. It measures the ease with which fluids are transported through porous materials under the influence of pressure gradient and is an extremely variable property of wood. In general, anatomical features of the wood such as pore size, pit aspiration, extractives, moisture content, and specimen flow length influence permeability.

Darcy's law is used to describe the steady-state flow of fluids through wood. In this case conductivity is called permeability and Darcy's law for liquids is written as [Siau, 1984]:

$$k = \frac{QL}{A\Delta P} \quad (1)$$

where  $k$  = permeability  $\text{cm}^2$  (liquid)/ atm sec,  $Q$  = volumetric flow rate,  $\text{cm}^3/\text{sec}$ ,  $L$  = length of specimen in the flow direction, cm,  $A$  = cross-sectional area of specimen perpendicular to flow direction,  $\text{cm}^2$ ,  $\Delta P$  = pressure differential, atm.

In order to express permeability only as a function of porous structure, another parameter, the specific permeability, is used. Specific permeability is given from the product of permeability with viscosity of a fluid and has units of darcy (or  $\text{cm}^3/\text{cm}$ ).

Comstock [1970] modelled the ratios of longitudinal-to-tangential permeabilities of softwoods between 10000:1 and 40000:1. Approximate values of permeability for different species are reported in Siau [1984], where species like red oaks had permeability as high as 200 darcys. The pine sapwood was among the most permeable softwoods (up to 8 darcys), whereas the spruces and cedars were usually lower, in the range of 0.1 darcys.

#### **2.4.4.1 Flow of Fluids Through a Porous Medium**

Unsteady-state transport is an important flow in wood treatments, because it is present whenever wood is heated, impregnated with liquids, evacuated or dried. By using the integrated form of Darcy's law, Siau [1984] described the unsteady-state transport of liquids into a porous body during the full-cell (Bethell) process. The penetration and the fractional volumetric retention of liquid for flow through both ends of a parallel side specimen were found proportional to the square root of time. For species with permeability less than 2 darcys, Bramhall [1971] observed a linear relationship between the logarithm of permeability and the length. In such species, although the penetration was proportional to the square root of time, the fractional volumetric retention was not.

Flow of an incompressible liquid through a porous medium can be described by the following equation [Perry, 1984]:

$$\frac{\Delta P}{L} = \alpha \mu U + \beta \rho U^2 \quad (2)$$

where  $\Delta P$  = pressure differential,  $L$  = Length of the medium,  $U$  = velocity of liquid movement,  $\mu$  = dynamic viscosity of the liquid,  $\rho$  = liquid density,  $\alpha$  = viscous resistance coefficient, and  $\beta$  = inertial resistance coefficient.

For purely viscous flow, the second term (involving  $U^2$ ) of equation 2 becomes negligible. Assuming that  $\alpha = k^{-1}$ , the resulting equation is the same as Darcy's law (eq.1) for an incompressible flow through porous media. The pressure differential,  $\Delta P$ , is given by the difference of the sum of external pressure  $P_{ex}$ , hydrostatic pressure  $P_h$ , capillary pressure,  $P_c$ , and the sum of partial pressures of air,  $P_a$ , and water vapour,  $P_v$  [Malkov *et al.* 2003].

$$\Delta P = (P_{ex} + P_h + P_c) - (P_a + P_v) \quad (3)$$

In the absence of the external pressure, the penetration of liquid into submerged porous bodies can be simplified as follows. Initially, liquid flow is driven through the lumens of the tracheids into the matrix by hydrostatic and capillary pressure and resisted by pressure of air and water vapour (fig.7). The influence of capillary pressure can be described by Jurin's Law:

$$P_c = \frac{2\gamma \cos \theta}{r} \quad (4)$$

where  $r$  = radius of capillary,  $\gamma$  = surface tension (N/m), and  $\theta$  = wetting (contact) angle.

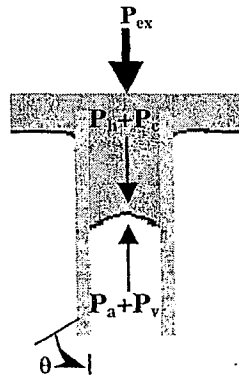


Figure 7. Schematic presentation of liquid penetration into a submerged porous body

The liquid flow ceases when pressure equilibrium takes place. At this stage, the further movement of liquid would be possible due to the dissolution of the entrapped air into the surrounding liquid and diffusion toward the surface. Assuming that the entrapped air is an ideal gas, the concentration of air as a function of coordinate and time can be found based on the second Fick's Law for diffusion and Henry's Law for gas solubility [Malkov *et al.* 2003]. Hudson and Shelton [1969] found that an initial application of pressure followed by cutting discs from the butt increases dramatically the flow rate of water-borne preservatives into green southern pine poles.

#### 2.4.4.2 Impregnation Model

Kazi *et al.*[1998] developed a model for impregnation of green softwood and hardwood with NaOH solution. The following assumptions were made:

- Chemical impregnation follows diffusional laws that can be modeled based on Fick's second Law of diffusion.

- For cylindrical samples, radial and tangential directional diffusion will be considered and diffusivities on these directions are independent of position.
- In addition, heat transfer and kinetics of chemical reaction are considered negligible.

Radial and axial directions were tested separately by isolating the respective surfaces. By uncoupling the second Fick's law in cylindrical coordinates, the radial concentration profile was given by:

$$\frac{\partial C}{\partial t} = D_r \left[ \frac{1}{r} \frac{\partial}{\partial r} \left( r \frac{\partial C}{\partial r} \right) \right] \quad (5)$$

where  $D_r$  = diffusion constant in radial direction,  $C$  = concentration at position  $r$ , and  $r$  = radial direction.

The initial and boundary conditions were:

I.C.:  $C=0$  at  $0 \leq r \leq a$  at  $t = 0$

B.C.:  $C=C_0$  at  $r = a$  at  $t > 0$

B.C.:  $\frac{\partial C}{\partial r} = 0$  at  $r = 0$  at  $t > 0$

where  $C_0$  = chemical concentration at the edge,  $a$  = radius of the cylindrical sample, and  $r$  = any radius of the cylindrical sample.

The analytical solution of equation (5) satisfying the above initial and boundary conditions was given as:

$$\frac{C}{C_0} = 1 - 2 \sum_{n=1}^{\infty} \left[ \frac{J_0(r\beta_n/a)}{\beta_n J(\beta_n)} \exp - \frac{\beta_n^2 D_r t}{a^2} \right] \quad (6)$$

where  $\beta_n$  = roots of  $J_0(\beta_n) = 0$ ;  $n=1,2,3,4,\dots etc.$ , and  $J$  = Bessel's function

The axial concentration profile was given by:

$$\frac{\partial C}{\partial t} = D_z \left[ \frac{\partial^2 C}{\partial z^2} \right] \quad (7)$$

where  $D_z$  = diffusion in axial direction,  $C$  = concentration at position  $z$ , and  $z$  = axial direction.

The initial and boundary conditions were:

I.C.:  $C=0$  at  $z > 0$  at  $t = 0$

B.C.:  $C=C_0$  at  $z = 0$  at  $t > 0$

B.C.:  $C=0$  at  $z = \infty$  at  $t > 0$

where  $C_0$  = chemical concentration at the edge.

The analytical solution of equation 7, for infinite length sample, with above initial and boundary conditions is given by [Crank, 1970]:

$$\frac{C}{C_0} = 1 - \operatorname{erf} \frac{z}{2\sqrt{D_z t}} \quad (8)$$

Figure 8 shows the concentration profiles that were obtained by experimental results (X-ray) and the impregnation model for radial and axial directions. Even though there was some scattering due to non-smoothness of sample surfaces, in general a good agreement was found between model and experimental data in all cases studied in this work.

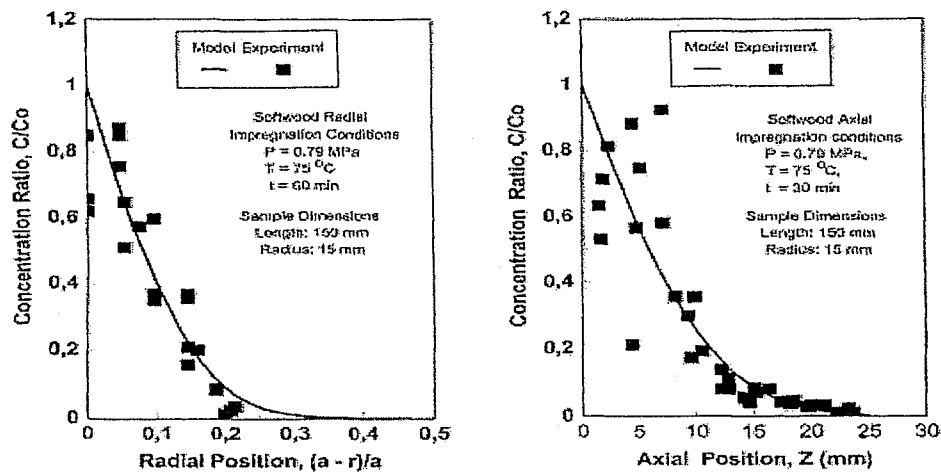


Figure 8. Concentration profiles (radial and axial) following softwood impregnation with NaOH [Kazi *et al.* 1998].

## 2.5 Raman Phenomena

Raman and Krishnan first discovered the Raman effect experimentally in 1928 in the course of researches on molecular light scattering. In a publication in *Nature*, Raman showed that “the spectrum of the new radiation... consists mainly of a narrow range of wavelengths clearly separated from the incident spectrum by a dark space” [Lewis and Edwards. 2001].

When monochromatic light of energy  $h\nu_0$  encounters a sample, light may be scattered in different directions. If the collision with a molecule is perfectly elastic, the scattered photon will have exactly the same energy as the incident photon (Rayleigh scattering). However the collision may be inelastic and the molecule will undergo a quantum transition to a “virtual” higher energy state with the result that the scattered photon loses energy. The transition is instantaneous, with no transfer of population into the virtual

state. This scattering process with shifted frequency gives rise to Stokes lines in a Raman spectrum where shifts are equivalent to the energy changes involved in transitions of scattered species. If the molecule is already in an energy level above the lowest one, the scattered photon may gain energy, leading to anti-Stokes lines. The Stokes lines are “mirrored” by an identical pattern of the anti-Stokes lines, but the intensities are greater in the Stokes side because at temperature equilibrium the number of molecules in a high state of energy is quite small compared to the number in the ground level. By convention Stokes Raman shifts, which are usually recorded as the Raman spectrum, are assigned a positive number even though they are a negative frequency shift. As it can be inferred, a Raman spectrum consists of scattered intensity plotted vs. energy, where each peak corresponds to a given Raman shift from the incident light energy  $h\nu_0$  [McCreery, 2000]. In practice the positions of Raman bands cannot be expressed in units of wavelengths because the bands are measured as shifts from the exciting wavelength. Raman bands are preferentially expressed in units of wavenumbers ( $\text{cm}^{-1}$ ), which are directly proportional to the energy.

Raman scattering is formally reminiscent of fluorescence. In fact, they are radically different with regard to mechanisms. In fluorescence the incident photon is totally absorbed by the molecule that is raised to an excited electronic state. After a certain life time (up to  $10^{-6}$  seconds) the molecule undergoes de-excitation and reradiates light with lower energy. Instead, during Raman effect the photon is never absorbed as a whole, but rather perturbs the molecule and induces it to a vibrational or rotational transition [Szymanski, 1967].

Fluorescence is a highly competitive effect with Raman. Sometimes fluorescence from the analyte or impurities in the sample is much stronger than Raman scattering, resulting in a large background. Fortunately, fluorescence emission can be quenched. By adding a reactive species (quencher) that is able to take away the energy of the excited molecules by collision, fewer molecules are able to fluoresce and consequently the intensity of emission is reduced by an amount proportional to the concentration of quencher [Gillbert and Baggott, 1991].

### 2.5.1 Polarizability and Selection Rules

In the case of inelastic collision the oscillating electric field  $\mathbf{E}$  (vector) of the incident light induces a polarization  $\mathbf{P}$  in the molecule's electron cloud (fig.9, pg.35). This induced dipole radiates scattered light via exchanging energy with rotations or vibrations in the molecule. Polarization  $\mathbf{P}$  (vector) scales with the polarizability,  $\alpha$ , and the incident electric field,  $\mathbf{E}$  [McCreery, 2000]:

$$\mathbf{P} = \alpha \mathbf{E} \quad (9)$$

Polarizability is the property of the sample that determines the degree of scattering. It is a tensor (anisotropic) that measures the degree to which the electrons in the molecule can be displaced relative to the nuclei when electromagnetic radiation (*i.e.* in visible region) falls into the molecule [Hollas, 2000]

A useful classical derivation from equation 9 is the following relationship for vibrational Raman scattering [McCreery, 2000]:

$$P = \underbrace{\alpha_{\text{equil.}} E \cos 2\pi\nu_0 t}_{\text{Rayleigh}} + \underbrace{\frac{1}{2} \left( \frac{\partial \alpha}{\partial Q} \right)_{\text{equil.}} [EQ (\cos 2\pi(\nu_0 \pm \nu) t)]}_{\text{Stokes and anti-Stokes}} \quad (10)$$

where the term  $Q$  refers the normal modes of vibrations ( $3N-6$  for non-linear polyatomic molecules with  $N$  atoms). In equation 10, the first term represents Rayleigh scattering, the second term Stokes ( $\nu_0-\nu$ ) Raman scattering and anti-Stokes ( $\nu_0+\nu$ ) Raman scattering. Two important implications arise from equation 10: first, only vibrations that change polarizability and consequently  $\left(\frac{\partial\alpha}{\partial Q}\right)_{equil.} \neq 0$  yield Raman scattering and second,

polarization and scattering intensities are linear with the laser intensity.

In polyatomic molecules each of the normal vibrations that are "allowed" by the harmonic oscillator selection rule is given by:

$$\Delta\nu_i = \pm 1, \pm 2, \pm 3, \dots$$

This means that only a limited number of Raman lines are observed, where  $\Delta\nu_i = \pm 1$  are the strongest (*fundamentals*) and  $\Delta\nu_i = \pm 2, \pm 3$ , account for *overtone and combination* transitions, which usually are very weak.

Polarizability changes upon vibration and selection rules for vibrational transitions represent further selection rules that involve symmetry properties of molecules. Although, the discussion of symmetry properties of vibrational coordinates goes beyond the scope of this review, it is worth mentioning something regarding the selection rules. In a quantum-mechanical consideration, the intensity of Raman scattering associated with a transition between two energy levels  $n \rightarrow m$  depends on the transition moment integral [Szymanski, 1967]:

$$\int \psi_m^* \alpha \psi_n dQ \quad (11)$$

where  $\psi_m^*$  and  $\psi$  are the time-independent wave functions of the energy levels and the integral is extended over the whole range of coordinates. The above integral will vanish

unless  $\psi_m^*$  and  $\alpha$  both belong to the same *symmetry species*. Hence a vibration is Raman active only if at least one component of polarizability is of the same symmetry species as the vibration itself.

### 2.5.2 Rotational Raman effect

In general, a vibrational transition is accompanied by rotational transitions, so the resulting Raman effect is vibration-rotation. If the molecule is isotropic, no pure rotational effect is possible. Raman is a “two photon process” where for each photon there is a change of rotation quantum number,  $\Delta J = \pm 1$ , thus for 2-photons  $\Delta J = \pm 2$ . Classically this selection rule can be explained by considering a polarizability ellipsoid that rotates with the molecule. Measured in a space-fixed rather than a molecule-fixed direction, polarizability changes at twice the frequency of rotation since the configuration of the ellipsoid is repeated every  $\pi$  radians. Practically pure rotational Raman spectra are observed in molecules with no permanent dipole and only for gaseous samples and molecules of low moment of inertia, the rotational structure may be resolvable [Szymanski, 1967].

### 2.5.3 Quantitative Analysis

The intensity of Raman scattered light from a sample,  $I_{\text{Raman}}$ , is proportional to:

$$I_{\text{Raman}} \propto I_{\text{Laser}} N (\nu_{\text{laser}} - \nu_{\text{vibration}})^4 \quad (12)$$

where  $N$  is the number of scattering molecules and  $\nu$  is the frequency in Hertz [Pelletier 2004]. In the case of modern instruments, photons are counted instead of measuring watts, and the following relationship is derived [McCreery, 2000]:

$$P_{Raman} = P_{laser} \sigma_j^0 \bar{\nu}_{laser} (\bar{\nu}_{laser} - \bar{\nu}_{vib})^3 D dz \quad (13)$$

where  $P$  has units of photons/second,  $D$  is the number density of scatters with units of molecules/cm<sup>3</sup>,  $dz$  is the pathlength of the laser in the sample,  $\sigma_j^0$  is a frequency independent Raman scattering cross section (cm<sup>6</sup>/molecule), and  $\bar{\nu}$  is expressed in wavenumbers (cm<sup>-1</sup>). Frequency independent cross-section can be defined as:

$$\sigma_j^0 = \frac{\sigma_j}{(\bar{\nu}_{laser} - \bar{\nu}_{vib})^4} \quad (14)$$

where  $\sigma_j$  (cm<sup>2</sup>/molecule) is the integrated cross-section for Raman scattering in all directions. For a particular Raman band, cross-section is a parameter that is proportional to the probability of an incident photon being scattered as a Raman shifted photon at that Raman band [McCreery, 2000].

Expressions (12) and (13) indicate that Raman scattered intensity is proportional to the number of molecules in the sample volume probed by the instrument. This proportionality is the basis for most Raman quantitative applications. The principle of quantitative Raman analysis relies on the fact that the Raman spectrum of a sample is equal to the weighted sum of the Raman spectra of the components that make up the sample. The weights are determined by cross-sections and are proportional to the quantities of the components. The above principle is called "linear superposition" and works because Raman cross-sections are very small and there is practically no optical coherence between components in the sample. In fact, production of a single Raman photon may require 10<sup>8</sup> excitation photons and the probability that a scattered photon being influenced because of another scattering interaction is basically zero. However,

optical absorption of one or more components may plague the Raman signal by attenuating the excitation or scattered intensity [Pelletier, 2004].

### **2.5.3.1 Area Normalization**

The most important factors influencing intensities measured by Raman microscopy other than analyte concentration are fluctuation of laser power, optical path alignment, and surface topology. Internal standards are widely used in quantitative Raman analysis to provide correction for changes in sample properties and instrumental performance. An internal standard method is efficient when during a studied process there is no change in standard peak intensity. Internal standards are not necessarily limited to one single Raman peak; the integrated area of several peaks or even the entire Raman spectrum can be used as an internal standard [Hilborn *et al.* 2000]. Normalizing the intensity to an internal standard emphasizes two of the advantages for using Raman spectroscopy: non-invasive analysis and no need for sample preparation [Pelletier, 2004].

### **2.5.4 Raman Microscopy**

The hardware of a Raman system may be divided into four basic components: a laser, an optical sampling system, a wavelength separator, and a detector. The optical sampling system illuminates the sample with laser and collects the Raman scattering for input to the spectrometer [Lewis and Edwards. 2001]. In Raman applications, the 180° sampling geometry (fig.9), which inserts the laser beam collinearly with the collection axis, provides a means to couple a Raman spectrometer with an optical microscope.

Acquisition of a spectrum from a single point (*microspectroscopy*) is the simplest application of Raman Microscopy. Collection of spectra from several points (*mapping*) on the sample is another feature of Raman microscopy. Monitoring simultaneously more than one point in the sample (*imaging*) in order to have spatial resolution of a particular component in the sample and the possibility of depth profiling make the Raman microscopy a powerful technique for chemical analysis.

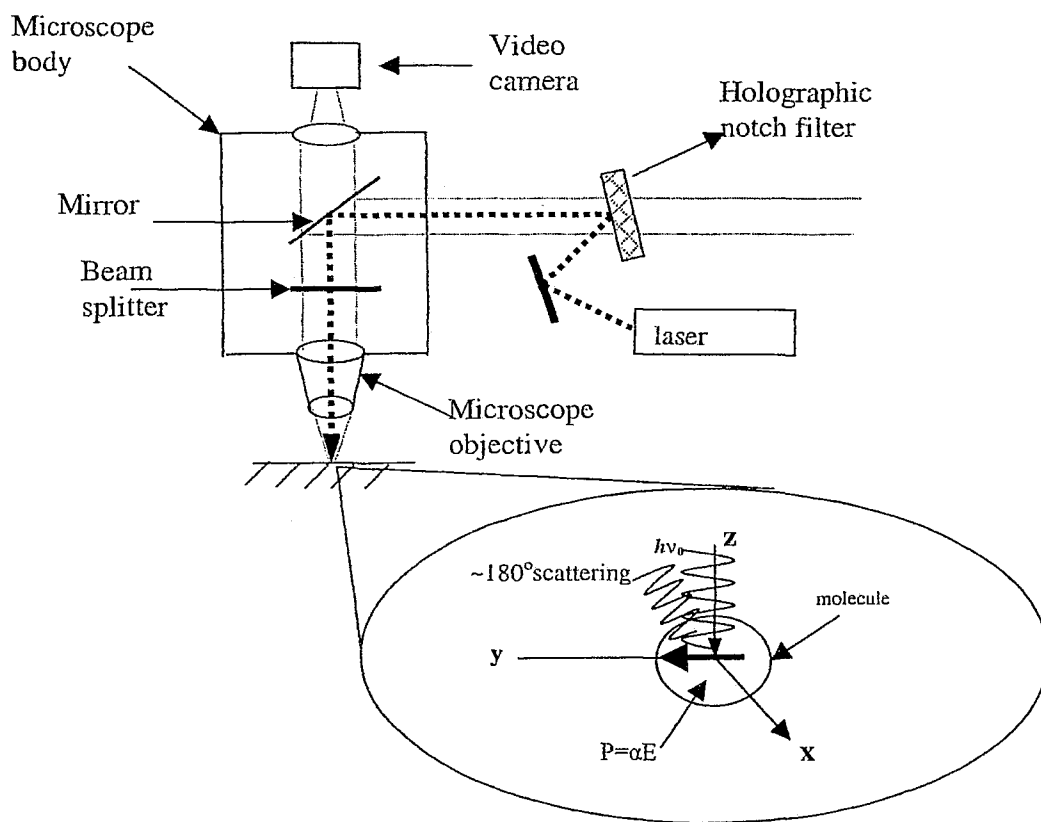


Figure 9. Schematic of a Raman Microscope and Polarization Induced in a Molecule's Electron Cloud by an Incident Electric Field ( $h\nu_0$ ). Only scattering in  $180^\circ$  is shown.

## 2.6 Application of Raman Spectroscopy in Wood Analysis

Raman spectroscopy has been used to study wood and its components in several studies. Raman spectra from wood are expected to have contributions from major compounds of wood such as cellulose, hemicellulose, lignin and extractives. For interpreting Raman spectrum of a complicated matrix like wood, not only the contribution of each component needs to be identified, but also the vibrational contributions from component-specific structural units and functional groups need to be assigned.

### 2.6.1 Spruce Spectra

Agarwal and Ralph [1997] approached the assignment of Raman spectral features of black spruce (*Picea mariana*) to its chemical components by using FT (Fourier Transform)-Raman spectroscopy. Most of the spruce Raman features were assigned to cellulose and lignin, where sharp and intense bands characterized cellulose since it is a highly ordered crystalline polymer. Overlapping of cellulose and lignin bands was found in very few positions of spruce spectra. Contribution from hemicellulose, which is a carbohydrate polymer with similar chemical bonds as cellulose, appeared to be broad and hidden under cellulose bands.

Table 1 reproduces the assignment of Raman bands over the 600-1600  $\text{cm}^{-1}$  range in the spectrum of black spruce as interpreted in the above study. Vibrational assignment for softwood-cellulose was done in terms of coupled vibrational modes, which together with softwood lignin vibrational contributions are listed in Table 2 [Agarwal *et al.* 1997].

Table 1. Raman Bands in the Spectrum of Black Spruce [Agarwal and Ralph. 1997].

| Shift (cm <sup>-1</sup> ) | Assignment   |
|---------------------------|--|
| 634 vw                    | Lignin   |
| 731 w                     | Lignin   |
| 787 w                     | Lignin   |
| 899 m                     | Cellulose  |
| 922 sh                    | Lignin   |
| 971 vw                    | Cellulose  |
| 1000 vw                   | Cellulose  |
| 1037 sh                   | Cellulose  |
| 1063 sh                   | Cellulose  |
| 1073 sh                   | Cellulose  |
| 1095 s                    | Cellulose, xylan <sup>a</sup> , glucomannan <sup>a</sup>   |
| 1123 s                    | Cellulose, , xylan <sup>a</sup> , glucomannan <sup>a</sup> |
| 1149 sh                   | Cellulose  |
| 1191 w                    | Lignin   |
| 1271 m                    | Lignin   |
| 1298 sh                   | Cellulose  |
| 1338 m                    | Cellulose  |
| 1377 m                    | Cellulose  |
| 1425 sh                   | Lignin   |
| 1456 m                    | Cellulose  |
| 1508 vw                   | Lignin   |
| 1602 vs                   | Lignin   |
| 1620 sh                   | Lignin   |

Note: vs-very strong, s-strong, sh-shoulder, m-medium, w-weak, vw-very weak. Band intensities are relative to other peaks in the spectrum.

<sup>a</sup> Only a very small contribution is expected.

Table 2. Band Assignment for Cellulose and Lignin in Black Spruce Spectrum. [Agarwal *et al.* 1997; *ibid.* 1999].

| Shift (cm <sup>-1</sup> ) | Assignment  |
|---------------------------|---|
| 634 vw                    | Skeletal deformation of aromatic rings, substituent groups and side chains.         |
| 731 w                     | Skeletal deformation of aromatic rings, substituent groups and side chains.         |
| 787 w                     | Skeletal deformation of aromatic rings, substituent groups and side chains.         |
| 899 m                     | HCC and HCO bending at C <sub>6</sub>   |
| 926 vw                    | CCH wag   |
| 971 vw                    | Heavy atom (CC and CO) stretching   |
| 1000 vw                   | Heavy atom (CC and CO) stretching   |
| 1037 sh                   | Heavy atom (CC and CO) stretching   |
| 1063 sh                   | Heavy atom (CC and CO) stretching   |
| 1073 sh                   | Heavy atom (CC and CO) stretching   |
| 1095 s                    | Heavy atom (CC and CO) stretching   |
| 1123 s                    | Heavy atom (CC and CO) stretching   |
| 1149 sh                   | Heavy atom (CC and CO) stretching + HCC and HCO bending                             |
| 1191 w                    | A phenol mode   |
| 1271 m                    | Aryl-O of aryl-OH and aryl-O-CH <sub>3</sub> ; guaiacyl ring (with C=O group) mode. |
| 1298 sh                   | HCC and HCO bending   |
| 1338 m                    | HCC and HCO bending   |
| 1377 m                    | HCC, HCO and HOC bending  |
| 1428 w                    | O-CH <sub>3</sub> deformation; scissoring; guaiacyl ring vibration                  |
| 1456 m                    | HCH and HOC bending   |
| 1508 vw                   | Aryl ring stretching, asymmetric  |
| 1601 vs                   | Aryl ring stretching, symmetric   |
| 1620 sh                   | Ring conjugated C=C stretch of coniferaldehyde                                      |

Note: vs-very strong, s-strong, sh-shoulder, m-medium, w-weak, vw-very weak.

## 2.6.2 Pine Spectra and Distinguishing Features of Hardwoods

Raman studies for characterization of the chemical structure of pine wood have also been reported [Shen *et al.*1998]. In pine, the spectral region between 2500 to 3500  $\text{cm}^{-1}$  appeared to have contributions from cellulose, hemicellulose and extractives. In the FT-Raman spectrum of pine (fig.10), a strong peak at  $\sim 2893 \text{ cm}^{-1}$  assigned to cellulose and hemicellulose was associated with a shoulder at  $\sim 2936 \text{ cm}^{-1}$  that was related to the presence of extractives and hemicellulose. This conclusion was contrary to the reported findings of Agarwal and Ralph [1997] that had assigned this peak to lignin.

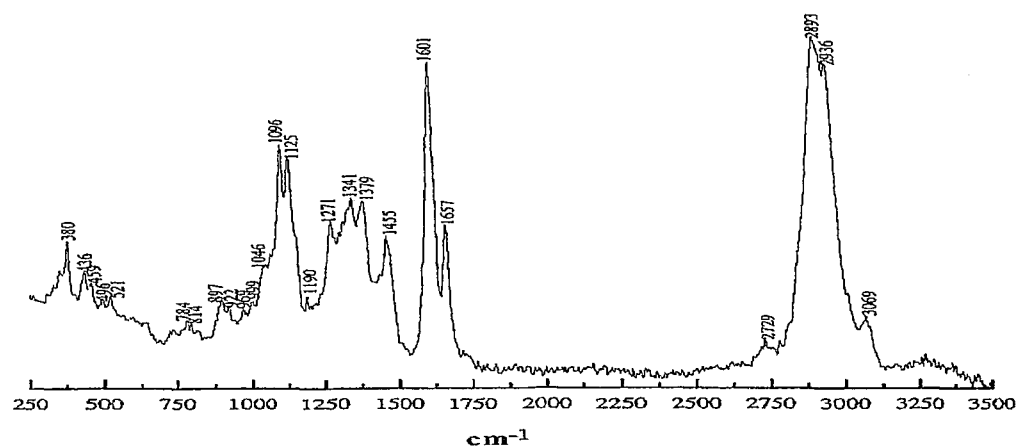


Figure 10. FT-Raman Spectra of Untreated Pine Wood. [Shen *et al.*1998].

In Raman spectra of pine, lignin was associated with a very intense peak and a shoulder located at  $\sim 1601 \text{ cm}^{-1}$  and  $\sim 1657 \text{ cm}^{-1}$  wavenumbers. In the 1000-1500  $\text{cm}^{-1}$  region overlapping peaks from cellulose, hemicellulose, lignin, and resins were observed. The intense peak and the shoulder located at  $\sim 1096/\sim 1125 \text{ cm}^{-1}$ , in agreement with previous studies [Agarwal and Ralph. 1997], were assigned to cellulose and hemicellulose due to the skeletal vibration also involving the CO stretching [Shen *et al.* 1998]. Special

attention was paid to the peaks at  $\sim 1271$  and  $\sim 1455$   $\text{cm}^{-1}$  since they appear almost invisible in the reference spectra of cellulose, hemicellulose, lignin, and wood resins. It was suggested that these peaks are due to lignin-carbohydrate complexes, which are very probable to occur in woody plants [Shen and Rosenholm. 1998].

The peak and the shoulder (fig.10) located at  $\sim 1341/\sim 1379$   $\text{cm}^{-1}$ . were related to the presence of cellulose and hemicelluloses, whereas in the high-energy end of Raman spectra ( $250\text{-}1000$   $\text{cm}^{-1}$ ) cellulose, hemicellulose and extractive contributions were detected [Shen *et al.* 1998]. Skeletal deformation of aromatic rings, substituent groups and side chains constitute the main motions over this region [Agarwal *et al.* 1997]. In species like *Artocarpus heterophyllus* (hardwood) that have heartwood rich in flavones and related compounds, a characteristic band from these compounds appears at  $1247$   $\text{cm}^{-1}$  [Yamauchi *et al.* 2003].

Shen *et al.* [1998] reported that in birch wood spectra, two peaks  $2893$  and  $2936$   $\text{cm}^{-1}$  are shifted at  $2907$  and  $2939$   $\text{cm}^{-1}$  and their ratio seems to be inverse to that of the pine wood. It was predicted that the ratio of these peaks could be used as a distinguishing feature between “soft” and “hard” woods. A shoulder at  $1740$   $\text{cm}^{-1}$  and the peak at  $1270$   $\text{cm}^{-1}$  (fig.10) can also be used as characteristic bands to distinguish between hardwoods and softwoods [Lavine *et al.* 2001; Griffiths *et al.* 1999]. The classification of wood categories based on the relative intensities of bands at  $1740$  and  $1270$   $\text{cm}^{-1}$  sometimes can lead to incorrect classification. Automated classification based on neural networks or genetic algorithms can be employed for differentiation of Raman spectra of hardwood from softwood with minimal incorrect classifications [Griffiths *et al.* 1999; *ibid.* 2001]

### 2.6.3 Lignin

Vibrations (C=C) of Guaiacyl (G) and Syringyl (S) skeletons have also been assigned to their individual Raman bands. Wariishi *et al.* [1997], investigated the region 1580 to 1620  $\text{cm}^{-1}$  wavenumbers, based on synthetic guaiacyl and syringyl spectral differences and peak component analysis. It was revealed that this spectral region had contributions from syringyl and guaiacyl in hardwood samples but only contribution from guaiacyl in softwood samples. A rapid alternative method to conventional chemical methods for determination of syringyl to guaiacyl ratio (S/G) was attempted in Wariishi's study. The S/G ratio has a huge influence on the rate of delignification and the quality of products in pulping processes. A good agreement between methods was found by investigating the relationship of peak area intensity of S/G ratio from NIR-FT Raman spectra and S/G ratio calculated from nitrobenzene oxidation.

Wariishi *et al.* [2002] showed that the lignin band at 1620  $\text{cm}^{-1}$  disappeared upon the reduction of carbonyl groups, whereas the band at 1660  $\text{cm}^{-1}$  (lignin) did not change its intensity. This fact and other spectral changes upon oxidation and hydrogenation suggested that 1620  $\text{cm}^{-1}$  and 1660  $\text{cm}^{-1}$  bands could be assigned to carbonyl groups and  $\alpha$ ,  $\beta$  unsaturated bonds, respectively.

Bond and Atalla [1999] observed the disappearance of lignin bands (1595  $\text{cm}^{-1}$ , 1620  $\text{cm}^{-1}$ , 1654  $\text{cm}^{-1}$ ) by exposure to 514.5 nm laser radiation (30 mW after plasma rejection) for 13 hours. While the cellulose band at 1098  $\text{cm}^{-1}$  remained unchanged (fig.11), the lignin band disappearance was related to the absorption of 514.5 nm photons by lignin molecules. The absorption initiated a complex series of photochemical, degradative reactions where the lignin macromolecules appeared to become disrupted. In addition,

Bond and Atalla [1999] found evidence of solubilized and degradation products including quinonoid structures.

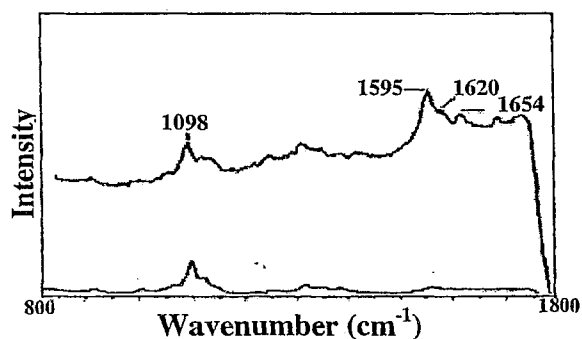


Figure 11. Raman Spectra Collected from a Single Location in the Latewood, Secondary Wall of Black Spruce. [Bond and Attalla, 1999]

Oldham *et al.* [1997] investigated the lignin content in wood pulp (pine) utilizing a Raman technique. By normalizing the area of the  $1600\text{ cm}^{-1}$  band to the cellulose band structure between  $1200$  and  $1010\text{ cm}^{-1}$ , the technique was compared with the traditional standard method (Kappa number, a chemical titration method that measures the degree of delignification) for determination of lignin. Pulp samples of moderate lignin content indicated a comparable accuracy and precision between the standard and Raman methods where the latter one has the advantages of being non-destructive, fast, and direct. These advantages and other qualities such as ease of analysis with heterogeneous materials and ease of analysing structural features of samples have been utilised to determine the proportion of cell types in native wood by Raman spectroscopy. Quantitative microscopy that is usually employed to determine the proportion of wood cells including fibers, vessels, ray and axial parenchyma, is a prolonged multistep procedure and requires time-consuming sample preparation. Ona *et al.* [1999] successfully obtained significant

correlations between conventionally measured and Raman predicted values for cell types in native wood. Applying the second derivative transformation of Raman spectroscopic data and the partial least-squares regression, the proportion of cell types for *Eucalyptus* native wood was determined regardless of age and colour.

Resonance and conjugation are two effects that make Raman spectroscopy capable of detecting a particular group or a structure at very low concentrations. The resonance Raman (RR) effect occurs when the incident laser wavelength is in resonance with an excited electronic state [Lewis and Edwards. 2001]. It is also known that the scattered intensity of certain vibrations is affected by the degree of  $\pi$ -electron conjugation between aromatic ring and substituent. Strong enhancement in scattering intensity is observed when one of these effects is present [Agarwal, 1999].

Agarwal and Atalla [2000] studied the dependence of Raman scattering on conjugated and non-conjugated lignin substructure models. Some of these models, such as stilbene and coniferaldehyde can be classified as chromophores and Raman spectroscopy is ideally suited for *in situ* studies of chromophore and non-chromophore lignin models. In general, chromophores contribute most strongly over the 1500-1700  $\text{cm}^{-1}$  region, which is free of lignocellulosic contributions, except for the strong 1600  $\text{cm}^{-1}$  lignin band. The authors determined that the intensity in lignin model compounds where both the phenyl and C=C or C=O group modes were present was enhanced due to a conjugation effect. Moreover, the variation of intensity for C=C or C=O vibrations was used for characterizing lignin models. It was shown that chromophores like stilbene

carboxaldehyde, stilbene methanol, and syringyl stilbene had the highest detection sensitivity in Raman, while non-conjugated models had the lowest one.

Although the structures and quantities of milled wood lignin (MWLs) are similar for softwoods, Agarwal and coworkers [McSweeney and Ralph, 1999] observed a significant decrease in intensity of the  $1600\text{ cm}^{-1}$  band when comparing loblolly pine MWL with spruce MWL. By investigating the influence of ring-conjugation to the intensity of the benzene ring mode at  $1600\text{ cm}^{-1}$ , it was explained that differences in concentration of conjugated structures are the reason for the lower intensity of the loblolly pine MWL.

#### 2.6.4 Mapping of Wood Compounds and Chemical Treatments

Bond and Atalla [1999] used the Raman bands at  $1098\text{ cm}^{-1}$  and  $1595\text{ cm}^{-1}$  for exploring cellulose and lignin molecules in the cell wall. Mapping of cellulose content in the cell walls confirmed that a maximum concentration occurs in the secondary wall ( $S_2$ ) layer, whereas declination to a minimum is observed near middle lamellae. By varying the plane of polarization of the incident light, it was concluded that on average the parallel intensity values of cellulose at  $1098\text{ cm}^{-1}$  were greater than perpendicular ones for all secondary wall locations. This was in agreement with the generally accepted fact that cellulose chain axes are preferentially oriented in planes parallel to the cell wall. In addition, the trend found for aromatic phenylpropane units in the  $S_2$  region showed that lignin concentration exhibits a minimum in the outer  $S_2$  and then increases in the middle lamellae region.

Bergström *et al.* [1999] studied the seasonal variation of pinosylvin concentration at the sapwood/heartwood boundary of Scots pine by Raman spectroscopy. Formation of

pinosylvin is considered as an event related to the transformation of sapwood to heartwood. Normalization to an internal standard of  $2891\text{ cm}^{-1}$  wavenumber was applied in order to obtain relative intensities for pinosylvin at the  $1636\text{ cm}^{-1}$  band (C=C stretching). Most of the trees sampled in this study showed a sharp increase in pinosylvin concentration at the sapwood/heartwood boundary, but the positions where maximum levels were detected varied considerably between trees. In another experiment, the pinosylvin level of individual trees was examined during one growing season. It was concluded that there is not any seasonal trend in the distribution pattern of pinosylvin concentration.

Yamauchi and Doi [2003] revealed that  $\text{B}(\text{OH})_3$  is the dominant boron species in Japanese cedar wood treated with boric acid solution. Boric acid is an effective water-borne fungicide and insecticide. The Raman spectrum of boric acid in the solid state was characterized by a symmetrical  $\text{BO}_3$  stretching vibration that appears at  $879\text{ cm}^{-1}$  ( $\nu_1$ ) and two other weaker lines at  $497$  and  $1167\text{ cm}^{-1}$ . The  $\nu_1$  band appeared slightly shifted in aqueous solutions ( $875\text{ cm}^{-1}$ ) where other features from Raman spectra of solid state could not be detectable [Servos and Clark. 1957; Yamauchi and Doi. 2003].

Yamauchi and Doi [2003] found that the relationship between normalized intensity  $\nu_1$  and increasing concentration of boric acid solution (fig.12) was far less linear compared to the relation between the weight gain of the treated wood and increasing concentration. Two possible explanations were provided by these workers: One accounted for the complex formation of boron with polyols that could entirely change the vibrational modes of B-O bonds and their Raman intensities may appear very weak. The other one was related to the precipitation of boric acid in form of microcrystals in the vicinity of the transverse

faces during air-drying. The  $\nu_1$  intensity obtained from microcrystals would be much stronger than that from the cell wall because of a greater number of  $B(OH)_3$  units per unit

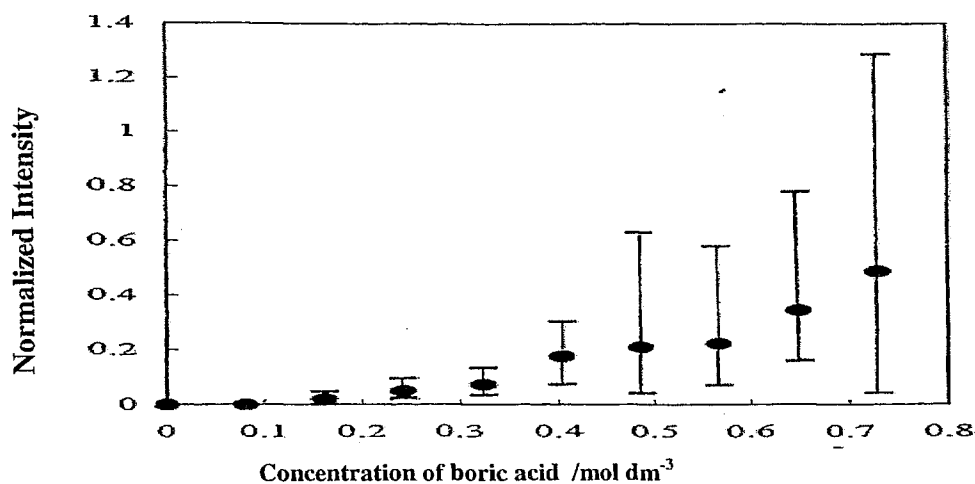


Figure 12. Changes in Intensity of  $\nu_1$  Band Intensity Obtained by Raman Measurements of Transverse Faces. The bars indicate the maximum to minimum range for measurements at a given concentration [Yamauchi and Doi, 2003].

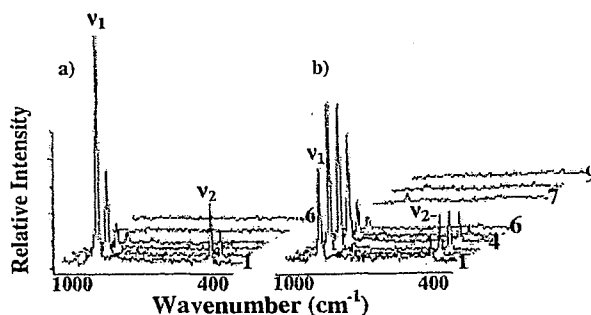


Figure 13. Line Maps of Various Raman Spectra in the Longitudinal Direction. a) Sap wood. b) Heart wood. The components due to wood constituents were subtracted from all spectra. Numbers 1..6..9 refer to distance from the grain, where each number corresponding to a difference of 0.5 mm. [Yamauchi and Doi, 2003].

In addition, Yamauchi and Doi [2003] investigated the distribution of boron species in the longitudinal direction in Japanese cedar samples. Raman line maps in the longitudinal direction showed a tendency of  $B(OH)_3$  microcrystals to accumulate near cut ends in long axial wood blocks. As figure 13 illustrates, the  $\nu_1$  band was undetectable outside a limited range of depth from the cut end. Although further investigations were required, it was suggested that the drying process and the cell wall structure were possible factors conditioning the distribution of boric acid microcrystals.

## Chapter 3

### METHODOLOGY

#### 3.1 Species

Spruce (*Picea spp.*) is the most abundant wood species in Canada, with approximately 40% of the total softwood volume corresponding to 7146 millions m<sup>3</sup> (Arnup *et al.*1988). White spruce (*Picea glauca*) also known as Canadian Spruce is an evergreen conifer with a relatively uniform, conical crown that prefers moist and cool climates. Botanically, it ranges from Newfoundland to Alaska and southward to the United States in New England and the Lake States [Lakehead University, 2002]. The wood of white spruce is light, soft, and straight grained. Its primary uses have been for frames, pulpwood, lumber, furniture, and boxes. EverDry Forest Product Ltd. provided samples of white spruce used in this study.

#### 3.2 Sample Preparation and Extraction

Wood blocks were cut with a band saw from sections of dried spruce boards that were free of knots or checks. Dimensions were: 7.3 (Tangential) x 2.7 (Radial) x 3.1 (Longitudinal) cm for the A-block, 7.1 (Tangential) x 2.6 (Radial) x 2.7 (Longitudinal) cm for the B-block and 8.6 (Tangential) x 2.6 (Radial) x 1.6 (Longitudinal) cm for the C-block. Propiconazole solution (50 %) in mineral spirits was also supplied courtesy of EverDry Forest Products Ltd. Each wood block was soaked in 200 ml solution of propiconazole in mineral spirits (CAS# 8052-41-3) for 48 hours. The concentration of treating solutions for A, B, and C blocks were 4 %, 2 % and 1 %, respectively. The

vessels containing wood blocks in propiconazole solutions were sealed and kept in dark during the soaking time. After the elapsed time, samples were removed from solutions and drip-dried for 15 minutes. The samples were then placed upon the radial face on a watch glass and left to dry in fumehood at ambient temperature for 36 hours to remove all the mineral spirits (undetectable by GC-MS).

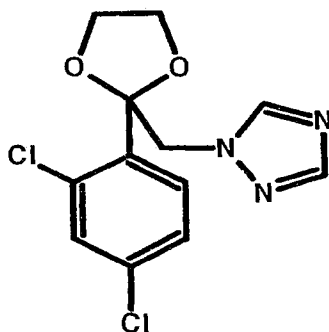
For Raman analysis a thin sliver (~ 3mm wide, tangential direction) with the long edge along the grains, was removed from the centre of the dried samples. A fine cut was obtained by using a knife since wood splits readily in longitudinal direction.

Samples for gas chromatography analysis were produced by milling layers of approximately 1.5 mm thick (longitudinal direction) from the remaining of the dried samples. The grinding was done in an Aciera F3 milling machine, where the last ~2 mm of the wood blocks could not be ground safely. These layers were also excluded from Raman analysis. Each milled layer was collected separately in a plastic bag and then was sifted with a 40-mesh sieve. The screened samples were weighed in an analytical balance and extracted using 25 mL of HPLC grade methanol for 4 hours in an Orbital Shaker (DS-500 VWR), at 200 rpm. Polar solvents like methanol are commonly used to extract pesticides from agricultural matrices since these solvents are miscible with water and penetrate the matrix effectively [AWPA, A24-94; Armstrong, 1999].

The extracts were vacuum filtered using a 0.45  $\mu\text{m}$  (PTFE) filter and quantitatively transferred to 25-mL volumetric flasks. The volume was made up to the mark with methanol and then 1.0 mL aliquots were transferred to GC vials. All GC vials were spiked with 50  $\mu\text{L}$  of the internal standard, azaconazole.

### 3.3 Internal standard

Azaconazole is also a triazole antifungal agent that has a similar structure to propiconazole [Zirngibl, 1998].



1-[[2-(2,4-dichlorophenyl)-1,3-dioxolan-2-yl]methyl]-1*H*-1,2,4-triazole

Figure 14. Azaconazole Structure

The azaconazole concentration was 1000 ppm, and was diluted with isooctane and isopropyl alcohol (90:10).

### 3.4 GC-MS Determination of Propiconazole

Analysis of extracts was performed on a Perkin Elmer Auto system XL GC interfaced to a Perkin Elmer TurboMass Mass Spectrometer and equipped with an autoinjector. The column used was a MDN-5S Supelco 35m x 0.25mm (i.d.) with a film thickness of 0.25  $\mu$ m. The stationary phase was a 95 % methyl and 5 % phenyl polysiloxane. Helium was used as the carrier gas under 300 kPa pressure and 2-mL/min flow. The injection volume was 1  $\mu$ L and the injector was set in the split mode (50:1). The injection port temperature was set at 250°C and the initial column temperature was 80°C, with 1.00 min hold time. The column was then ramped at 25°C/min to 350°C, where it was held for 7.00 min. The

temperature of the transfer line and MS Source were set at 250°C and 200°C, respectively.

Electron Impact (EI) was used as the ionization method, where the electron energy was set at 70 eV. Propiconazole enantiomer pairs co-elute [Armstrong, 1999]. From the total ion chromatograms (35-350 m/z) it was determined that two diastereoisomers, *cis* and *trans*, were fully resolved in a ratio of about 1:2. The retention times for the two isomers were 9.15 and 9.20 minutes, whereas for azaconazole the retention time was 8.69 minutes. Both propiconazole isomers produce identical mass spectra.

The mass spectrometer was operated in the Selected Ion Monitoring (SIM) mode. The selected ions were 69 m/z for propiconazole and 217 m/z for azaconazole. These ions were chosen since they represented the highest intensity among other ions in the propiconazole and azaconazole mass spectra [Katic, 2003]. Quantitative data were generated from background-free chromatograms (fig.15). In order to obtain the total propiconazole signal both peaks of *cis* and *trans* isomers were integrated.

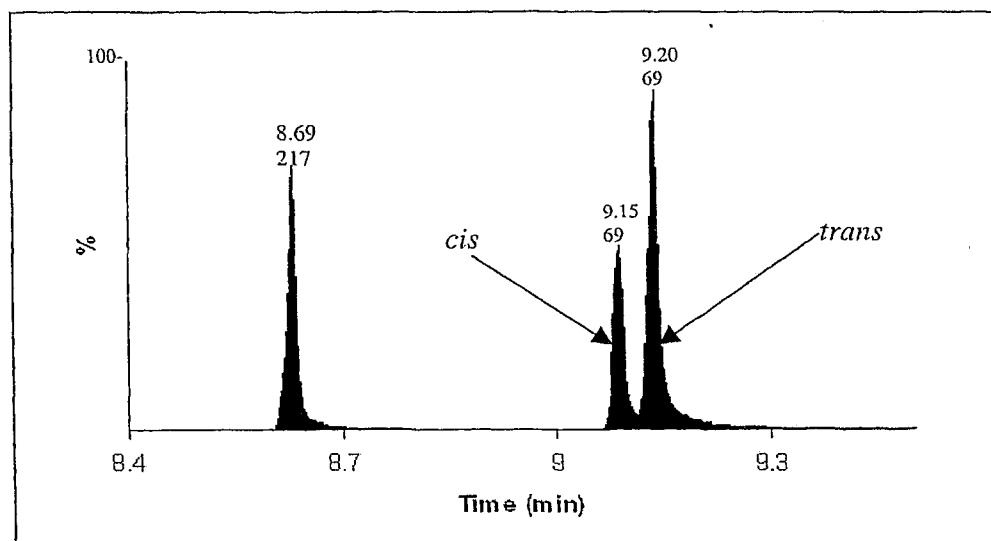


Figure 15. SIM Chromatogram

### 3.5 Raman Spectra

The Raman spectra were recorded using a Renishaw Raman Imaging Microscope, System 2000. In order to obtain a longitudinal depth profile, Raman spectra were measured on the radial face of the sliver that was removed prior to milling (fig.16). Within the area corresponding to a given milled layer, four different spectra were collected and their normalized intensities (see 4.1, pg 59) were averaged. Raman spectra were obtained only from points located in summerwood since it was found that summerwood contains more propiconazole per unit volume and produces spectra with higher SNR (signal to noise ratio) than springwood. Information about propiconazole distribution on late and early wood were obtained by recording, 1-D (dimensional) and 2-D mapping on different spots (radial face) of wood samples.

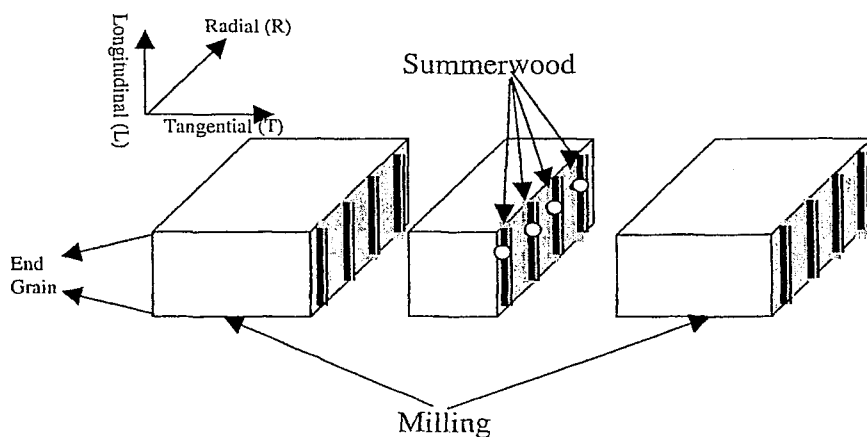


Figure 16. Raman Measurements Points on the Radial Face of Wood Blocks. Points (4) corresponding to the distance from end grain of a given milled layer.

Spectra were also recorded on the transversal face so that propiconazole deposits on wood surface made from solutions of different propiconazole concentration were compared.

### **3.6 Raman Instrument**

Renishaw System 2000 is a dispersive system that can acquire Raman spectra, Spectral Mapping and Global Images. Signal detection is achieved through the use of a Pelletier-cooled CCD (charge coupled device) array detector. Attached to the system unit, a microscope allowed laser light and/or the microscope illumination to fall on the sample. The microscope is equipped with a well-engineered stage that was capable of moving accurate x-y-z steps in a micron scale. In addition, a trinocular head that has a video camera and eyepieces is fitted to the microscope with the ability to select which one is to be employed.

#### **3.6.1 Overview of System Operation**

The following is a brief and simplified description of the grating light path in a System 2000 Raman instrument (fig.17). Laser light coming from a laser source enters the spectrometer via an alignment mirror and a laser attenuation filter wheel (not shown in the picture). Mirror B aligns the laser light through a fixed objective lens (C) and converges the beam into a 10  $\mu\text{m}$  pinhole that collimates laser light into a parallel beam by a second objective lens (D). The beam is reflected by two mirrors E and F onto the holographic notch filter (G) that reflects the beam out of the spectrometer and into the optical path of the microscope. In order to achieve a high spatial resolution, a high numerical aperture is required. A  $\times 50$  objective was used as a microprobe to focus and collect light in the  $180^\circ$  (backscattering) collection geometry. The additional advantage of collecting light in a large cone becomes a free pay off when (easy sampling and reproducible) backscattering scheme is used [Lewis and Edwards. 2001]. For this high-

NA, (Numerical Aperture=0.75) lens the lateral resolution was  $\sim 2 \mu\text{m}$  and the objective depth of field was  $\sim 5 \mu\text{m}$ .

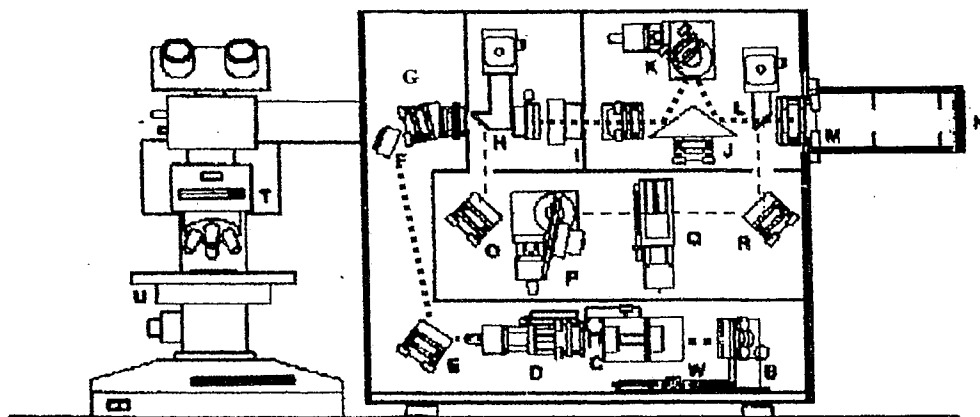


Figure 17. Schematic Diagram of Renishaw Raman System 2000. (---) Grating Light path, (---) Filter light path

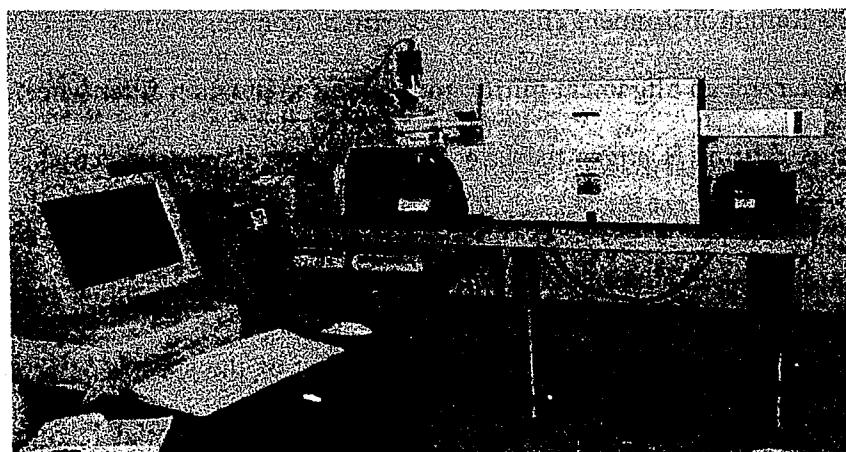


Figure 18. Renishaw Raman System 2000 at Ryerson University.

On the return path, the set of holographic (G) filters removes the Rayleigh component from the backscattered light, so that only the Raman light remains. The Raman light is

then passed through a lens and focused on to the slit assembly (I). This will prevent diverging components of Raman light reaching the CCD, therefore improving the accuracy and resolution of the grating spectrum. The Renishaw System 2000 can be operated in the confocal mode, so spectra is collected from well-defined regions of a sample. In the confocal mode, the slit is closed between 10 and 15 microns, with the depth of field  $\sim 5 \mu\text{m}$  for the  $\times 50$  objective. For this experiment, the slit opening was set at 50 microns, as it was necessary to collect signal from bigger volumes than the confocal ones.

After recollimation through another lens, the input side of the prism mirror (J) reflects Raman light onto a diffraction grating (K). The grating density of the diffraction grating was 1200 lines/mm. The diffraction grating assembly rotates and disperses the incident light that is then reflected off the output face of the mirror into focusing lens (M) and onto the detector (N). In the continuous scan option of extended data capture, the grating movements are in synchronization with the charge movement across the CCD array chip. A software-controlled shutter, (not shown in the picture) controls light exposure of the CCD camera that can collect a  $600 \text{ cm}^{-1}$  spectral window with  $2.5 \text{ cm}^{-1}$  spectral resolution. The limits between which fundamental molecular vibrations occur are from around  $50\text{-}4000 \text{ cm}^{-1}$ . For practical purposes,  $150\text{-}3600 \text{ cm}^{-1}$  usually suffices. In the produced spectra the Raman shift ( $\Delta\nu$ )( $\text{cm}^{-1}$ ) is automatically calculated as:

$$\Delta\nu (\text{cm}^{-1}) = \nu_{\text{Laser}} - \nu_{\text{Raman}} \quad (15)$$

The Renishaw System 2000 can also be used for Global Imaging via the Filter light path. When the laser beam is fully defocused, a  $\times 50$  objective could obtain Raman images from an area up to  $40 \mu\text{m}$  in diameter. In the filter light path, a wedge mirror (H) directs

the beam to the filter wheel assembly (P), which contains filters with approximately 20  $\text{cm}^{-1}$  bandpass and is angle-tuned to selectively pass the correct required Raman band. Raman light is then directed by the second beam diversion mirror (L) to the focusing lens (M) and detected by CCD camera.

### 3.6.2 Experiment Set-up

All spectra were collected at ambient temperature with the following experimental parameters:

|                          |                           |  |
|--------------------------|---------------------------|--|
| Light path               | Grating                   |  |
| Type of data             | Spectrum                  |  |
| Method of data capture   | Extended                  |  |
| Mode                     | Continuous                |  |
| Spectral Range           | 600-1200 $\text{cm}^{-1}$ |  |
| Detector Time            | 300 seconds               |  |
| Collection time/spectrum | ~10 minutes               |  |
| Cosmic Ray Elimination   | Off                       |  |
| Gain                     | High                      | 5 photogenerated electrons on the CCD correspond to a single count |
| Accumulation             | 1                         |  |
| Binning                  | 1                         |  |
| Power on the sample      | 100%                      |  |
| Laser beam               | Fully focused             |  |

### 3.6.3 Laser Source

Two lasers are suited to the Renishaw Raman Imaging Microscope, System 2000: an argon ion ( $\text{Ar}^+$ ) green (514.532 nm) laser and diode laser in the near-infra-red (785 nm) wavelength. It has been observed that when lignocellulosic materials are irradiated with 514.5 nm laser light, a strong emission of fluorescence is obtained [Agarwal, 1998]. Fluorescence intensity changes very slowly across the spectrum, so that the elevated baseline may be removed by software. Once the shot noise on the fluorescence background becomes large relative to the Raman signal the fluorescence can no longer be subtracted. A diode laser (785 nm) with output power of 30mW was the excitation source for this work since it was necessary to reduce fluorescence.

#### 3.6.3.1 Quenching Fluorescence

When light irradiates lignocellulosic materials, hemicellulose and cellulose absorb very little of the light energy, while lignin [Shen *et al.* 2000; Agarwal, 1998; Zhu and Gray. 1995] and extractives [Hillis, 1961] contribute to the most absorption. A number of Raman techniques have been developed to eliminate the fluorescence but none of them has been totally accepted [Oldham *et al.* 1997]. Preliminary studies of this work have involved application of different methods to quench the fluorescence emission from wood samples. In one attempt, wood samples were allowed to remain under irradiation by the laser beam for several hours. This method, which is known as drench quenching, works well with cellulosic samples with the laser beam apparently photodegradating

impurities on the sample [Agarwal, 1999]. Adding quencher molecules that contain heavy atoms (*e.g.* iodine-substituted organic compounds) was also tried as a quenching method. These compounds quench the fluorescence by enhancement of the intersystem crossing rate, increasing the yield of triplet excited molecules *via* a so called "spin-orbit" interaction [Gillbert and Baggott. 1991].

## Chapter 4

### RESULTS AND DISCUSSION

#### 4.1 Normalization Procedure

At the beginning of each experimental session Raman shift accuracy and instrumental response were ensured through calibration on a standard silicon wafer. Nonetheless, the Raman scattered signal is intrinsic to the material being analysed. In anisotropic materials like wood, which have extremely variable surface properties, the absolute Raman signals vary strongly with surface roughness. Quantitative analysis for such samples requires a normalization procedure.

Figure 19 illustrates the Raman spectra of spruce, spruce treated with propiconazole and pure propiconazole (99.7 %). The band area between 647 and 693  $\text{cm}^{-1}$  was chosen as the analytical region in this study. The intensity of this band was quite high and it was positioned on a region free of wood component features [Agarwal and Ralph. 1997]. The area between 985-1175  $\text{cm}^{-1}$  was used to normalize the analytical region. In the normalization band, cellulose and hemicellulose contribute with two strong peaks at 1095 and 1123  $\text{cm}^{-1}$  and a shoulder located at 1149  $\text{cm}^{-1}$ . Cellulose, which is the most abundant wood component, has the major contribution over this area. Typically, these cellulose peaks do not change throughout measurements therefore making them a good choice for internal standard. As figure 19 shows, the normalization region overlapped with some of the propiconazole peaks. Consequently, for the normalization procedure, this region was corrected by subtracting from it an estimate of the area due to propiconazole peaks.

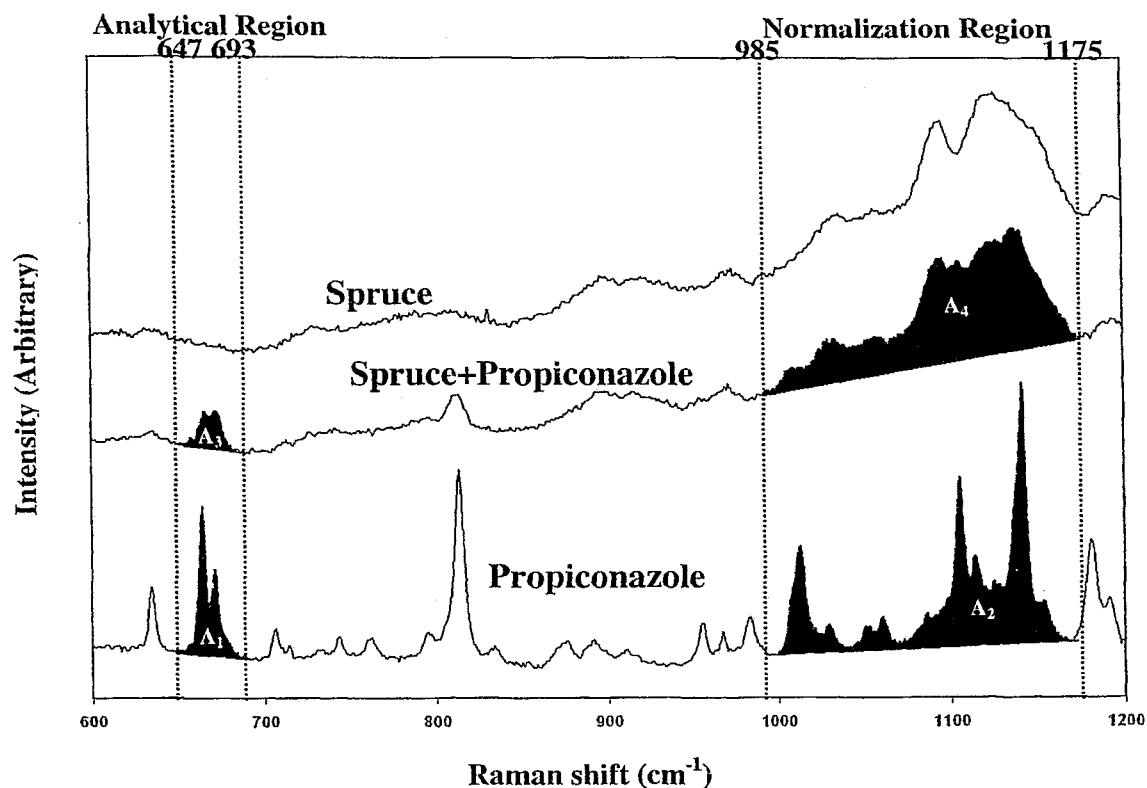


Figure 19. Raman Spectra of Spruce, Spruce treated with Propiconazole, and Standard Propiconazole (Janssen 99.7%).

The Normalized Raman Intensity was calculated as:

$$\text{Normalised Intensity} = \frac{A_3}{A_4 - \frac{A_2}{A_1} A_3} = \left( \frac{A_4}{A_3} - \frac{A_2}{A_1} \right)^{-1} \quad (16)$$

where:  $A_1$  – peak area for pure, standard propiconazole under the analytical region (647-693 cm<sup>-1</sup>);  $A_2$  – peak area for pure, standard propiconazole under the normalization region (985-1175 cm<sup>-1</sup>);  $A_3$  – peak area for propiconazole (647-693 cm<sup>-1</sup>) in treated spruce;  $A_4$  –

peak area for treated spruce (due to wood and propiconazole) under the normalization region (985-1175  $\text{cm}^{-1}$ ).

## 4.2 Fluorescence

Although fluorescence is not a scattering process, its signals appear in the same spectral range as Raman shifts. Fluorescence is highly undesirable in Raman studies of wood because it not only plagues the quality of spectra but, for certain species, completely masks their Raman features [Agarwal, 1999]. This limitation of visible Raman spectroscopy can be avoided by using a longer wavelength laser. Compared to the visible excitation (i.e. 514.5 nm), the 785 nm (NIR) laser is sufficiently lower in energy that the efficiency for promoting the electronic transitions responsible for fluorescence should be low. Moisture has also minimal effect on spectra since the NIR laser does not greatly excite  $\nu$  (O-H) in water [Wariishi *et al.* 2002].

Even at 785 nm excitation laser source, there are species that fluoresce. An investigation was conducted on samples from species such as white pine, red pine, southern pine, western red cedar, poplar, red maple, white spruce and aspen. Figure 20 represents the intensity at  $300 \text{ cm}^{-1}$  (chosen because no Raman peaks appear in this region) from Raman spectra normalized to the lignin band at  $1560\text{-}1720 \text{ cm}^{-1}$ . A correlation between the wood colour and the fluorescence emission seemed to exist. While spectra from white spruce and poplar (light coloured) exhibited the lowest fluorescence, in samples like cedar or southern pine (reddish-brown), the fluorescence totally overwhelmed the Raman signal. Furthermore, spectra from a different sample of red pine wood indicated that sapwood tended to fluoresce less than heartwood (fig. 21).

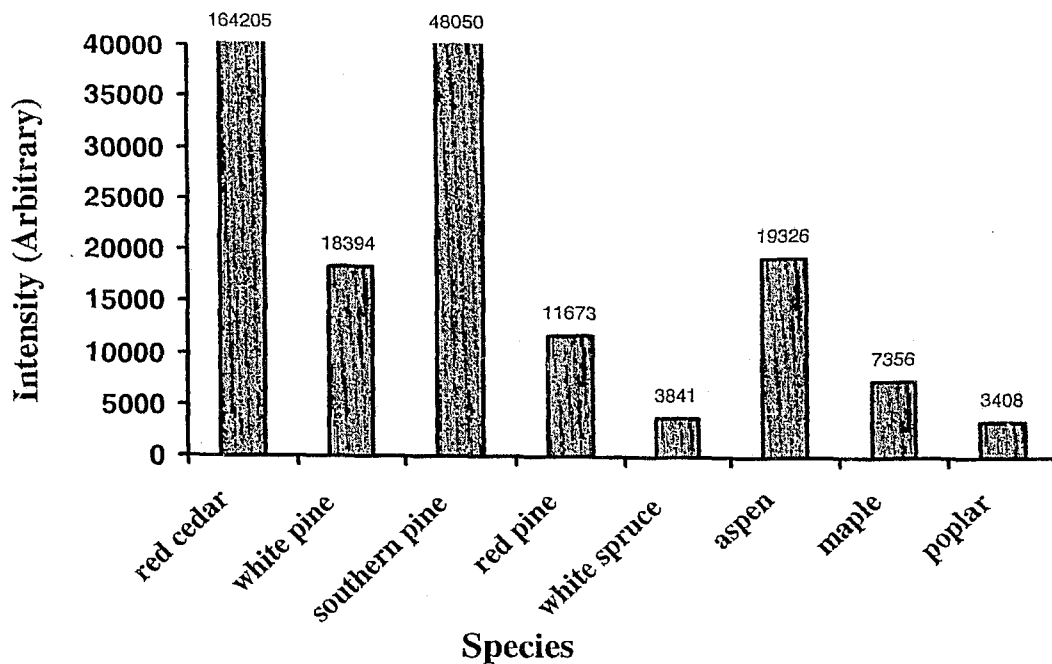


Figure 20. Different Species Intensity at  $300\text{ cm}^{-1}$  from spectra normalized to the lignin band ( $1560\text{-}1720\text{ cm}^{-1}$ ). Spectra collected for 10 seconds detector time, using 785 nm laser. Spectra included in Appendix A1.

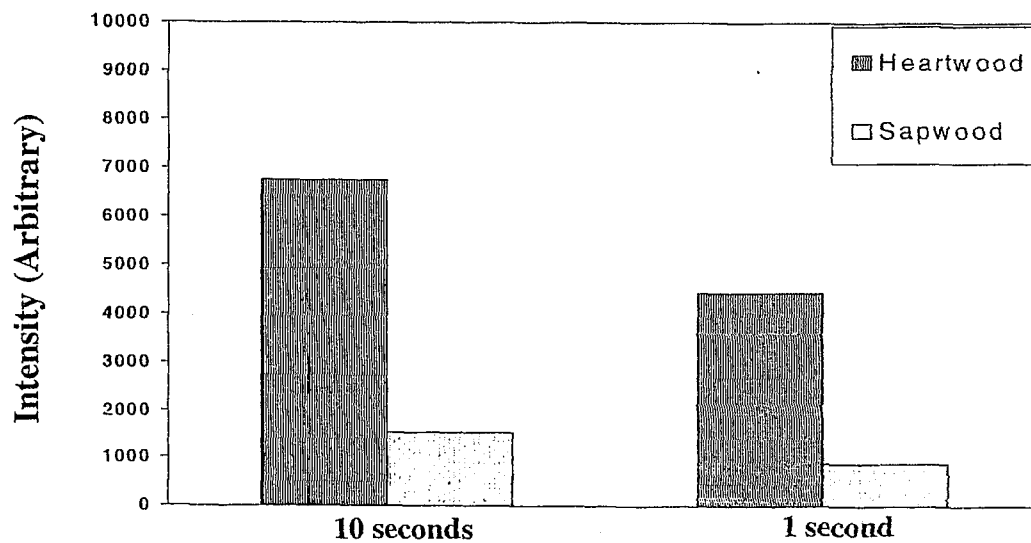


Figure 21. Red Pine Heartwood and Sapwood Intensities at  $300\text{ cm}^{-1}$  from spectra normalized to the lignin band ( $1560\text{-}1720\text{ cm}^{-1}$ ). Detector time 10 seconds and 1 second.

Based on these observations, the fluorescence emission can be linked to dark-coloured extractives present in wood species. Western red cedar and southern pine are well known as rich sources of extractives, while species like poplar are very low in extractive content [Chan-Yeung; Tsounis, 1968]. The biosynthesis of extractives is controlled genetically and hence each wood species tends to produce specific substances. On the other hand, these extraneous materials that impart colour to wood are deposited in certain morphological sites in the wood structure. Resins are primarily found in resin canals and parenchyma cells, whereas extractives like tannin, flavonoid, lignans, *etc.*, are most abundant in latewood. Phenolic compounds like catechin or tetrahydroxyflavan, which absorb light at shorter wavelengths than 500 nm, are predominantly located in heartwood while only traces are present in sapwood [Hillis, 1962; Sjöstoröm, 1993].

It is also noteworthy that aromatic groups contained in lignin or trace amount of impurities are capable of fluorescence [Oldham *et al.* 1997]. Some of the lignin chromophores (i.e.  $\alpha$ -carbonyls) that absorb above 300 nm are generally non-fluorescent, whereas structures like 3-methoxy-catechol, methoxy-*p*-benzoquinone, and methyl-*p*-quinone exhibit fluorescence when excited at 514.5 nm laser [Zhu and Gray. 1995; Agarwal, 1998].

Figure 22 shows the results of fluorescence quenching by different methods. All spectra were normalized to the lignin band at 1560-1720  $\text{cm}^{-1}$ . Some of the spectra, to a certain degree, exhibited reduction on fluorescent emission. Drench quenching ligno-cellulosic materials, usually is not as successful as in cellulosic materials, because lignin can be the source of fluorescence itself [Agarwal, 1999].

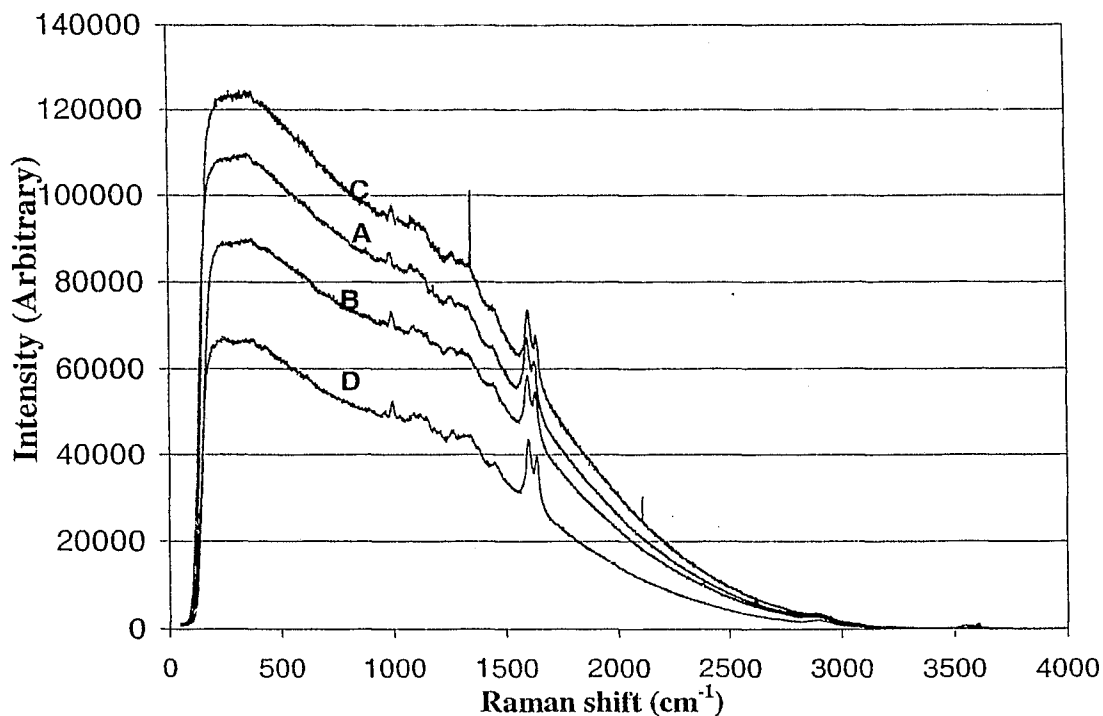


Figure 22. Quenching Fluorescence. A-white pine spectra; B-white pine after 2 hours irradiation by 514.5 nm laser; C-white pine spotted with methyl iodide; D-white pine after 3.5 hours irradiation by 514.5 nm laser; spectra collected for 100 sec detector time, using 785 nm excitation source.

Better results were particularly obtained after 3.5 hours photobleaching with 514.5 nm laser (D-spectrum). The average number of excitation and emission cycles that occur for a particular fluorophore before photobleaching is dependent upon the molecular structure and the local environment. In this case, the green laser (514.5 nm) has apparently caused photon-induced chemical changes or covalent modifications, so that some of the fluorophores have lost their ability to fluoresce. Spin/orbital interactions are expected to become larger in the presence of  $\text{CH}_3\text{I}$  on the pine wood. Spectrum C (fig. 22) indicates that the change in spin was not favourable thus the fluorescence is very high.

### 4.3 Distribution of Propiconazole

#### 4.3.1 Deposition on Wood Surface

For these experiments, samples of white spruce were soaked in 0.20-5.0 % solution of propiconazole. Raman spectra of the surface of the samples were recorded. Figure 23 illustrates the plot of normalized Raman intensity versus concentration of propiconazole treating solution. Each point on the curve represents the average normalized intensity of five different spectra taken on the transverse face of propiconazole treated samples. All Raman spectra were recorded in the range  $600-1500\text{ cm}^{-1}$  by accumulating two spectra. Typically, SNR (signal to noise ratio) improves by the square root of the number of spectra accumulated. The rest of experimental conditions were the same as described in section 3.5.2.

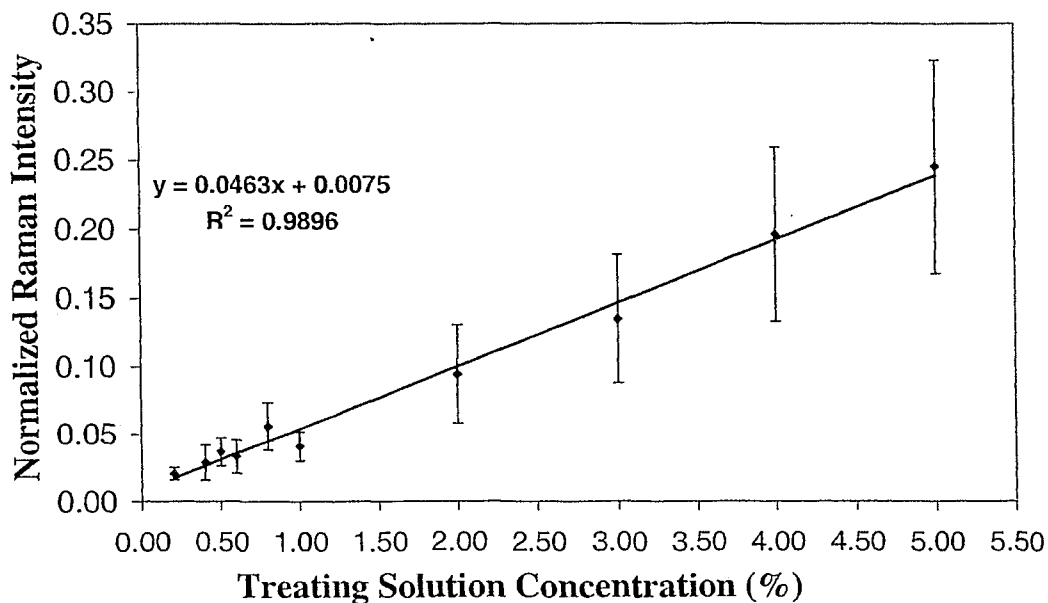


Figure 23. Raman Surface Calibration Curve. The error bars represent the standard error of the mean normalized intensity.

Raman surface calibration curve exhibits two significant results. First, the normalized Raman signal is linear with the concentration of the soaking solution; a correlation coefficient ( $R^2$ ) of 0.9896 was obtained. The signal strength and linearity of the surface calibration curve pronounce the capability of Raman Microscopy for determining propiconazole in wood. Data from GC-MS analysis have shown that the total propiconazole concentration in treated wood samples was directly proportional to the concentration of treating solution [Katic, 2003]. Therefore, the normalized Raman intensity can be alternatively plotted against the propiconazole concentration in wood.

Second, the large error bars indicate an inhomogeneous distribution of the propiconazole on the wood surface. Wood is an anisotropic and porous material with very heterogeneous surface chemistry. Mapping measurements on the transverse surface (fig. 24) show the non-uniform distribution of propiconazole. Improvement in variability of signal could probably be achieved by using a larger spot size of the excitation beam. A larger diameter of the laser spot can be obtained by using low- or medium-power objectives. However, when using low N.A. (numerical aperture) probes, the collected (and the processed) signal strength decreases rapidly compared to high power objectives (i.e.  $\times 50$ ) [McCreery, 2000]. Fibre optic devices with poorer spatial resolution might be more appropriate for routine analysis.

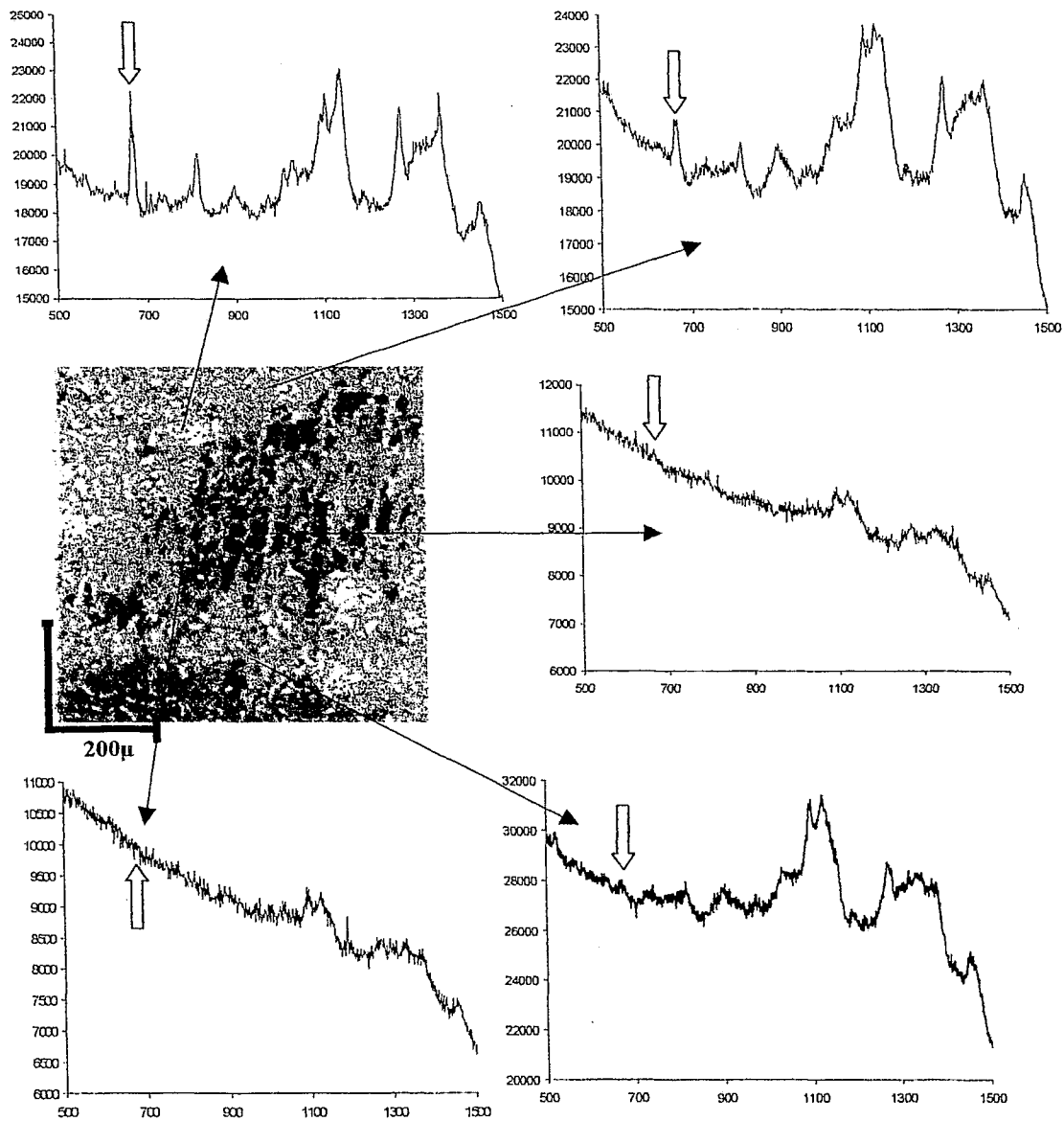


Figure 24. Mapping Measurement on Transversal Surface of a Propiconazole Treated Sample. Axes on the spectra are Intensity (counts) vs. Raman shift ( $\text{cm}^{-1}$ ). ( $\Rightarrow$ ) pointing to the propiconazole peak

### 4.3.2 Mapping Measurements of Propiconazole Distribution in Seasonal Wood

Mapping spectra were collected on the radial face of propiconazole treated samples. All spectra were recorded by setting the spectral accumulation at 3. The rest of the experimental set up is described in section 3.5.2. Due to the topological features, a long working distance objective ( $\times 20$ ) was used for conducting mapping analyses. Although it does not provide the highest spatial resolution, a  $\times 20$  objective is suitable for discriminating among wood structures. With a numerical aperture (NA) of 0.40, the laser beam diameter at the focal spot is in the range of 4.7 - 4.9 micron.

SNR (signal to noise ratio) was one of the distinguishing characteristics of spectra from seasonal wood. It was observed that spectra from springwood had lower a SNR than spectra from summerwood. Typically, SNR tracks the square root of integration time. For a given time and detection performance the SNR is nearly linear with the cross section-number density product for the analyte of interest [McCreery, 2000]. In earlywood the density of wood at the laser spot is smaller than in latewood. Therefore, less propiconazole (adsorbed to the cell wall) is present in the sampling volume of springwood. Apparently by decreasing cross section-number density product for propiconazole (lower signal) in springwood the SNR is likely to get degraded.

Figure 25 depicts the differences on integrated signal of the analytical region ( $647\text{-}693\text{ cm}^{-1}$ ) from Raman spectra of earlywood and latewood. The signals are not normalized to the wood band, so they do not represent the concentration of propiconazole. There was a significant intensity change in the analytical band of seasonal wood spectra. Eighteen microns from the initial position, which corresponds to the springwood, the integrated intensity increased steeply. Moving further into the

summerwood the analytical signal remained at higher levels than in springwood. Repeated mapping analyses (1-D and 2-D) have shown very similar behaviour with these results.

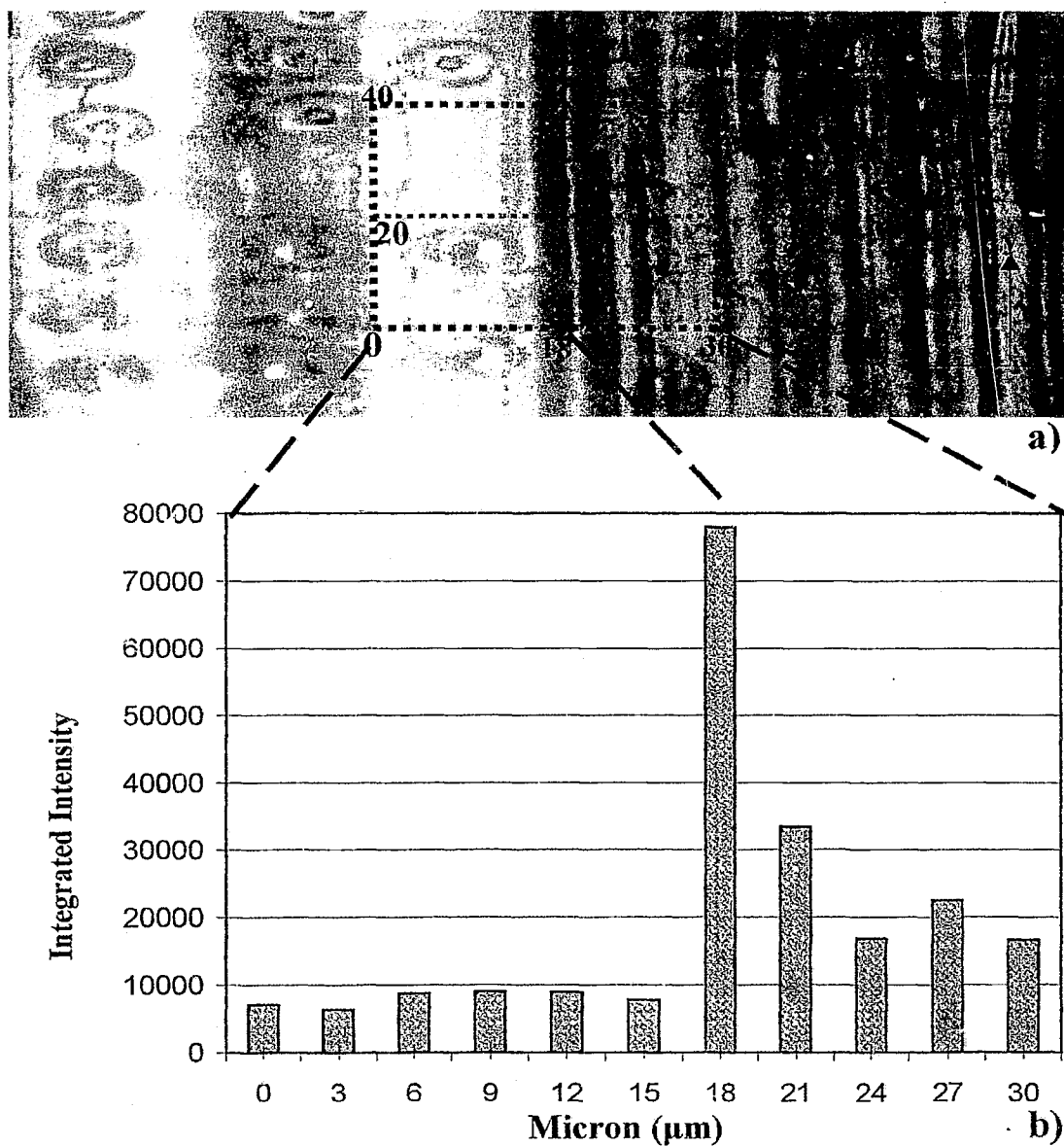


Figure 25. a) White Light Image from 2-D Mapping Measurements. b) Average integrated intensity of analytical region ( $647-693 \text{ cm}^{-1}$ ). Spectra were collected every  $3\mu$  in the x-direction. Integrated intensity was averaged over three different levels separated by  $20 \mu\text{m}$  distance (y-direction).

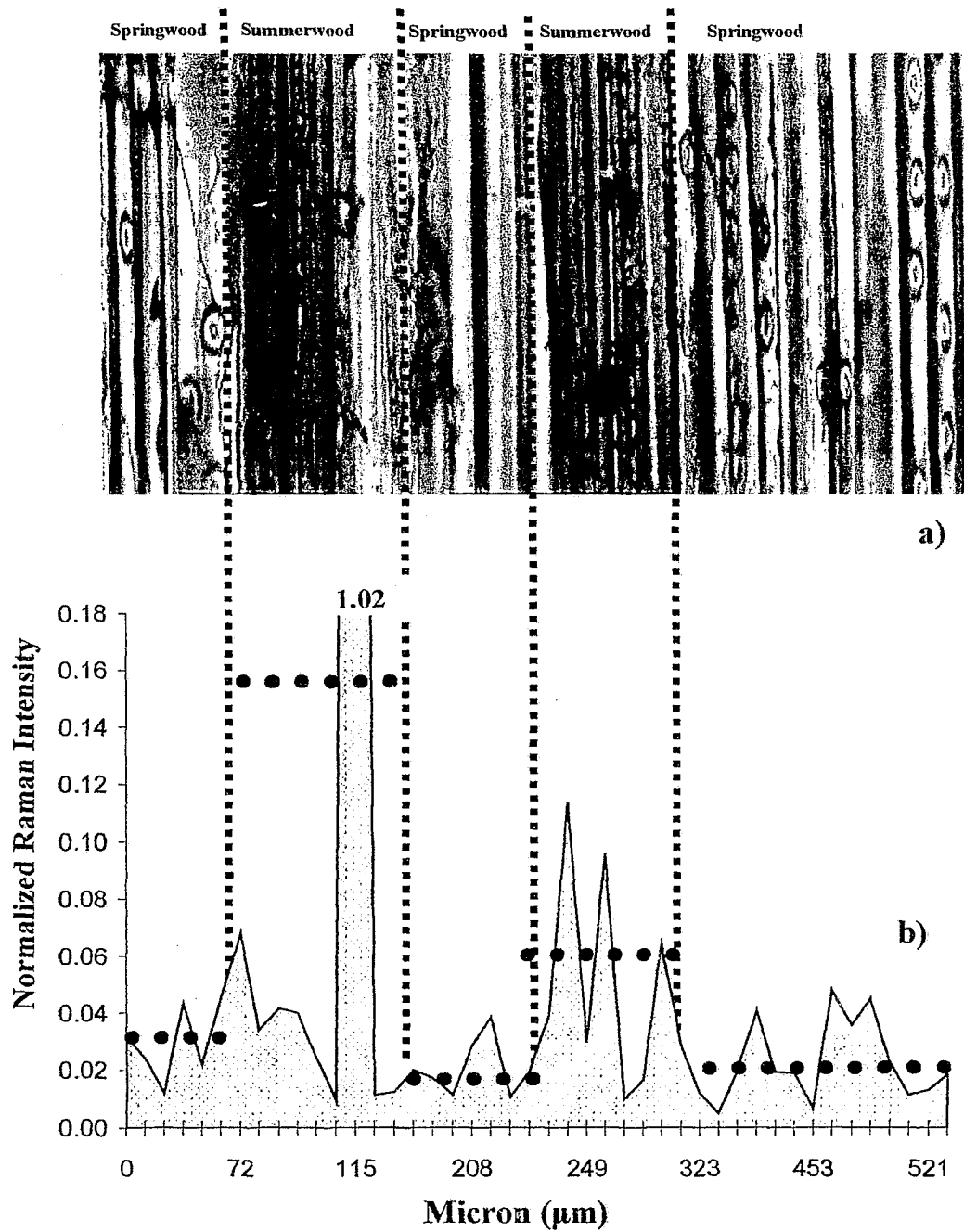


Figure 26. a) White Light Image b) Normalized Raman Intensity from 1-D mapping over 500  $\mu$  on the radial face. Spectra were collected on points over a straight line. ● ● represents the average of the normalized intensity on the selected region.

The normalized Raman intensities from mapping measurements over a wider range on the radial face are plotted on figure 26. Even though the data exhibited scattering, on average, the normalized intensity of propiconazole in summerwood was higher than in springwood. The explanation for such trend might be related to the propiconazole concentration in the cell wall. The structure of earlywood is less dense and has more pit openings than summerwood. Analyses of propiconazole soaked samples have shown evidence of blooming (section 4.4). It is likely that during drying propiconazole diffuses out of earlywood structures more easily and some of the moving molecules get trapped on the denser interface of the summerwood.

Based on these results, all Raman spectra for determination of propiconazole depth of penetration were sampled from summerwood.

#### 4.4 GC-MS Determination of Propiconazole Depth Profile

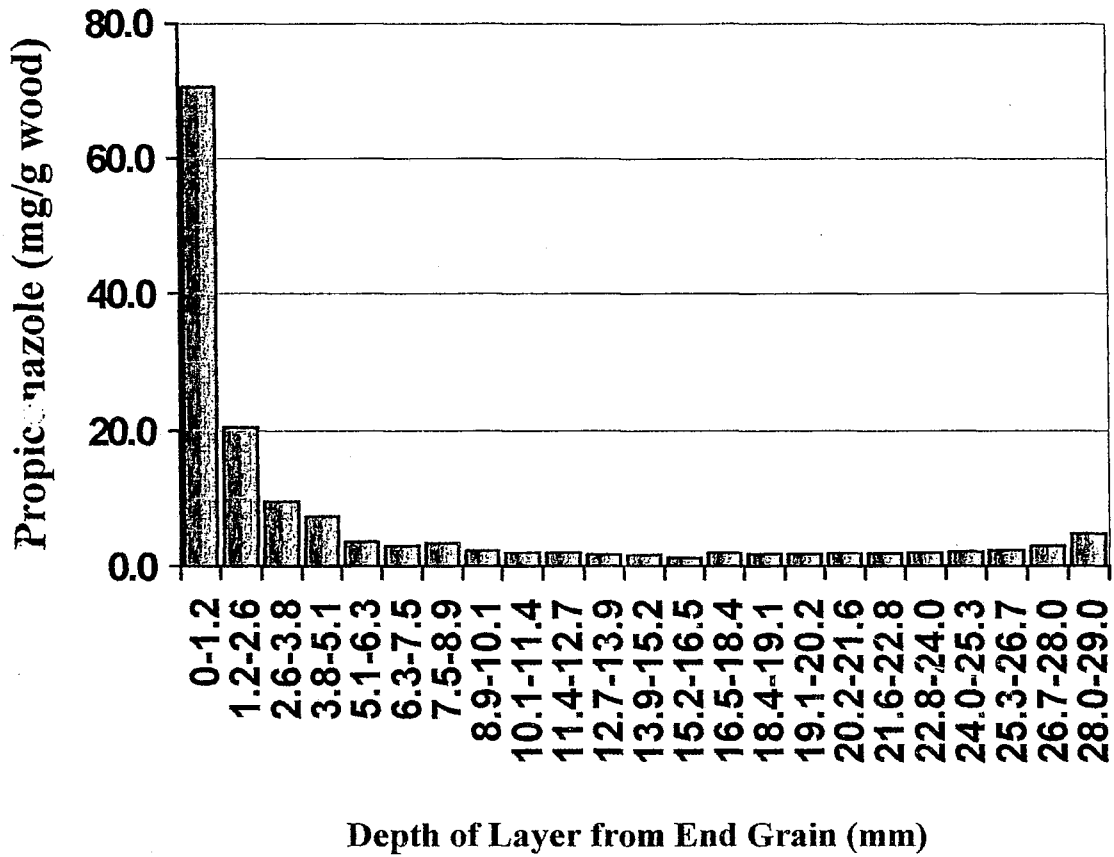


Figure 27. Depth Profile of Propiconazole in Block A by GC-MS (soaked in 4 % solution). Quantitation was performed using the internal standard calibration curves. Only calibration curves with correlation coefficients of .99 were accepted.

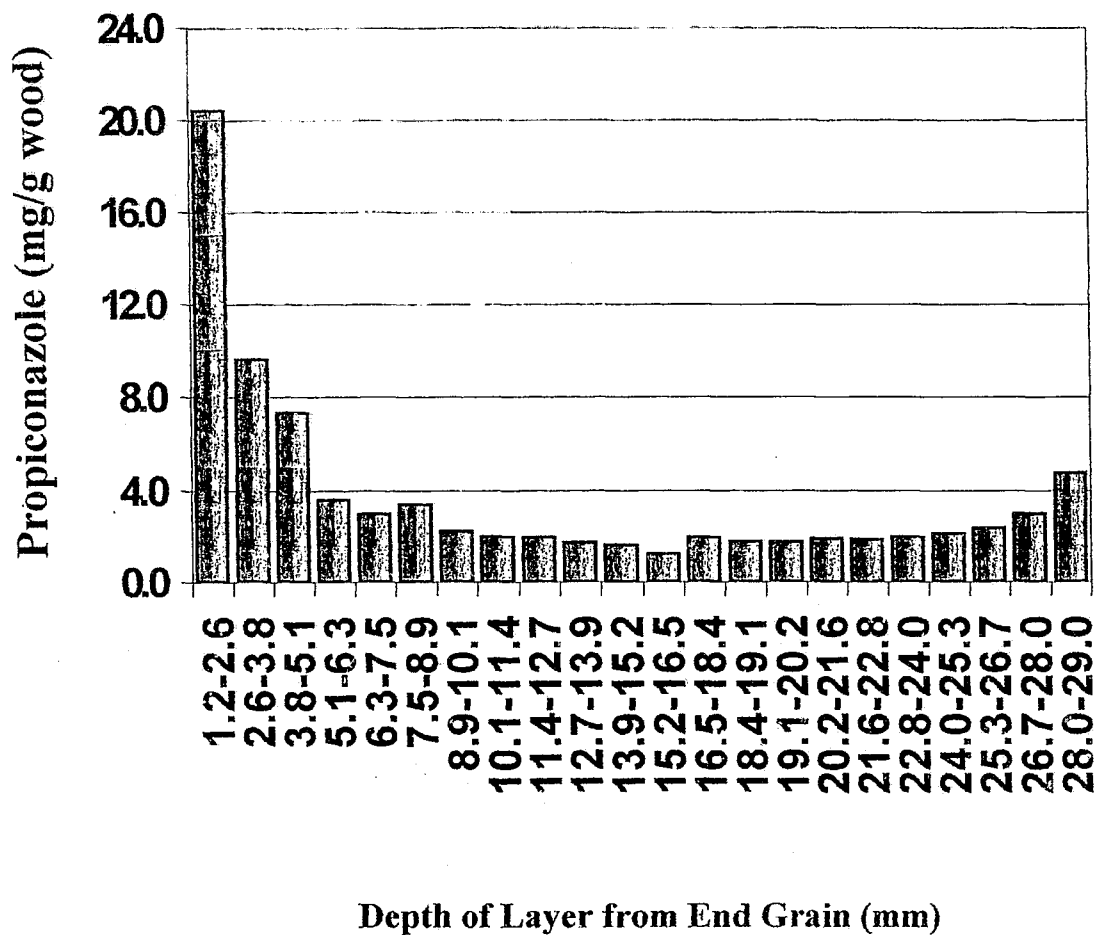


Figure 28. Surface-Excluded Depth Profile of Propiconazole in Block A by GC-MS (soaked in 4 % solution).

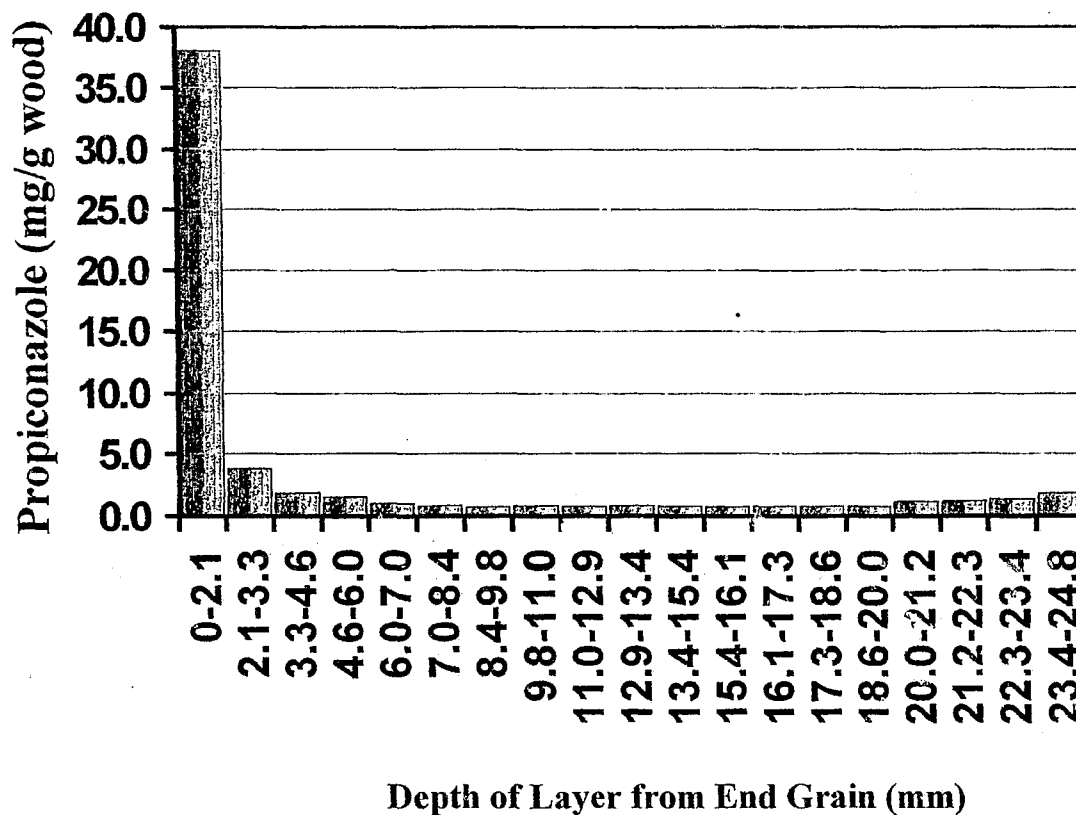


Figure 29. Depth profile of propiconazole in block B by GC-MS (soaked in 2 % solution). Quantitation was performed using the internal standard calibration curves. Only calibration curves with correlation coefficients of .99 were accepted.

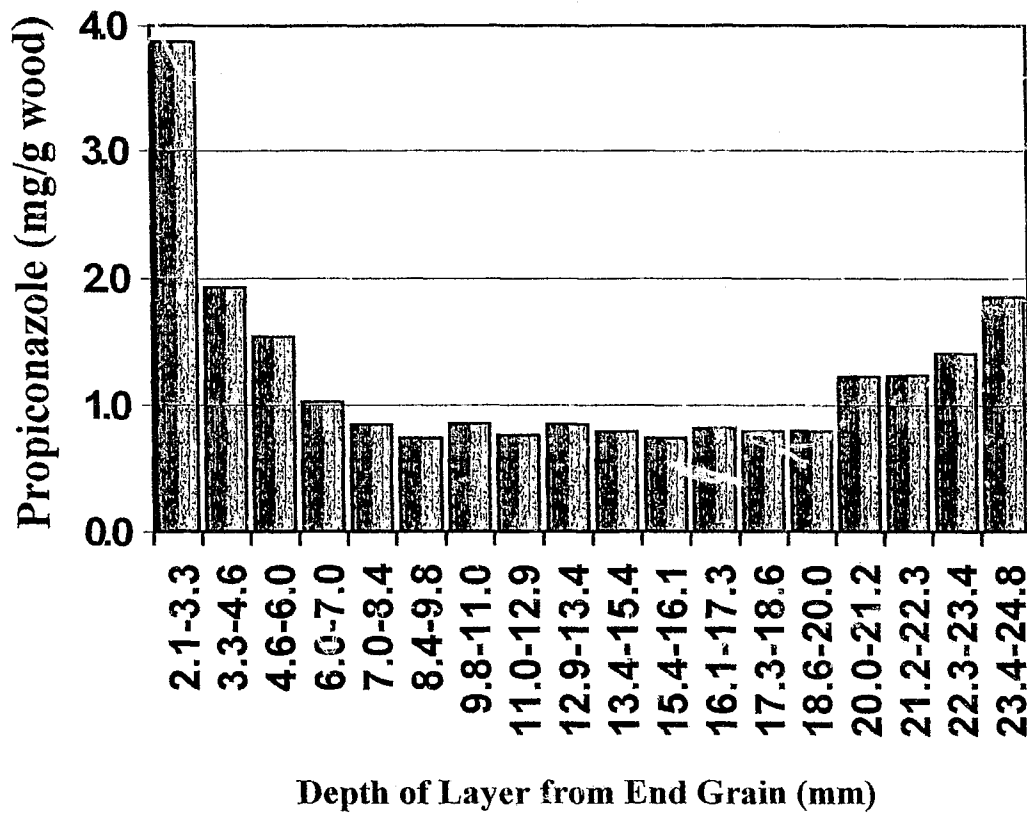


Figure 30. Surface-Excluded Depth Profile of Propiconazole in Block B by GC-MS (soaked in 2 % solution).

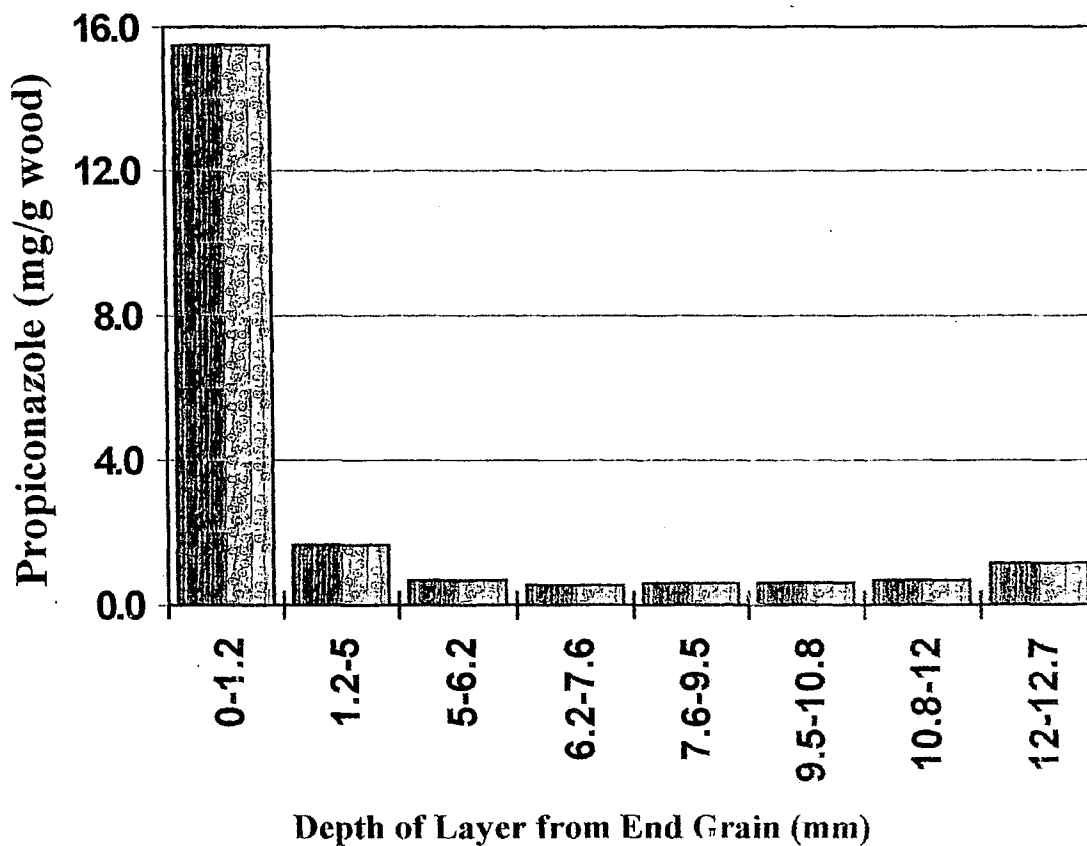


Figure 31. Depth Profile of Propiconazole in Block C by GC-MS (soaked in 1 % solution). Quantitation was performed using the internal standard calibration curves. Only calibration curves with correlation coefficients of .99 were accepted.

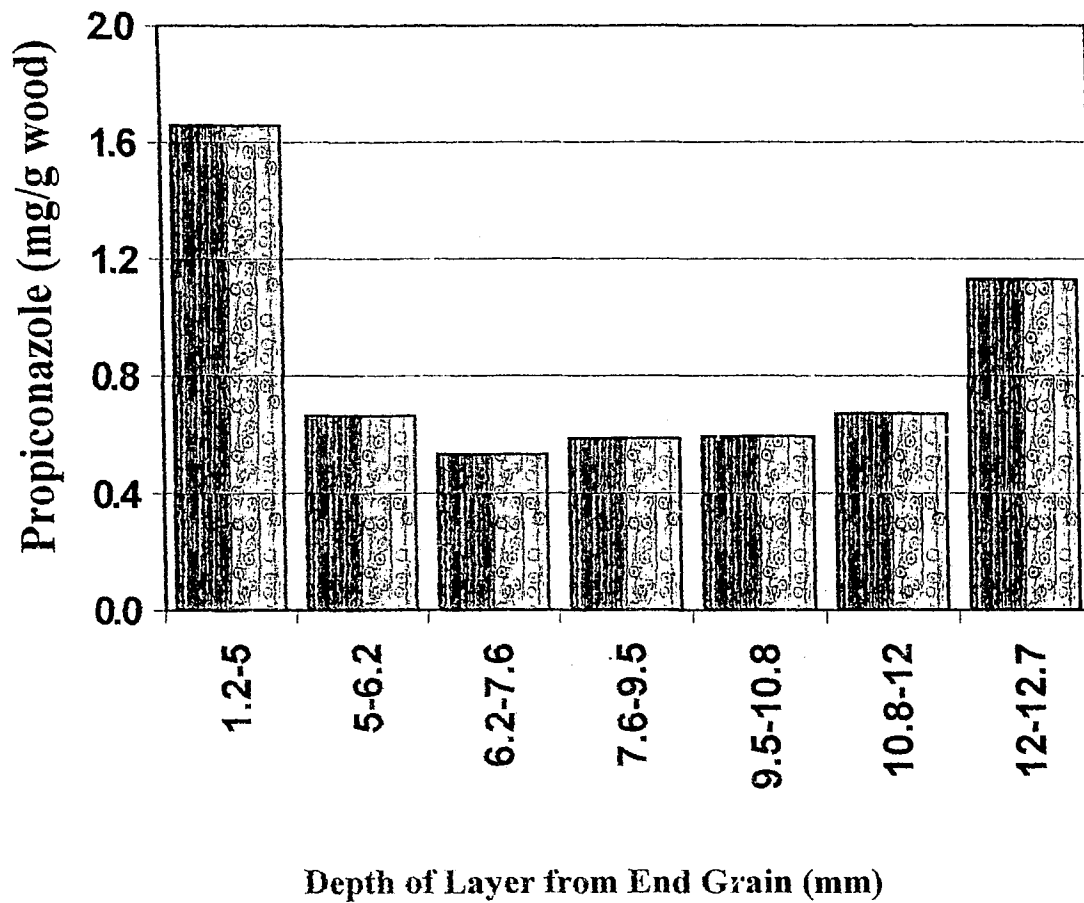


Figure 32. Surface-Excluded Depth Profile of Propiconazole in Block C by GC-MS (soaked in 1 % solution).

Figures 27-32 show the distribution of propiconazole in the longitudinal direction of samples soaked in 1%, 2%, and 4% solutions of propiconazole. The bars represent the concentration determined by GC-MS in each layer. The deposition level of propiconazole on the soaked samples (A, B, C) conformed to the standard proposed by AWPA (American Wood Preserver's Association). For example, a concentration of about 696 ppm was obtained from the first layer of 1.1 mm, in the block (A) soaked in 4% solution. The AWPA (Standard P8) standard recommends an average retention level of 600 ppm within 1.5 mm of the end grain for wood that is not in contact with the ground or severe weather conditions.

As the GC depth profiles illustrate, the distribution of propiconazole along the grain was consistent with depth profiles described by Schoknecht and Bergmann [2000] and Malkov *et al.* [2003]. The propiconazole concentration decreased from high values on the first layers toward a flat minimum in the middle of the sample. In addition, the GC depth profiles had similar shapes with the axial concentration profiles obtained and modeled by Kazi *et al.* [1998]. However, the diffusional mechanism described by Kazi *et al.* [1998] refers to the impregnation of green wood (lumens are filled with unbound water), and the application of the Fick's second law in the longitudinal direction considers only one end of the wood block to be in contact with the treating solution.

Comparing the propiconazole concentration between first and subsequent layers in all samples, revealed noteworthy differences between their concentrations. From the first to the second layer the propiconazole concentration dropped by almost 70 %, 92 %, and 93 % for A, B, and C-blocks, respectively. In addition, Raman analysis showed that propiconazole was highly concentrated on the transverse surface. These results implicate

two scenarios: propiconazole has “bloomed” to the surface, as the sample dried or there is incomplete penetration of the treating solution. Previous experiments indicated that the weight gain of soaked samples increased with the concentration of treating solution [Katic, 2003] and the wood blocks could be saturated with the treating solution prior to 24 hours soaking time. Contradicting the incomplete penetration, these facts emphasize the idea of blooming toward the surface of drying samples.

During soaking time, due to the two polar functional groups (dioxolane and triazole moiety), propiconazole molecules would be adsorbed by the cell wall. The strength of intermolecular interactions with cellulose depends among others on sterical factors. Also, amounts of water, if present, will compete with cellulosic material for adsorption [Armstrong, 1999]. However, having a relatively high solubility in mineral spirits (> 10%) the extent of propiconazole adsorption on the cellulosic material should be low. Typically, the mineral spirits, as a non-swelling fluid, tend not to penetrate the cell wall. Without entering into many details of the drying process it can be envisioned that after drying has started a convective flow is established through cell cavities (lumens) and pits. The gradient of the mineral spirits content (in the longitudinal direction) causes a capillary flow headed for the transversal surfaces. As a result, not only molecules of propiconazole remaining in the solution are transported towards the surface, but also some of the adsorbed molecules are likely to be “washed” off from the cell wall.

#### 4.5 Raman Depth Profiles

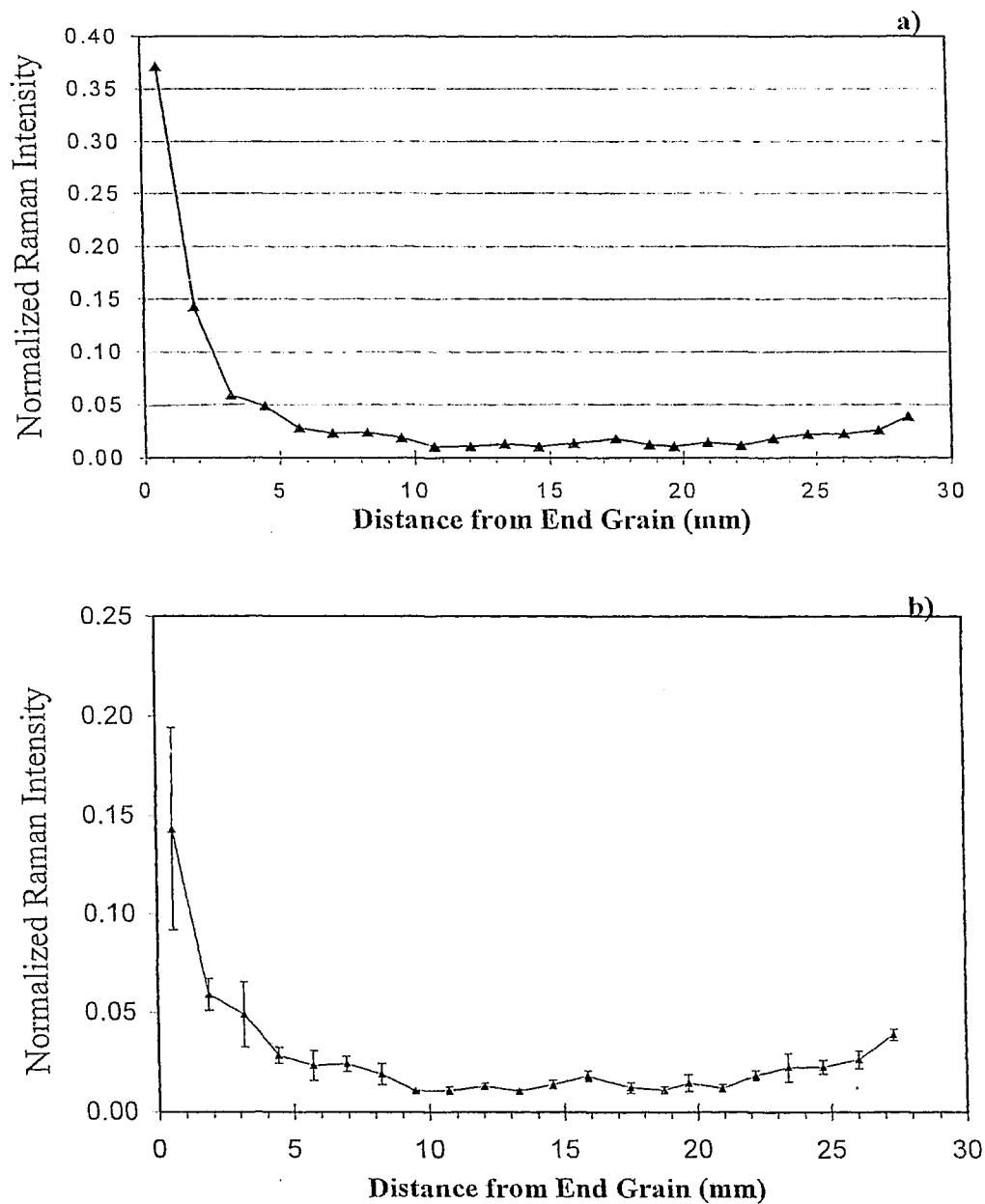


Figure 33. Raman Depth Profiles for Block-A (soaked in 4% propiconazole solution). a) surface included, b) surface excluded. The error bars represent the standard error of the mean normalized intensity.

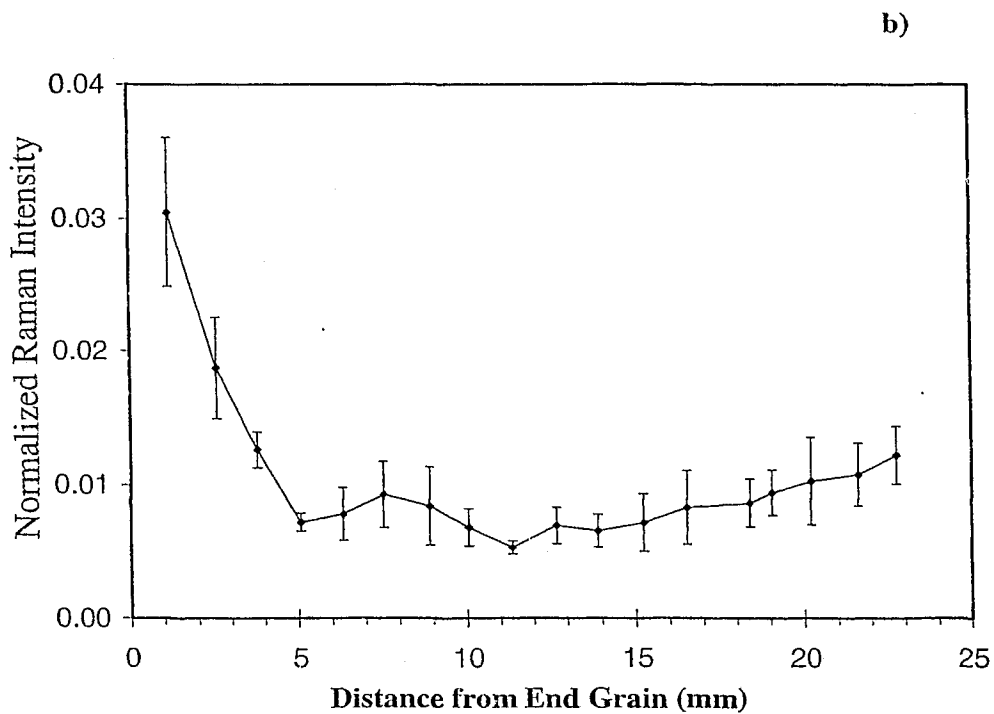
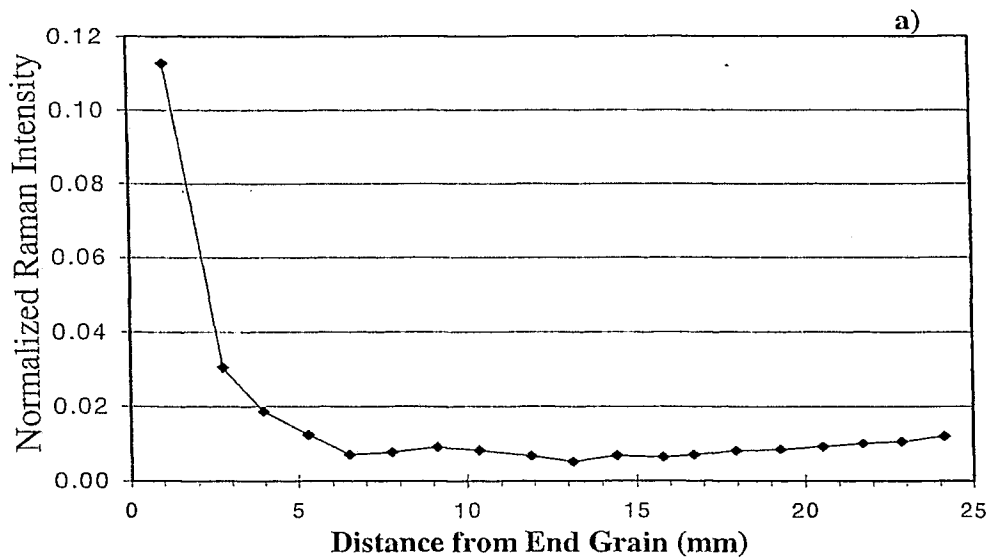


Figure 34. Raman Depth Profiles for Block-B (soaked in 2% propiconazole solution). a) surface included, b) surface excluded. The error bars represent the standard error of the mean normalized intensity.

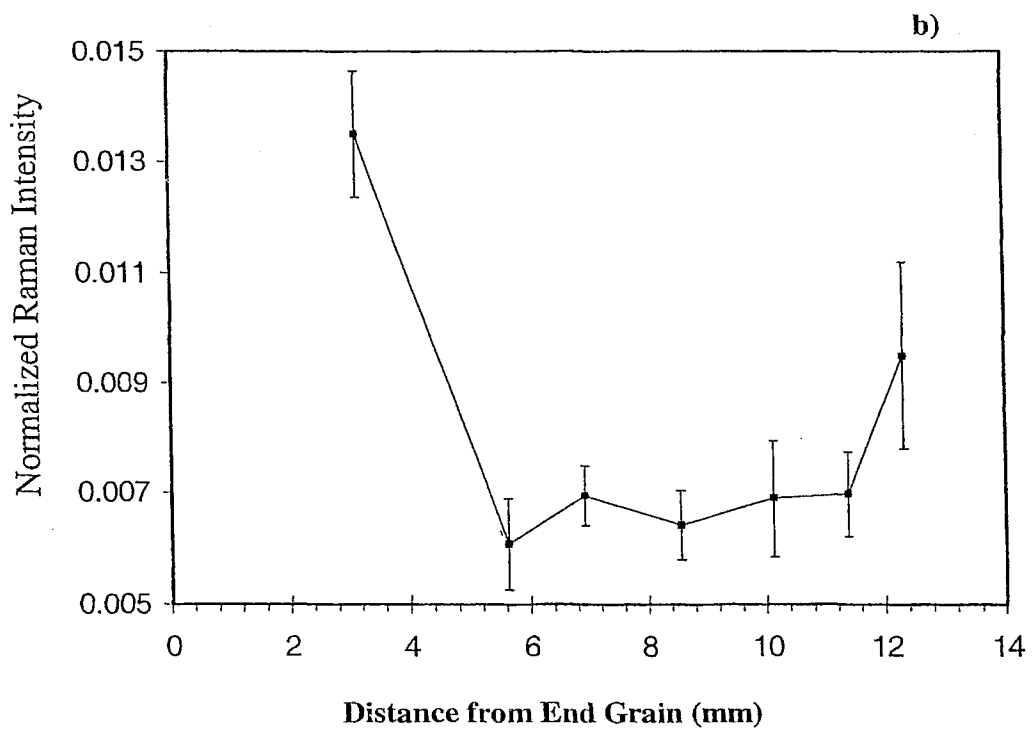
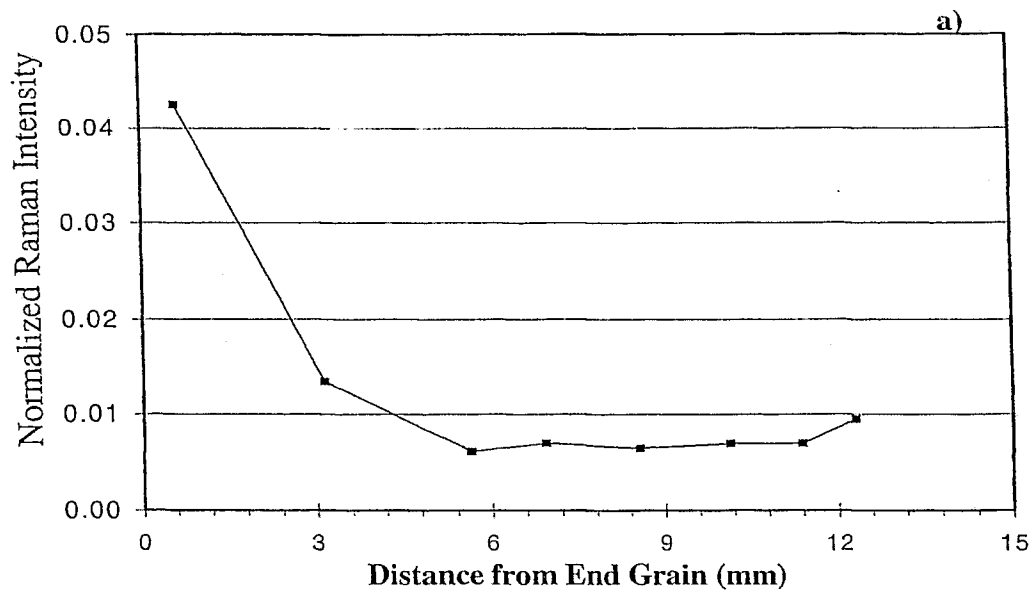


Figure 35. Raman Depth Profiles for Block-C (soaked in 1% propiconazole solution). a) surface included, b) surface excluded. The error bars represent the standard error of the mean normalized intensity.

Figures 33-35 show Raman profiles in the longitudinal directions. Each point on the graphs represents the average normalized intensity of four different spectra taken on the radial face. Comparison of a) and b) profiles in all soaked samples highlights the differences in concentration between the first two layers, as mentioned in the previous section. The Raman profiles had similar shapes with the depth profiles obtained by GC-MS analysis. However, Raman depth profiles exhibited more deviations from the "bowl" shape compared to GC-MS curves. The uncertainty in the Raman can be explained by considering the sampling volume of Raman Microscope. The use of a high numerical aperture objective ( $\times 50$ ,  $NA=0.75$ ) has the unique advantages of transmitting the most power and collecting most signal with  $\sim 2\mu\text{m}$  spatial resolution. The volume sampled by the spectrometer is the overlap between the focused laser beam diameter ( $\sim 2\mu\text{m}$ ) and the depth of focus ( $\sim 7\mu\text{m}$ ). On the other hand, the GC-MS data is derived from a volume at least  $10^4$  times larger and consequently the scattering should be smaller. The large error bars reflect the inhomogeneity in the distribution of propiconazole at a given layer. As mapping analysis showed, even within summerwood propiconazole was not uniformly distributed. It is likely that a bigger sampling volume (larger laser spot) or averaging the Raman signal on more spectra could produce smoother curves and smaller error bars.

The first points on the a)-curves of fig. 33-35 refer to the first layer of each of the blocks. Spectra, as for all layers, were collected on the radial face leaving the transverse surface out. The edge of the blocks usually was vulnerable to the knife edge resulting in damaged or smashed fibers. Since GC-MS data include the transverse surface concentration, and spectra were collected on damaged surfaces (radial), the first points of depth profiles were not used on the calibration curve.

#### 4.6 Calibration Curve

Figure 36 represents the calibration curve associated to the relationship between Raman and GC-MS data.

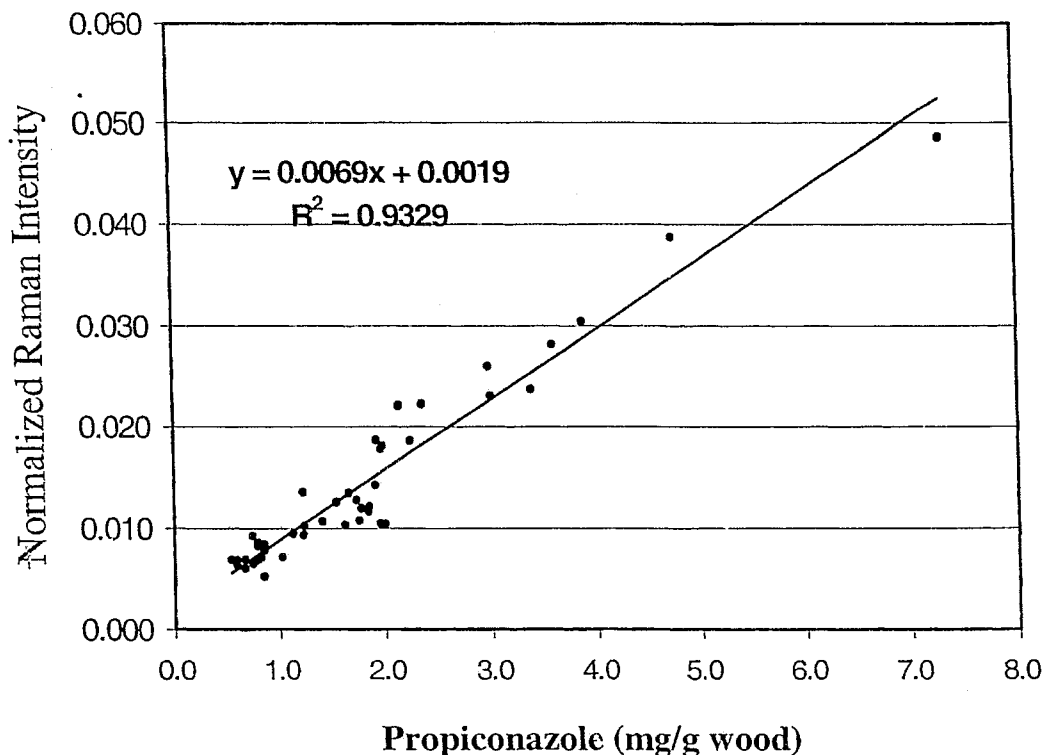


Figure 36. Calibration Curve constructed by plotting the average normalized Raman intensity at analytical region ( $647-693\text{ cm}^{-1}$ ) to the propiconazole concentration determined by GC-MS.

Data points over 7 mg/g were excluded from the calibration curve because they had low weight and skewed the line of regression. These points were also not relevant to the depth analysis due to very high concentrations only observed at the transverse

surfaces. The calibration curve indicates a linear relationship, with  $R^2=0.9329$ . Data are weighted toward low concentrations, especially around 1 mg/g. The low concentration points refer to the propiconazole concentration on the interior parts of the samples. As GC (and Raman) depth profiles depicted, within a certain region in the middle of the blocks, the propiconazole concentration was characterized by rather constant values. The increase of propiconazole concentration (fig.36) is associated with data points monotonically distributed around the regression line. The standard deviation about regression was:  $S_r = 0.0024$ . At 95 % significance level, the confidence limits for the slope (b) and intercept (a) were:  $b = 0.0069 \pm 0.0006$  (g wood /mg) and  $a = 0.0019 \pm 0.0012$ . The confidence limits (95 %) for concentrations determined by the unweighted regression line are shown in figure 37.

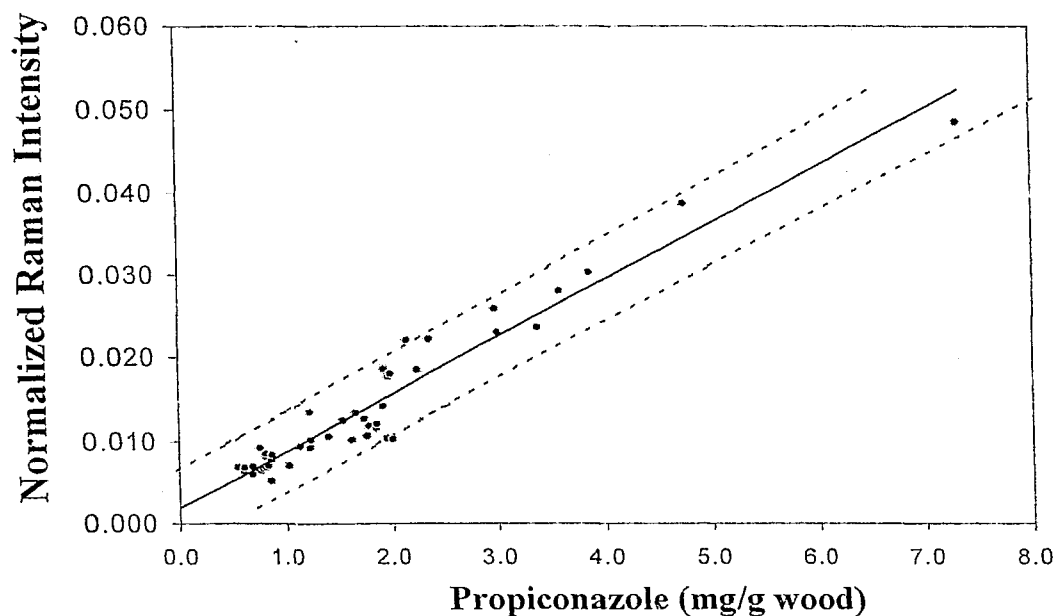


Figure 37. (---) 95 % Confidence Limits for the Unweighted Regression Line.  $t = 2.01$

#### 4.6.1 Raman Predicted Concentration

Another block of wood with dimensions 8.5 (T) x 2.4 (R) x 1.3 (L) cm was soaked (and analyzed) under the same conditions as the previous blocks (A, B, C) in 3 % propiconazole solution. The Raman depth profile for this block is plotted in figure 38.

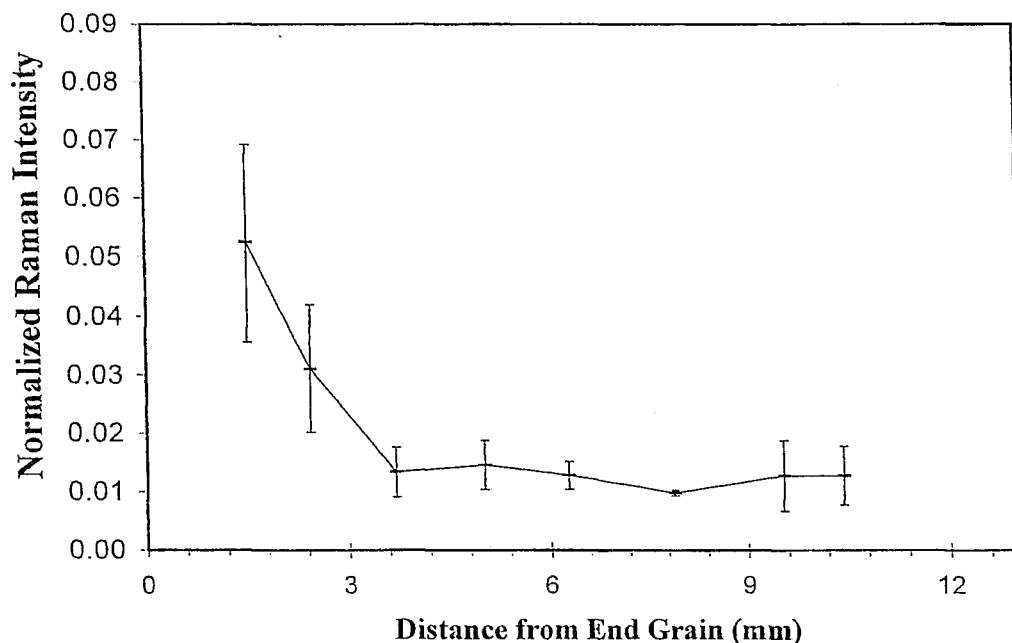


Figure 38. Raman Depth Profiles for the Block Soaked in 3% Propiconazole Solution. Surface (first layer excluded) excluded. The error bars represent the standard error of the mean normalized intensity.

Based on the data of the Raman depth profile and the regression equation of the calibration curve, the propiconazole concentration (mg/g) was calculated. Computation of propiconazole concentration involves error because the slope, the intercept and the Raman signal are subject to a known error. Figure 39 shows the plot of the predicted values against distance from end grain. Error bars represent the error in predicted concentration by using the regression line equation. Since each data point in the

calibration curve (fig.36) and in the Raman depth profile (fig.38) is derived from four Raman readings, they are considered as one set of readings when calculating the error in the predicted concentrations.

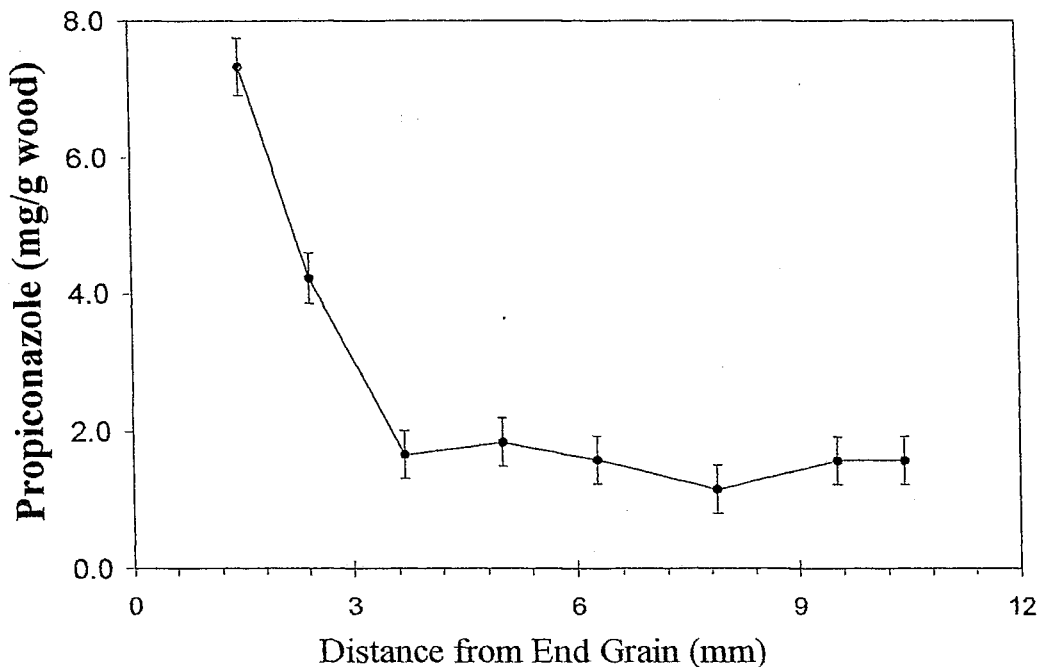


Figure 39. Predicted Concentration From the Regression Line Equation.

In figure 40 the predicted concentrations are plotted together with the GC-MS measured values. The bars represent the GC-MS-determined concentrations for each layer of the sample soaked in 3 % solution. The predicted concentrations are represented by points since they are predicted from the average of normalized Raman signal over four points in the corresponding layer. The predicted values, except for the value of the second layer, exhibit deviations in the range of 20 % (Table B2, Appendix B). Some of the predicted concentrations (first and last points) show very small percent deviation from the GC-MS measured concentrations and in general the residuals appear to be normally

distributed. The high percent deviation of the second point could be as a result of inhomogeneous distribution of propiconazole within the second layer. It is possible that the points sampled by Raman have adsorbed more propiconazole than other regions in this layer due to structural features not detectable by the microscope.

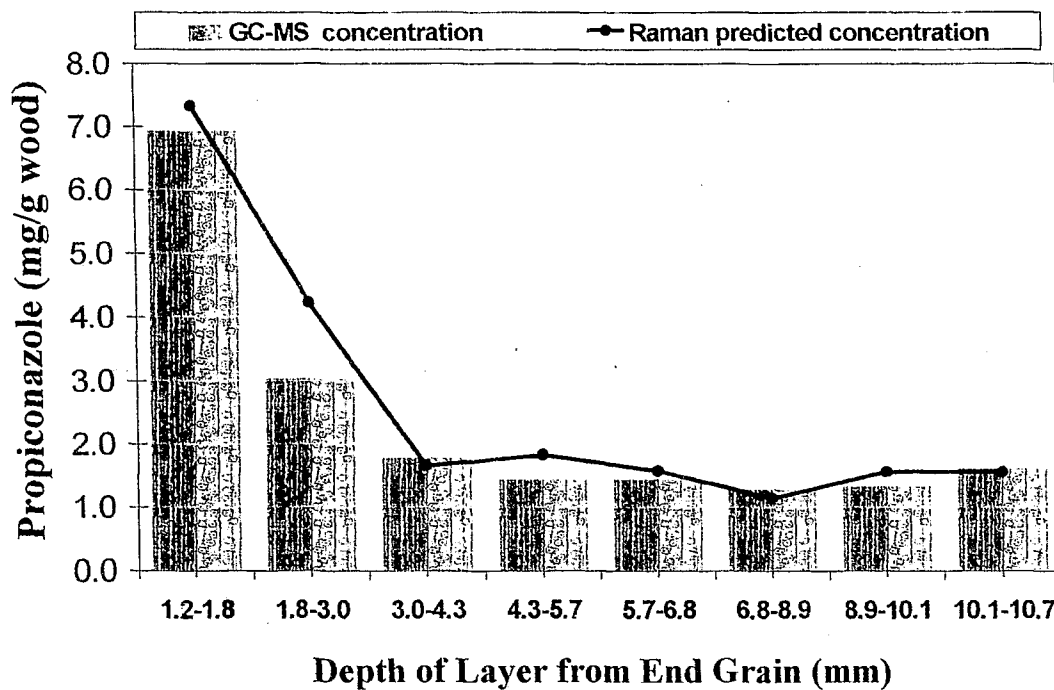


Figure 40. GC-MS Measured Concentration and Raman Predicted Values based on the regression equation of the calibration curve.

#### 4.6.2 Weighted Regression Lines

When plotting Raman Normalized Intensities versus GC-MS concentrations (fig.36), a main assumption was that errors on the x-direction were negligible (compared to the error from Raman measurements). Also, it was assumed that the absolute error in the y-direction was constant. By plotting the calibration curve together with standard deviations

(Figure B1, Appendix B), it appears that the error bars become larger as the concentration increases. This situation suggested a weighted regression line, where the calculated line passes close to points with the smallest standard deviations. This is achieved by giving each point an individual weight ( $w_i$ ) inversely proportional to the variance ( $s^2$ ) of that point ( $w_i \propto 1/s^2$ ) [Miller and Miller, 1988]. Application of the weighted regression line showed that the slope and the intercept of the calibration curve were:  $b = 0.0049$  (g wood/mg) and  $a = 0.0029$ .

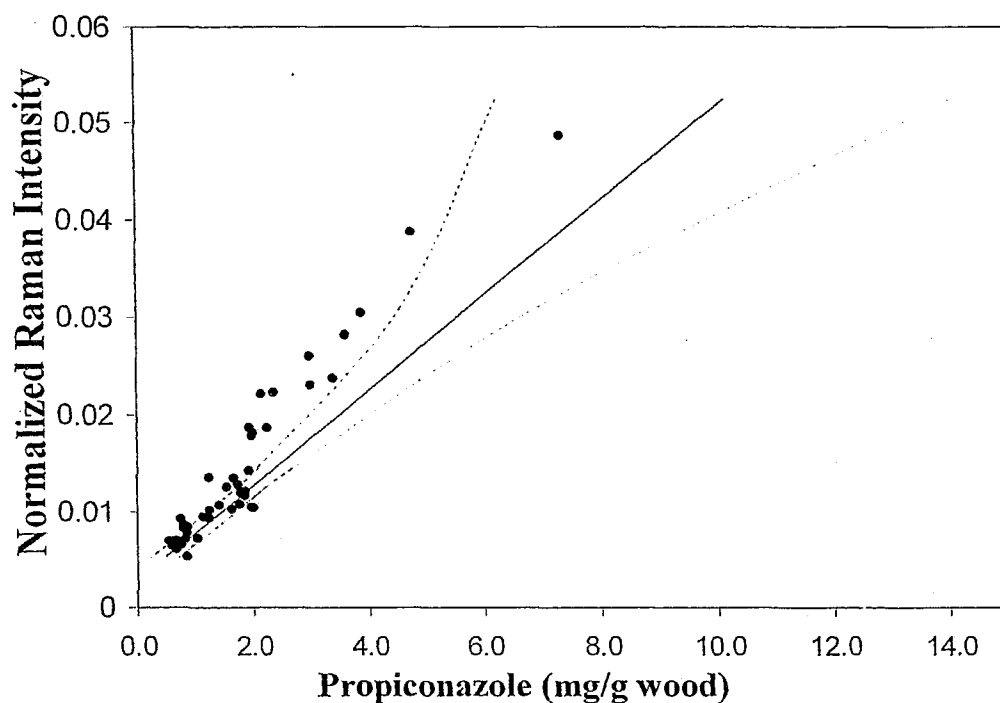


Figure 41. (---) 95 % Confidence Limits for Predicted Concentration by Using Weighted Regression Line.

Figure 41 depicts the confidence limits of Raman predicted concentrations based on the weighted regression equation ( $y = 0.0049x + 0.0029$ ). The confidence intervals increase with the increasing propiconazole concentration. Compared to the unweighted

regression line, the confidence limits become smaller for the less concentrated points, and bigger for higher concentrations (Table B1, Appendix B). Consequently the predicted concentrations from weighted regression calculations should be closer to reality. However, this is not the case, when compared to the GC-MS measured concentrations. In fact, there is one major drawback with these calculations. The weighted regression procedure is not appropriate for the distribution of the observed SD (standard deviations) values. In a perfect situation the absolute error increases linearly with the concentration and the weighted centroid (co-ordinates of  $\Sigma_i w_i x_i / n$  and  $\Sigma_i w_i y_i / n$ ) is much closer to the origin of the graph than the unweighted centroid. The weighting given to each point ensures that the weighted regression line has an intercept closer to the point with the smallest standard deviation. In fact, there are data points with small SD that correspond to high concentrations and vice-versa (Appendix B1). The point with the smallest SD corresponds to the concentration of 2 mg/g. By forcing the regression line closer to this point, the resulting intercept is larger compared to the unweighted regression line. Apparently, the unweighted regression line is more appropriate for predicting concentrations from the calibration curve.

## Chapter 5

### GENERAL CONCLUSIONS

This work was undertaken to explore the suitability of Raman Microscopy for analyzing propiconazole in wood matrixes. The study demonstrated the potential of Raman as a rapid analytical technique for determination of propiconazole distribution in the longitudinal direction. While it lacks the precision of the more traditional GC-MS, the Raman technique has the advantage of fast applicability. From comparison of data of three spruce blocks soaked in different propiconazole solutions (4%, 2% and 1%) a linear relationship was obtained. The correlation coefficient ( $R^2$ ) for the calibration curve was equal to 0.9329 and indicates that there was significant correlation between Raman and GC-MS results. An increase in the number of calibration points, especially between 3-5 mg/g, is likely to make the method more quantitative. The regression equation of the calibration curve was used to predict the depth profile of concentration from a sample soaked in 3 % propiconazole solution. The results indicated that Raman technique could be applied, with reasonable accuracy, for analyzing propiconazole in wood.

The large standard deviations associating with some of the measured Raman signals were due to the inhomogeneous distribution of propiconazole. Raman microscopy revealed that propiconazole preferentially adsorbed to summerwood and that propiconazole was nonuniformly distributed within summerwood.

The application of the Raman technique to other wood species was hindered by the interference of fluorescence. Raman measurements on several wood species or morphological wood (heartwood and sapwood) correlated the fluorescence emission to

dark-colored extractives. Different quenching methods could not totally eliminate the fluorescence background from wood spectra.

### 5.1 Recommendations

Some recommendations are listed as follows:

- Although this work was limited to white spruce, future research should involve the use of a longer wavelength (i.e. 1064 nm) excitation laser to determine propiconazole in other wood species.
- Based on the satisfactory results for quantifying propiconazole in wood, Raman microscopy can be recommended to analyze other antifungal agents or treatments in woody plants.
- For *in situ* analyses, the development of a commercial instrument equipped with a fiber optic probe (larger beam diameter) and a longer wavelength excitation source, is suggested.

Appendix A

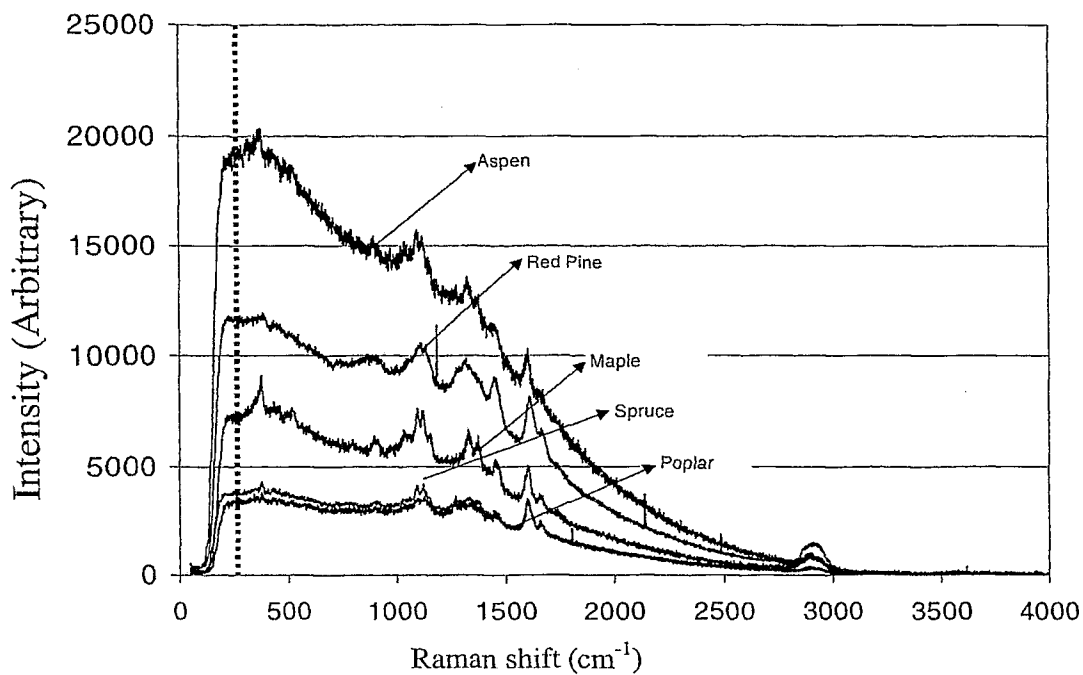
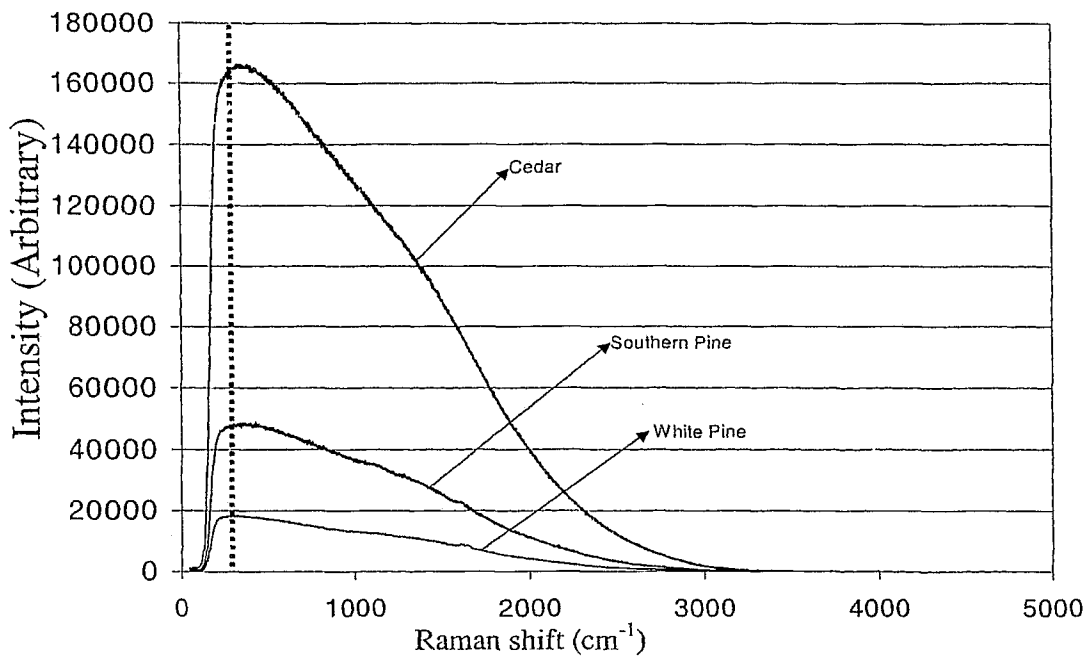


Figure A1. Raman Spectra of Different Species normalized to the lignin band at 1560-1720 cm<sup>-1</sup>.

Appendix B

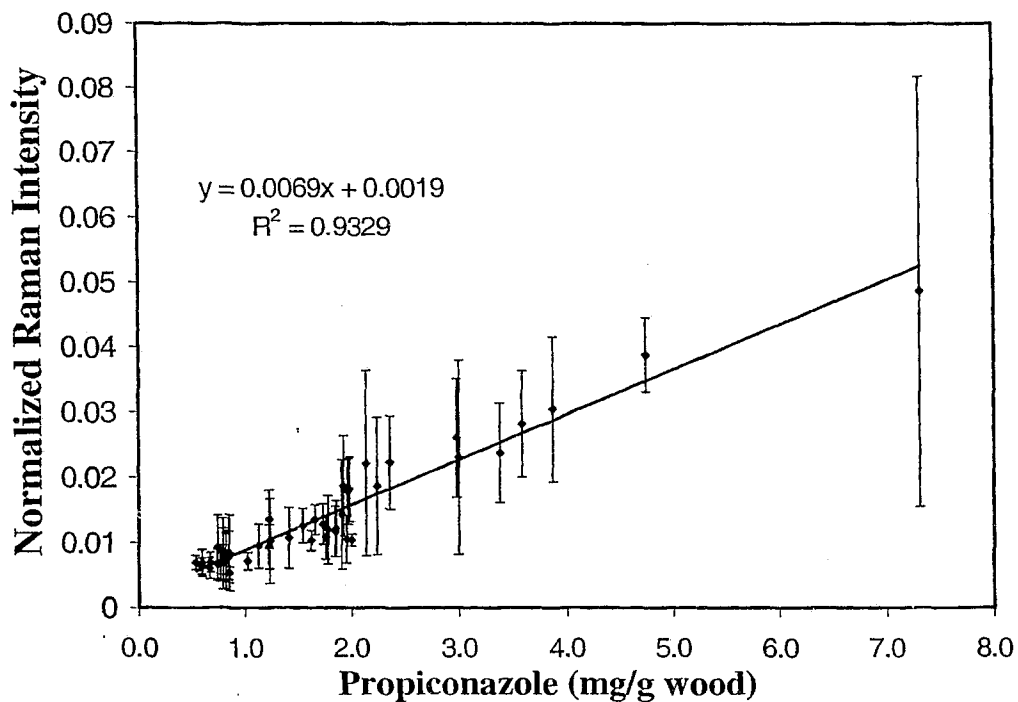


Figure B1. Calibration Curve. The error bars represent  $\pm 1$  SD (Standard Deviation).  
LOD (limit of detection) = 1.05 mg/g

| Conc <sup>a</sup><br>(mg/g) | Conc <sup>b</sup><br>(mg/g) | (S <sub>X<sub>ow</sub></sub> ) <sup>c</sup> | (+ t*S <sub>X<sub>ow</sub></sub> ) <sup>d</sup><br>(mg/g) | (- t*S <sub>X<sub>ow</sub></sub> ) <sup>d</sup><br>(mg/g) | Conc <sup>e</sup><br>(mg/g) | (S <sub>X<sub>o</sub></sub> ) <sup>f</sup> | (+ t*S <sub>X<sub>o</sub></sub> ) <sup>h</sup><br>(mg/g) | (- t*S <sub>X<sub>o</sub></sub> ) <sup>h</sup><br>(mg/g) |
|-----------------------------|-----------------------------|---|---|---|-----------------------------|--|--|--|
| 6.93                        | 10.11                       | 1.93  | 14.00   | 6.23  | 7.33                        | 0.42                                       | 8.17   | 6.48   |
| 3.04                        | 5.75                        | 0.59  | 6.93  | 4.56  | 4.23                        | 0.37                                       | 4.96   | 3.49   |
| 1.79                        | 2.14                        | 0.13  | 2.40  | 1.87  | 1.66                        | 0.35                                       | 2.37   | 0.95   |
| 1.45                        | 2.38                        | 0.14  | 2.67  | 2.09  | 1.84                        | 0.35                                       | 2.54   | 1.13   |
| 1.45                        | 2.02                        | 0.13  | 2.28  | 1.77  | 1.58                        | 0.35                                       | 2.29   | 0.87   |
| 1.29                        | 1.41                        | 0.11  | 1.63  | 1.19  | 1.15                        | 0.35                                       | 1.86   | 0.44   |
| 1.34                        | 2.00                        | 0.13  | 2.26  | 1.75  | 1.57                        | 0.35                                       | 2.28   | 0.86   |
| 1.63                        | 2.01                        | 0.13  | 2.26  | 1.75  | 1.57                        | 0.35                                       | 2.28   | 0.86   |

Table B 1. Predicted Concentration Values by Unweighted and Weighted Regression lines. 95% confidence limits are calculated for  $t = 2.01$ . a) GC-MS measured concentration. b) Predicted concentration by weighted regression equation. c) Standard Deviation of predicted concentration. d) Confidence intervals for calculated concentrations. e) Predicted concentration by the unweighted regression equation. f) Standard Deviation of predicted concentration. h) Confidence intervals for calculated concentrations.

| E <sub>r</sub> (%) <sup>a</sup> | E <sub>r</sub> (%) <sup>b</sup> |
|---------------------------------|---------------------------------|
| 45.98                           | 5.76                            |
| 89.03                           | 39.01                           |
| 19.14                           | -7.31                           |
| 64.60                           | 26.91                           |
| 39.92                           | 9.39                            |
| 9.12                            | -11.29                          |
| 49.85                           | 17.25                           |
| 23.36                           | -3.48                           |

Table B 2. Relative Error in the Predicted Concentration. a) Predicted by weighted regression equation. b) Predicted by unweighted regression equation.

## References:

Adler, E., **Lignin Chemistry Past, Present and Future**. Wood Sci. Technol. 11:169 - 218. (1977).

Agarwal,P.U., **An Overview of Raman spectroscopy as Applied to Lignocellulosic Materials**. Advances in Lignocellulosics Characterization, Atlanta, GA: TAPPI Press: Chap. 9: 2001-225. (1999).

Agarwal,P.U, McSweeny,J.D., Ralph,S.A., **An FT-Raman Study of Softwood, Hardwood, and Chemically Modified Black Spruce MWLS**. In: Proceedings of the 10<sup>th</sup> international symposium on wood and pulping chemistry, main symposium; June 7-10; Yokohama, Japan. Atlanta, GA: TAPPI Press. Vol. 2: 136-140. (1999).

Agarwal,P.U, Atalla,H.R., **Using Raman Spectroscopy to Identify Chromophores in Lignin-Lignocellulosics**. ACS symposiums series 742. Lignin:historical, biological, and material perspectives.Washington,DC:American Chemical Society: Chapter 11.250-264. (2000).

Agarwal,P.U., **Assignment of the Photoyellowing-related 1675 cm<sup>-1</sup> Raman/IR Band to p-Quinones and its Implications to the Mechanism of Colour Reversion in Mechanical Pulps**. Journal of Wood Chemistry and Technology,18(4),381-402. (1998).

Agarwal,P.U., Ralph,A.S., **FT-Raman Spectroscopy of Wood: Identifying Contributions of Lignin and Carbohydrates Polymers in the Spectrum of Black Spruce.** Applied Spectroscopy, v51, Nr11. (1997).

Agarwal,P.U., Ralph,S.A., and Atalla,H.R., "**FT Raman Spectroscopic Study of Softwood Lignin**", Proc.9<sup>th</sup> International Symposium Wood Pulp Chemistry., Canadian Pulp Paper Ass., Montreal, Canada, Poster Presentation, 8-1. (1997).

Armstrong, D.S., **Microwave-Assisted Extraction for the Isolation of Trace Systemic Fungicides from Woody Plant Material.** Department of Chemistry, Virginia Polytechnic Institute and State University. Blacksburg, Virginia, USA. (1999).

Arnup,R.W., Campbell,B.A., Raper,R.P., Squires,F.M., Virgo,D.K., Wearn,H.H., and White,G.R., **A Silviculture Guide for the Spruce Working Group in Ontario.** Science and technology series. V 4.Ministry of Natural Resources, Ontario.pp.1,67. (1988).

AWPA. American Wood-Preservers' Association. **Standard Method for the Analysis of Wood and Solutions for Propiconazole by GC.** A24-94.

AWPA. American Wood-Preservers' Association. **Proposed Standard for Propiconazole for Inclusion in Standard P8, Oil born Preservatives,** Attachment C.

(AWPI), AMERICAN WOOD PRESERVERS INSTITUTE [www.preservedwood.com](http://www.preservedwood.com)  
(2000).

Bergström,B., Gustafsson,G., Gref,R., Ericsson,A., **Seasonal Changes of Pinosylvin Distribution in the Sapwood/heartwood Boundary of *Pinus sylvestris***. Springer-Verlag Heidelberg., Vol. 14, Number 2.(1999).

Bond,J.S., Atalla,H.R., **A Raman Microprobe Investigation of the Molecular Architecture of Loblolly Pine Tracheids**. 10th International Symposium on Wood and Pulping Chemistry, Main Symposium, 1999 June 07-10, Yokohama, Japan. Atlanta, GA : TAPPI Press,.,:p. 96-101. (1999).

Bramhall,G., **The Validity of Darcy's law in the Axial Penetration of Wood**. Wood Science Technology 5:121-134. (1971).

Chang-Yeung,M., **Western Red Cedar Asthma**. Canadian researchers tackle occupational disease.

Ciba-Geigy. **Technical Information Bulletin for Propiconazole Fungicide**. Greensboro,NC 15 pp.

Comstock,G.L., **Directional Permeability of Softwoods**. Wood Fiber 1:283-289. (1970).

Crank,J., **The Mathematics of Diffusion**. Oxford University Press,London. (1970).

Dence,C.W., In:**Methods in Lignin Chemistry**.Spring-Verlag. (1992).

Douglas,J.G., **Stabilization of the Wood Cell Wall**. Kentucky. (1987).

Ekman,R., **Analysis of Lignans in Norway Spruce by Combined Gas chromatography – mass spectrometry**. Holzforschung 30, 79-85. (1976).

EverDry Forest Products. <http://www.everdry.ca/index.html> (2003).

EXTOXNET (Extension Toxicology Network) **Pesticide Information Profile on Propiconazole** Cornell University. Web site:  
<http://pmep.cce.cornell.edu/profiles/extoxnet/metiram-propoxur/propiconazole-ext.html>  
(Publication date 10/97, last updated 12 19 2001).

Fengel,D., Stoll,M., **Über die Veränderung des Zellquerschnitts, der Dicke der Zellwand und der Wandschichten von Fichtenholz-Tracheiden innerhalb eines Jahrrings**. Holzforschung 27,1-7. (1973).

Fengel,D., Wegener,G., **Wood , Chemistry, Ultrastructure, Reactions**. Walter de Gruyter, Berlin. (1984).

Forest Products Society.,**Wood Handbook: Wood as an Engineering Material**. Forest Products Laboratory. U.S. Department of Agriculture. (1999).

Gilbert,A., Baggott,J., **Essentials of Molecular Photochemistry**. Oxford Blackwell Scientific Publications. (1991).

Griffiths,R.P., Lewis,R.I., Yang,H., **Raman Spectrometry and Neural Networks for the Classification of Wood types.2.Kohonen Self-organizing Maps**. *Spechtrochimica Acta*,Part A 55,2783-2791. (1999).

Herbert,H., **Critical Annotations to the Use of Azole Antifungals for Plant Protection**. *Antimicrobial Agents and Chemotherapy*, p. 2987-2990, Vol. 45, No. 11. (November 2001).

Hilborn,G.J., Manson,E.A., Lee,S.S., Han,Y.Z., **Method to Determine Chemical Composition Distribution of Matte Coating Surfaces Using Raman Microscopy**. V:54.No.6. (2000).

Hillis,E.W., **Wood Extractives and their Significance to the Pulp and Paper Industries**. Academic Press,New York. (1962).

Hollas,M.J., **High Resolution Spectroscopy**. Second Edition, John Wiley & Sons. (2000).

Hsiang,T., Yang,L. and Barton,W., **Baseline Sensitivity and Cross-resistance to Demethylation-inhibiting Fungicides in Ontario Isolates of *Sclerotinia homoeocarpa*** *European Journal of Plant Pathology* 103: 409-416. (1997).

Hudson,M.S., Shelton,S.V., **Longitudinal Flow of Liquids in Southern Poles**. Forestry Product Journal. 19(5):25-32. (1969).

Hughes,A.S., **The Tools at Our Disposal** . First Workshop COST Action E22 Environmental Optimization of Wood Protection. Lisbona, Portugal . (2004).

Lewis,I.R., Edwards,G.M., **Handbook of Raman spectroscopy: from the research laboratory to the process line**. New York : Marcel Dekker. (2001).

Katic,S., **Analysis of Propiconazole in Spruce by GC-MS**. Ryerson University, Toronto. Fourth Year Thesis Report. (2003).

Kazi,K.M., Jollez,P., Chornet,E., **Preimpregnation :An Important Step for Biomass Refining Process**. Biomass and Bioenergy Vol. 15, No. 2, pp. 125-141. (1998).

LaFuente,M.T., Tadeo, J.L., **GLC Multiresidue Analysis of Postharvest Fungicides in Citrus Fruits**, Fresenius Z Analytical Chemistry, 328, 105. (1987).

Lakehead University, Faculty of Forestry and the Forest Environment, **Ontario's Northwest Forest**. <http://www.borealforest.org/index.php> (2002).

Lavine,K.B., Davidson,E.C., Moores,J.A., Griffiths,R.P., **Raman Spectroscopy and Genetic Algorithms for the Classifications of Wood Types**. Applied Spectroscopy,V55,No8. (2001).

Malkov,S.Y., Kuzmin,A.V., Baltahikov,P.V., Tikka,P., **Modelling the Process of Water Penetration into Softwood Chips**. Journal of Pulp and Paper Science. (2003).

McCreery,L.R., **Raman Spectroscopy for Chemical Analysis**. v.157. Wiley-Interscience. (2000).

Miller,C.J., Miller,N.J., **Statistics for Analytical Chemistry**; Second Edition. Ellis Horwood Ltd.Chichester. (1988).

Milton,T.F., **The Preservation of Wood. A Self Study Manual for Wood Treaters**. University of Minnesota, [www.extension.umn.edu](http://www.extension.umn.edu). (2002).

Ona,T., Sonoda,T., Ito, K., Shibata, M., Ootake, Y., Ohshima, J., Yokota, S., Yoshizawa, N., **In situ Determination of Proportion of Cell Types in Wood by Fourier Transform Raman Spectroscopy**. Analytical Biochemistry. 268(1) 43-48. (1999).

Panshin.A.J., De Zeeuw.C., **Textbook of Wood Technology** .New York. (1980).

Pelletier,M.J., **Quantitative Analysis Using Raman Spectrometry**. Applied Spectroscopy. V: 57. (2003).

Perry,J.H., **Chemical Engineer's Handbook**. 6<sup>th</sup> edition, McGraw-Hill, Tokyo. (1984).

PMRA. **Pest Management Regulatory Agency; Regulatory Note**, Reg. 2000-06.  
www.hc-sc.gc.ca/pmra-arla.

Schoknecht,U., Bergmann,H., **Preservative Penetration-determination of Active Substances in Wood**. Holz als Roh- und Werkstoff 58, 380-386. (2000).

Servos,R.R., and Clark,H.M., **Vibrational Spectra of Normal and Isotopically Labelled Boric Acid**. Journal of Chemical Physics.26:1175-1178. (1957).

Shen,J., Zhou,J., Vazquez,O., **Experimental Study of Optical Scattering and Fiber Orientation Determination of Softwood and Hardwood with Different Surface Finishes**. Applied Spectroscopy, V54, No12. (2000).

Shen,Q., Rosenholm,J.B., **Characterization of the Wettability of Wood Resin by Contact Angle Measurements and FT-Raman Spectroscopy**. in "Progress in lignocellulosic characterization". 237-248.TAPPI Press. (1998).

Shen,Q., Rahiala,H., Rosenholm,J.B., **Evaluation of the Structure and Acid-Base Properties of Bulk Wood by FT-Raman Spectroscopy**: Vol. 206, No 2 , pages 558-568. (1998).

Siau,F.J., **Transport Processes in Wood**. New York . (1984).

Sjöstoröm,E., **Wood Chemistry Fundamentals and Application**, 2<sup>nd</sup> (Ed). Academic Press, San Diego. (1993).

Stephen,S., **Preservative Treated Wood**. Shutesbury, Massachusetts,  
[http://www.umass.edu/bmatwt/publications/articles/preservative\\_treated\\_wood.html](http://www.umass.edu/bmatwt/publications/articles/preservative_treated_wood.html)  
(1996).

Stipes,R.J. Campana R.J., **Introduction and Evaluating liquid Fungicides for Control of DED, Methods for Control of Plant Pathogens**, American Phytopathological Society, St. Paul, Minnesota. (1986).

Szymanski,A.H., **Raman Spectroscopy .Theory and Practice**. Plenum Press, New York. (1967).

Tsounis.G., **Wood as Raw Material** . Pergamon Press, Oxford . (1968).

Vialaton,D., Baglio,D., Ana Paya-Perez, Bo Larsen, and Claire Richard,  
**Phototransformation of Propiconazole In Aqueous Media**. Journal of Agricultural Food Chemistry 49,5377-5382. ( 2001).

Wariishi,H., Takayama,M., Johjima, T., Yamanaka, T., Tanaka, H., **Spectrochimica Acta, Fourier Transform Raman Assignment of Guaiacyl and Syringyl Marker Bands for Lignin Determination Part A**, 53.1621-1628. (1997).

Wariishi,H., Kihara,M., Takayama,M., Tanaka,H., **Determination of the Carbonyl Groups in Native Lignin Utilizing Fourier Transform Raman Spectroscopy.** Spectrochimica Acta Part A 58, 2213-2221. (2002).

Wayne,S.J., **Preservative Treated Wood in the Landscape.** University of Nevada. (1994).

Yamauchi,S., Doi,S., **Raman Spectroscopic Study on the Behaviour of Boric Acid in Wood.** Journal of Wood Science. 49:227-234. (2003).

Yamauchi,S., Shibutani,S., Doi,S., **Characteristic Raman bands for Artocarpus heterophyllus heartwood.** Journal of Wood Science. 46:466-468. (2003).

Zhu,H.J., Gray,G.D., **Photoyellowing of Lignin Rich Paper :Interaction of Excited States with Selected Additives.** Journal of Photochemistry and Photobiology A:Chemistry 87,267-273. (1995).

Zirngibl,L. **Antifungal Azoles, A Comprehensive Survey of their Structures and Properties.** Wiley-VCH. (1998).